

NASA Contractor Report 4763

# Evaluation of the MV (CAPON) Coherent Doppler Lidar Velocity Estimator

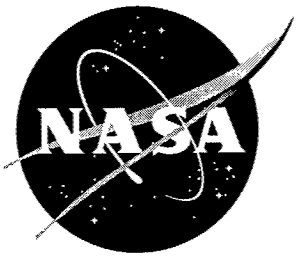
---

*B. Lottman and R. Frehlich*

Grant NAG8-253  
Prepared for Marshall Space Flight Center

---

January 1997



# Evaluation of the MV (CAPON) Coherent Doppler Lidar Velocity Estimator

---

*B. Lottman and R. Frehlich*

*Cooperative Institute for Research in Environmental Sciences (CIRES)*

*University of Colorado • Boulder, Colorado*

National Aeronautics and Space Administration  
Marshall Space Flight Center • MSFC, Alabama 35812

Prepared for Marshall Space Flight Center  
under Grant NAG8-253

---

January 1997

## Contents

1	Introduction	1
2	Typical Parameter Regimes	1
3	Velocity Estimator Performance	3
4	Potential Uses	4
5	Computational Effort	4
6	Results M=10	5
7	Results M=16	9
8	Results M=32	10
9	Results M=64	12
10	Results M=128	13
11	Results M=512	14
12	Acknowledgements	16
	Appendix A, M=16	17
	Appendix B, M=32	21
	Appendix C, M=64	27
	Appendix D, M=128	32
	Appendix E, M=512	37

## List of Tables

Table 1. Parameter regime for a typical $2\mu m$ and $10\mu m$ LAWS type lidar.	2
Table 2. Parameter regime for a typical $2\mu m$ and $10\mu m$ boundary layer lidar.	2
Table 3. Parameter regime for typical $2\mu m$ and $10\mu m$ LAWS type lidar observing a thick cloud.	3
Table 4. Parameter regimes evaluated in this paper.	3
Table 5. Computational effort for the CAPON Estimator based on estimator order $p$ , oversampling $os$ , and the number of data points in the range cell $M$ .	4
Table 6. Model Fit Parameters for $M=10$ , $\Omega=0.2$ and $0.3$ .	8
Table 7. Model Fit Parameters for $M=16$ , $\Omega=0.2$ , $0.3$ , $0.5$ and $1.0$ .	10
Table 8. Model Fit Parameters for $M=32$ , $\Omega=0.2$ , $0.3$ , $0.5$ , $1.0$ , $2.0$ , and $3.0$ .	11
Table 9. Model Fit Parameters for $M=64$ , $\Omega=0.3$ , $0.5$ , $1.0$ , $2.0$ , and $3.0$ .	13
Table 10. Model Fit Parameters for $M=128$ , $\Omega=0.5$ , $1.0$ , $2.0$ , $3.0$ , and $7.0$ .	14
Table 11. Model Fit Parameters for $M=512$ , $\Omega=7.0$ and $10.0$ .	15

## List of Figures

Figure 1. Estimator performance as a function of oversampling $os$ and order $p$ for $M=32$ and $\Omega=0.5$ .	3
Figure 2. Estimator performance vs. computational effort for $M=512$ and $\Omega=7.0$ .	5
Figure 3. Performance vs. oversampling $os$ for $M=10$ and $\Omega=0.2$ .	6
Figure 4. Performance vs. oversampling $os$ for $M=10$ and $\Omega=0.3$ .	6
Figure 5. Performance vs. order $p$ for the CAPON estimator for $M=10$ and $\Omega=0.2$ .	6
Figure 6. Performance vs. order $p$ for the CAPON Estimator for $M=10$ and $\Omega=0.3$ .	6
Figure 7. Single realizations of the CAPON estimates for $M = 10$ and $\Omega=0.2$ for $\Phi=1,10,50,1000$ with optimal estimator parameters.	7
Figure 8. Single realizations of the CAPON estimates for $M=10$ and $\Omega=0.3$ for $\Phi=1,10,50,1000$ with optimal estimator parameters.	7
Figure 9. PDF of the Velocity Estimates using the CAPON estimator with $M=10$ and $\Omega=0.2$ for $\Phi=1,10,50,1000$ .	7

Figure 10. PDF of the Velocity Estimates using the CAPON estimator with $M=10$ and $\Omega=0.3$ for $\Phi=1,10,50,1000$ .	7
Figure 11. Performance of the CAPON estimator with $M=10$ and $\Omega=0.2$ and 0.3 using optimal estimator parameters. Best fit model is (-).	8
Figure 12. Optimal parameters for the CAPON estimator with $M=10$ and $\Omega=0.2$ and 0.3.	8
Figure 13. Minimum estimator order $p$ with $M=10$ and $\Omega=0.2$ and 0.3 for no greater than 5the good estimates.	8
Figure 14. Performance of the CAPON estimator with $M=16$ and $\Omega=0.2, 0.3, 0.5,$ and 1.0 using optimal estimator parameters.	9
Figure 15. Optimal parameters for the CAPON estimator with $M=16$ and $\Omega=0.2,$ 0.3, 0.5, and 1.0.	9
Figure 16. Minimum estimator order $p$ with $M=16$ and $\Omega=0.2, 0.3, 0.5,$ and 1.0 for no greater than 5% and 10% increase in the standard deviation $g$ of the good estimates.	9
Figure 17. Performance of the CAPON estimator with $M=32$ and $\Omega=0.2, 0.3, 0.5,$ 1.0, 2.0, and 3.0 using optimal estimator parameters.	10
Figure 18. Optimal parameters for the CAPON estimator with $M=32$ and $\Omega=0.2,$ 0.3, 0.5, 1.0, 2.0, and 3.0.	11
Figure 19. Minimum estimator order $p$ with $M=32$ and $\Omega=0.2, 0.3, 0.5, 1.0, 2.0$ and 3.0 for no greater than 5% and 10% increase in the standard deviation $g$ of the good estimates.	11
Figure 20. Performance of the CAPON estimator with $M=64$ and $\Omega=0.3, 0.5, 1.0,$ 2.0, and 3.0 using optimal estimator parameters.	12
Figure 21. Optimal parameters for the CAPON estimator with $M=64$ and $\Omega=0.3,$ 0.5, 1.0, 2.0, and 3.0.	12
Figure 22. Minimum estimator order $p$ with $M=64$ and $\Omega=0.3, 0.5, 1.0, 2.0$ and 3.0 for no greater than 5% and 10% increase in the standard deviation $g$ of the good estimates.	12
Figure 23. Performance of the CAPON estimator with $M=128$ and $\Omega=0.5, 1.0, 2.0,$ 3.0, and 7.0 using optimal estimator parameters.	13
Figure 24. Optimal parameters for the CAPON estimator with $M=128$ and $\Omega=0.5,$ 1.0, 2.0, 3.0, and 7.0.	14

Figure 25. Minimum estimator order  $p$  with  $M=128$  and  $\Omega=0.5, 1.0, 2.0, 3.0$  and  $7.0$  for no greater than 5% and 10% increase in the standard deviation  $g$  of the good estimates. 14

Figure 26. Performance of the CAPON estimator with  $M=512$  and  $\Omega=7.0$  and 10.0 using optimal estimator parameters. 15

Figure 27. Optimal parameters for the CAPON estimator with  $M=512$  and  $\Omega=7.0$  and 10.0. 15

Figure 28. Minimum estimator order  $p$  with  $M=512$  and  $\Omega=7.0$  and 10.0 for no greater than 5% and 10 % increase in the standard deviation  $g$  of the good estimates. 15

# 1 Introduction

The first coherent Doppler lidars were based on the  $CO_2$  laser [1, 2, 3, 4]. More recently, solid state Doppler lidars have been successfully operated [5, 6, 7]. Coherent Doppler lidar is under consideration for measurements of the global wind field from space [[3, 8, 9]]. A coherent Doppler lidar operating at wavelength  $\lambda$  can estimate the radial component of the velocity  $v = \lambda f/2$  as a function of range for every transmitted pulse by estimating the Doppler frequency shift  $f$ . The Probability Density Function (PDF) provides a complete statistical description of an estimator. For the better velocity estimators, the PDF is characterized by a fraction  $b$  of uniformly distributed bad estimates or random outliers and a distribution of good estimates centered on the true mean velocity. Frehlich and Yadlowsky[10] investigated the performance of mean-frequency estimators by modeling the distribution of good estimates as a Gaussian PDF with standard deviation  $g$ . Approximately universal curves of performance of velocity estimates (and mean-frequency estimates) are produced by plotting the standard deviation  $g$  normalized by the signal spectral width in velocity space  $w_v = \lambda w/2$  versus the parameter  $\Phi = SNR \cdot M$  for fixed  $\Omega = wMT_s$  where  $w$  is the signal spectral width,  $T_s$  is the sampling interval of the complex data, SNR is the Signal-to-Noise Ratio, and  $M$  is the number of complex data points per observation.  $\Omega$  is fixed for fixed range resolution and fixed transmitted pulse length, the typical comparison case for lidar performance. For shot-noise dominated operation, the parameter  $\Phi = \eta_H N_e$  where  $\eta_H$  is the heterodyne efficiency ( $\eta_H \approx 0.4$  in the far field. The far field condition is usually valid for space-based platforms.) and  $N_e$  is the average number of photo-electrons per estimate.  $\Phi$  is the average number of coherent photo-electrons per estimate. The parameter  $\Omega$  is proportional to the number of independent samples of the signal per range gate, sometimes called the “speckle count”.

Anderson [11] proposed the Minimum Variance (MV) or CAPON spectral estimator for

space-based measurements of winds. Assuming  $\Phi$  and  $\Omega$  are known, we evaluate the performance of the CAPON estimator where the auto-regressive coefficients up to order  $p$  are determined from the biased covariance estimates and the Yule-Walker solution [10, 12, 13]. The optimal order  $p$  and the optimal sampling interval for estimating the maximum of the spectral estimate  $S(f)$  for the CAPON estimator are determined by minimizing the standard deviation of the good estimates. Various parameter regimes will be considered.

## 2 Typical Parameter Regimes

A variety of parameter regimes relevant to space-based measurements are evaluated in this paper. The basic space-based parameters were determined by the following criteria;

- 1)A velocity search space  $v_s$  of 50 m/s was selected. The sampling interval  $T_s$  for complex data is given by  $T_s = \lambda/(2v_s)$ . The sampling interval for 2 and 10  $\mu m$  lidar is 20 and 100 ns respectively.
- 2)For numerical weather prediction, current models use a 1 km height resolution. This implies a 1.5 km range cell (line of sight) for typical satellite scanning geometries. The range resolution is  $\Delta p + \Delta r$  where  $\Delta p$  is the distance the pulse moves per velocity estimate, i.e.,  $\Delta p = MT_s c/2$  where  $c$  [m/s] is the speed of light.  $\Delta r$  [m] is the full width half max (FWHM) spatial extent of the pulse, i.e.  $\Delta r = \Delta t c/2$  where  $\Delta t$  [s] is the FWHM temporal extent of the pulse. A  $\Delta p$  of 1500m was selected. Since  $M = 2\Delta p/(T_s c)$ ,  $M = 500$  and  $100$  for 2 and 10  $\mu m$  lidars respectively. For a large  $\Delta p$  the spectral width  $w$  of the returned signal is usually dominated by wind turbulence. The lidar signal is approximated as a Gaussian with a spectral width in velocity space  $w_v$  of 1 m/s and since  $w = 2w_v/\lambda$ ,  $w$  is 1 and 0.2 MHz for a 2 and 10  $\mu m$  lidar respectively.  $\Omega = wMT_s$  where  $\Omega$  is proportional to the speckle count.  $\Omega = 10.0$  and  $2.0$  for a 2 and 10  $\mu m$  lidar respectively.

Examples of parameter regimes for a 2 $\mu m$  and 10 $\mu m$  LAWS type lidar are shown in Table 1.

$\lambda$	$T_s$	$w$	$\Delta p$	M	$\Omega$
2	20	1.0	1536	512	10.2
2	20	1.0	768	256	5.1
2	20	1.0	384	128	2.5
10	100	0.2	1920	128	2.5
10	100	0.2	960	64	1.3
10	100	0.2	480	32	0.6

**Table 1.** Parameter regime for a typical  $2\mu m$  and  $10\mu m$  LAWS type lidar.  $\lambda$  is in  $\mu m$ .  $T_s$  is in  $ns$ .  $w$  is in  $MHz$ .  $\Delta p$  is in  $m$ .

Typical lidar parameters for boundary layer measurements are also of interest. The basic parameters for the typical boundary layer lidar are based on the following;

1)  $50 m/s$  was selected for the velocity search space.  $2$  and  $10 \mu m$  was selected for lidar wavelength  $\lambda$ . The sampling time  $T_s$  for complex data for a  $2$  and  $10 \mu m$  lidar is  $20$  and  $100 ns$  respectively.

2) The boundary layer is typically  $1000 m$  in depth. To characterize activity within the layer, measurements are usually taken at least every  $100 m$ . A range cell length  $\Delta p$  of  $48m$  was selected and  $M = \frac{2\Delta p}{T_s c}$  or  $M = 16$ .

For a small  $\Delta p$  the spectral width  $w$  of the returned signal is determined by the transmitted pulse (pulse dominated) and not wind turbulence. For a  $2 \mu m$  example, the FWHM pulse width  $\Delta t$  is  $0.3 \mu s$ . The spectral width  $w$  (pulse dominated) is  $w = \sqrt{\ln 2/2}/\pi\Delta t$  or  $w = 0.1873/\Delta t$  and  $\Omega = wMT_s$  or  $\Omega = 0.2$ .

For very large spectral width  $w$ , the velocity search space becomes comparable with  $w$ . In this regime the PDF's do not have a uniform layer of outliers and the two parameter model is not valid. The upper bound on  $\Omega$  is when the  $16\sigma$  spectral width of the signal approaches the full velocity search space. For example, for  $M = 16$ ,  $16w \leq 1/T_s$ , or  $wT_s \leq 1/16$ , therefore  $\Omega = wMT_s \leq M/16$ , or  $\Omega \leq 1$ .

Examples of typical parameter regimes for the  $2\mu m$  and  $10\mu m$  boundary layer lidar are shown in Table 2.

For a LAWS system, observation of thick clouds is of interest. Thick clouds generate a signal similar to a hard target return and the signal

spectral width is determined by the transmitted pulse.

The basic parameter set for thick cloud observation using a LAWS type system is determined as follows;

1) Sampling interval is selected based on a velocity search space of  $50 m/s$  and the lidar wavelength  $\lambda$ . The sampling interval  $T_s$  for  $2$  and  $10 \mu m$  lidar is  $20$  and  $100 ns$  respectively.

2) The observation time  $MT_s$  is determined as a fraction of the FWHM of the transmitted pulse  $\Delta t$ .  $MT_s = k\Delta t$ ; where  $k$  is a user defined constant, which is related to  $\Omega$  by  $\Omega = k\sqrt{\ln 2/2}/\pi$  or  $\Omega = .1873 k$ .  $\Delta t$  determines  $M$ .

$\lambda$	$T_s$	$\Delta t$	$\Delta p$	M	$\Omega$
2	20	0.30	48	16	0.2
2	20	0.20	48	16	0.3
2	20	0.12	48	16	0.5
2	20	0.06	48	16	1.0
2	20	0.60	96	32	0.2
2	20	0.40	96	32	0.3
2	20	0.24	96	32	0.5
2	20	0.12	96	32	1.0
2	20	0.06	96	32	2.0
2	20	0.04	96	32	3.0
2	20	0.80	192	64	0.3
2	20	0.48	192	64	0.5
2	20	0.24	192	64	1.0
2	20	0.12	192	64	2.0
2	20	0.08	192	64	3.0
10	100	0.94	150	10	0.2
10	100	0.62	150	10	0.3
10	100	1.50	240	16	0.2
10	100	1.00	240	16	0.3
10	100	0.60	240	16	0.5
10	100	0.30	240	16	1.0

**Table 2.** Parameter regime for a typical  $2\mu m$  and  $10\mu m$  boundary layer lidar.  $\lambda$  is in  $m$ .  $T_s$  is in  $ns$ .  $\Delta t$  is in  $\mu s$ .  $\Delta p$  is in  $m$ .

This regime is similar to the high SNR small range gate scenario for boundary layer measurements. The parameter sets for the thick cloud target with various transmitted pulse widths for  $2\mu m$  ( $T_s=20ns$ ) and  $10\mu m$  ( $T_s=100ns$ ) are shown in Table 3.

Tables 1 through 3 give the general regimes of

interest. The parameter sets evaluated in this paper are shown in Table 4.

2 $\mu m$				10 $\mu m$			
$\Delta t$	$k$	M	$\Omega$	$\Delta t$	$k$	M	$\Omega$
0.20	1.0	10	0.2	1.00	1.0	10	0.2
0.13	1.6	10	0.3	0.63	1.6	10	0.3
0.32	1.0	16	0.2	1.60	1.0	16	0.2
0.20	1.6	16	0.3	1.00	1.6	16	0.3
0.11	2.7	16	0.5	0.59	2.7	16	0.5
0.64	1.0	32	0.2	3.20	1.0	32	0.2
0.40	1.6	32	0.3	2.00	1.6	32	0.3
0.24	2.7	32	0.5	1.18	2.7	32	0.5
0.80	1.6	64	0.3	2.37	2.7	64	0.5
0.47	2.7	64	0.5				
0.95	2.7	128	0.5				

**Table 3.** Parameter regime for typical 2 $\mu m$  and 10 $\mu m$  LAWS type lidar observing a thick cloud.  $\Delta t$  is in  $\mu s$ .

M	$\Omega$							
	0.2	0.3	0.5	1.0	2.0	3.0	7.0	10.0
10	X	X						
16	X	X	X	X				
32	X	X	X	X	X	X		
64	X	X	X	X	X	X		
128	X	X	X	X	X	X	X	
512						X	X	

**Table 4.** Parameter regimes evaluated in this paper.

### 3 Velocity Estimator Performance

Simulations of complex coherent Doppler lidar data were produced by the method described in Frehlich and Yadlowsky[10]. This produces data with a specified auto-covariance function which is chosen as a Gaussian function defined by the parameters  $\Phi$ ,  $\Omega$ , and  $M$  [see Eq. (22) of Ref.[10]]. This is a good approximation for 2 $\mu m$  coherent lidars[14].

For the CAPON estimator, performance is a function of both estimator order and oversampling. Oversampling refers to sampling the spectral function at smaller intervals to improve es-

timator accuracy. In velocity space, the sampling interval  $\Delta v = v_s/(M os)$  where  $os$  is the oversampling.  $os = 1$  means that the spectral function is sampled with  $M$  data points. The maximum value of the spectral estimate and the two closest neighbors are fit to a parabola. The velocity that produces the peak of the parabola is selected as the estimate. The value of  $x$  that maximizes  $f(x)$  for uniformly sampled  $x_k$  is

$$x_{peak} = x_1 + \frac{f(x_2) - f(x_0)}{2(2f(x_1) - f(x_0) - f(x_2))}$$

where  $x_0$  is the index of the spectral function to the left of the peak,  $x_1$  is the index of the spectral function at the peak, and  $x_2$  is the index of the spectral function to the right of the peak.

Generally, performance is less sensitive to oversampling than estimator order. Examples of oversampling and order sensitivity for  $M = 32$  and  $\Omega = 0.5$  are shown in Fig. 1. Performance is normalized by the minimum standard deviation of the good estimates for each regime  $g_{min}$ .

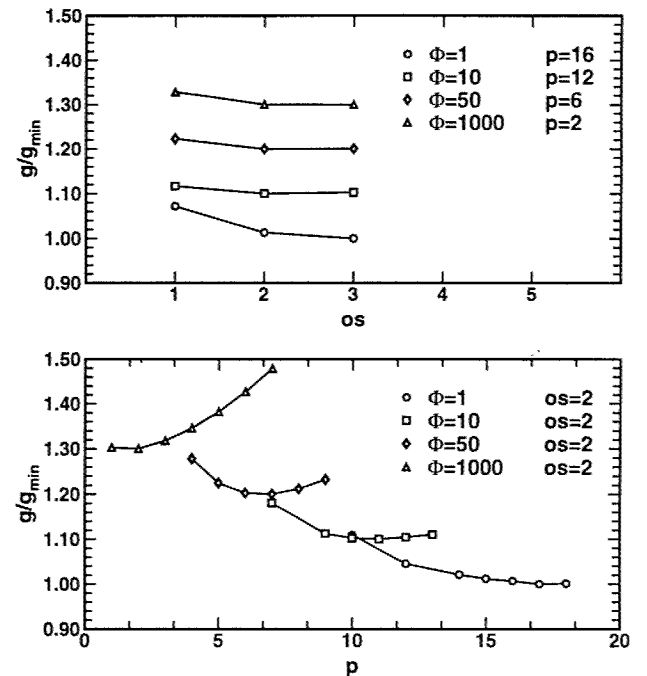


**Figure 1.** Estimator performance as a function of oversampling  $os$  and order  $p$  for  $M=32$  and  $\Omega=0.5$ . Curves are offset by 0.10. The  $1\sigma$  error bars are less than the symbol size.

The technique for determining the optimal estimator parameters ( $p$ ,  $os$ ) for given basic pa-

rameters ( $M$ ,  $\Omega$ ,  $\Phi$ ) is to first determine optimal oversampling  $os$  with an approximate optimal order, then determine optimal order  $p$  using the oversampling result  $os$ . Parameters that give the best performance within the statistical limitations of the simulation are considered the optimal parameters.

For large  $M$  with large  $\Omega$ , estimator accuracy does not improve with oversampling ( $os = 1$  produces the best performance). For the  $M = 512$   $\Omega = 7.0$  and  $10.0$  cases order sensitivity is computed but oversampling sensitivity is not computed.

The results of each parameter set include: performance as a function of oversampling and order, single realizations of the CAPON spectral estimates, and PDF's for the velocity estimators for a subset of cases using optimal estimator parameters.

## 4 Potential Uses

The standard deviation of the good estimates  $g$  and the fraction  $b$  of uniformly distributed bad estimates can be used to generate simulated velocity data for a given parameter regime. To generate velocity data, velocity values are drawn from one of two random number generators. The good estimates are represented by a Gaussian random variable with standard deviation  $g$ , while the bad estimates are represented by a uniform random variable over the velocity search space  $v_s$ . Selection of a good or bad estimate is based on the parameter  $b$ , the fraction of uniformly distributed bad estimates.

For a LAWS type mission, the final data product will be generated from multiple shots in a resolution cell with a specified scanning configuration e.g. a conical scan[9]. The desired data product is the average wind vector over the resolution cell in 3D. The PDF of any multishot velocity algorithm can be derived from the single shot PDF's using a Monte Carlo analysis.

## 5 Computational Effort

Computational effort for complex data is shown in Table 5. *Flops* are complex floating point operations[15].

	Multiplications (flops)
Autocorrelation	$(2M - p)(1 + p)/2$
AR coefficients	
Yule Walker	$p^2 + p$
$\psi_{MV}$ coefficients	$p(p + 1)/2$
FFT	$M os \log_2(M os)/2$
Total(Approx)	$(M + p)(1 + p) + M os \log_2(M os)/2$
	Additions (flops)
Autocorrelation	$(2M - p)(1 + p)/2 + M$
AR coefficients	
Yule Walker	$p^2 + p$
$\psi_{MV}$ coefficients	$p(p + 1)/2$
FFT	$M os \log_2(M os)$
Total(Approx)	$(M + p)(1 + p) + M + M os \log_2(M os)$

**Table 5.** Computational effort based on estimator order  $p$ , oversampling  $os$ , and the number of data points in the range cell  $M$ . *flops* are complex floating point operations.

For a typical  $2\mu m$  LAWS regime ( $M = 512$ ,  $\Omega = 10.0$ ), the maximum optimal order  $p$  is about 12 and optimal oversampling  $os$  is 1. Thus the dominant terms for computational effort are  $(2M - p)(1 + p)/2 + M \log_2(M)/2$  for complex multiplications and  $(2M - p)(1 + p)/2 + M + M \log_2(M)$  for complex additions.

Computational effort (total of complex multiplications and additions) for a typical LAWS regime ( $M=512$ ,  $\Omega=7.0$ ) versus estimator performance is shown in Fig. 2. The solid lines represent the total computational effort whereas the dashed lines are the computational effort for the FFT portion of the estimation routine. For this case, computational effort is not dominated by the FFT portion of the estimation routine.

Since computational effort for the CAPON estimator depends on order  $p$ , a reduced order reduced performance (reduced from optimal) esti-

imator may be of interest for regimes that require high optimal estimator order  $p$ . A reduced order estimator tends to increase the standard deviation of the good estimates  $g$ .

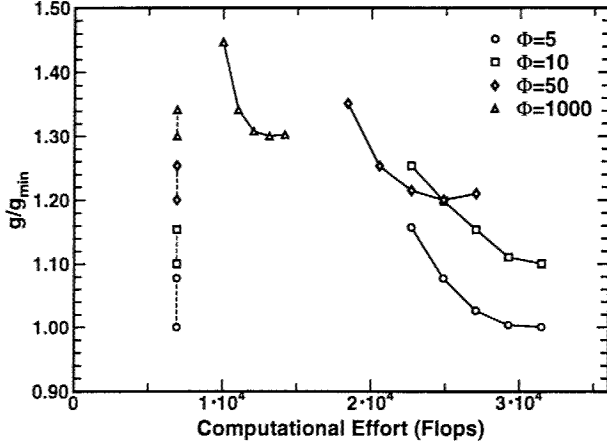


**Figure 2.** Estimator performance vs. computational effort for  $M=512$  and  $\Omega=7.0$ . Points on curve refer to performance for different filter order. Solid curves are the total complex operations in *flops*. Dashed curves are the complex operations (*flops*) for the FFT portion of the estimation routine.

Order reduction is considered for cases where  $g$  increases no more than 5% and 10%. Performance results due to relaxed estimator order are included.

## 6 Results M=10

For this set, performance of the estimator will be evaluated for the  $\Omega=0.2$  and  $\Omega=0.3$  cases. For larger  $\Omega$ , the signal spectral width becomes comparable to the velocity search space.

As oversampling  $os$  increases, performance approaches a constant. Optimal oversampling is the minimum oversampling where the performance does not degrade more than the statistical variations in the estimates for  $g$ . For  $\Omega=0.2$  and 0.3, optimal oversampling  $os$  is 3. For the low  $\Phi$  cases, oversampling can improve the standard deviation of the good estimates  $g$  for this parameter regime by up to 20%. Performance vs. oversampling  $os$  for  $\Omega=0.2$  and 0.3 are shown in Fig. 3 and Fig. 4.

There is a tendency for performance to in-

crease with order  $p$  to the optimal performance, then gradually decrease. In addition, optimal order decreases with increasing  $\Phi$ . Estimator order sensitivity for  $\Omega=0.2$  and 0.3 are shown in Fig. 5 and Fig. 6.

Single realizations of the spectral estimates can provide insight into the optimal performance of an estimator. There is a tendency for the width of the signal spectral peak to increase for increased  $\Phi$ . Intuitively one might think that a wider spectrum will produce a larger estimation error  $g$ . Results from simulations show that at large  $\Phi$  the wider spectral function has less error and requires less oversampling for optimal performance. Single realizations of the spectral estimates for  $\Omega=0.2$  and 0.3 are shown in Fig. 7 and Fig. 8. The tick marks represent a sampling of the spectral estimate with  $os = 1$ . The realizations demonstrate that the oversampling resolves the peak.

The PDF of the estimators are characterized by a clump of good estimates and uniformly distributed bad estimates. The PDF's were modeled by both a single Gaussian component (—) and a double Gaussian component (—) for the good estimates. The vertical lines indicate the boundary region for estimating the standard deviation of the good estimates  $g$  without assuming a model for the PDF. The parameters of the PDF were estimated using a maximum likelihood algorithm on the histograms (ML-PDF)[16]. These parameters were used to define a region around the mean velocity that permits an estimate of  $g$  without assuming a model for the PDF.

The bias of the good estimates  $\Delta v$  and the  $1\sigma$  error bars are also calculated. For most cases the bias is less than 1/1000 of the standard deviation of the good estimates  $g$  and is not statistically different than the error bars. This means there is statistically no significant bias for the good estimates. The PDF's for  $\Omega=0.2$  and 0.3 are shown in Fig. 9 and Fig. 10. Cases of  $\Phi = 1, 10, 50$ , and 1000 are reasonable fits with little bias.

A summary of the performance for the  $M=10$  and  $\Omega=0.2$  and 0.3 is shown in Fig. 11. A summary of the optimal order and oversampling is shown in Fig. 12.

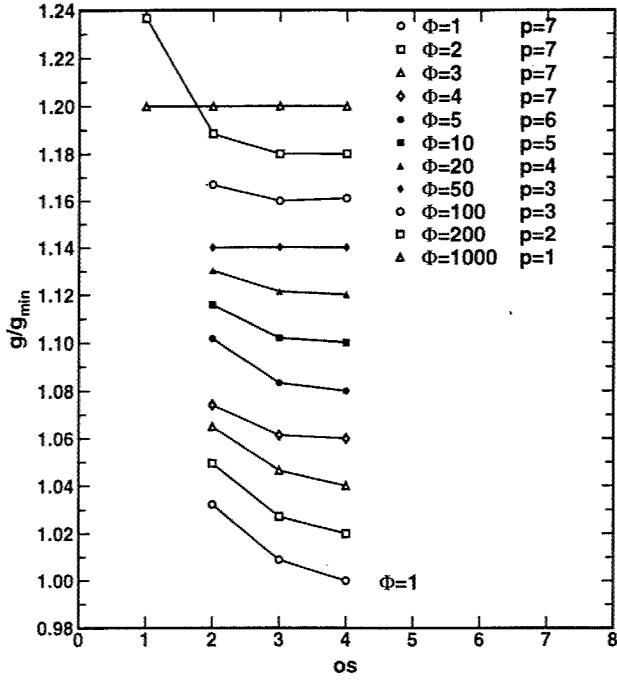


Figure 3. Performance vs. oversampling  $os$  for  $M=10$  and  $\Omega=0.2$ . Curves are offset by 0.02.  $1\sigma$  error bars are less than the symbol size.

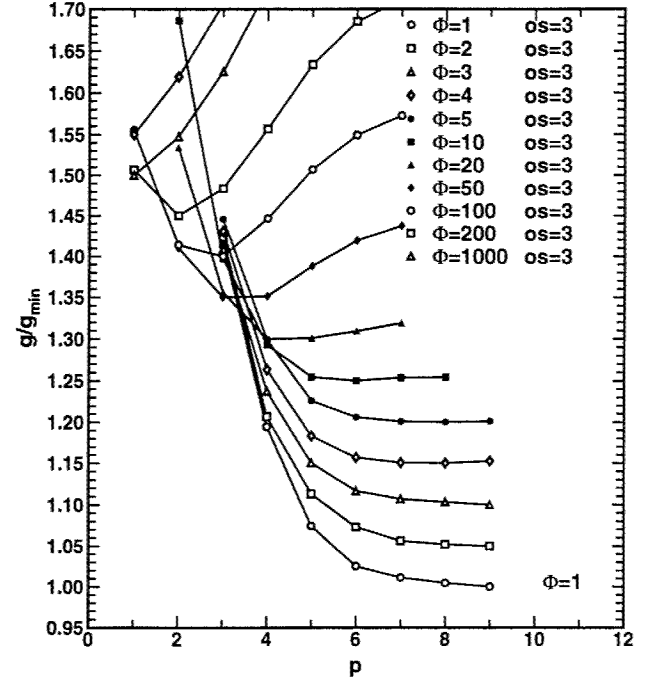


Figure 5. Performance vs. order  $p$  for  $M=10$  and  $\Omega=0.2$ . Curves are offset by 0.05.  $1\sigma$  error bars are less than the symbol size.

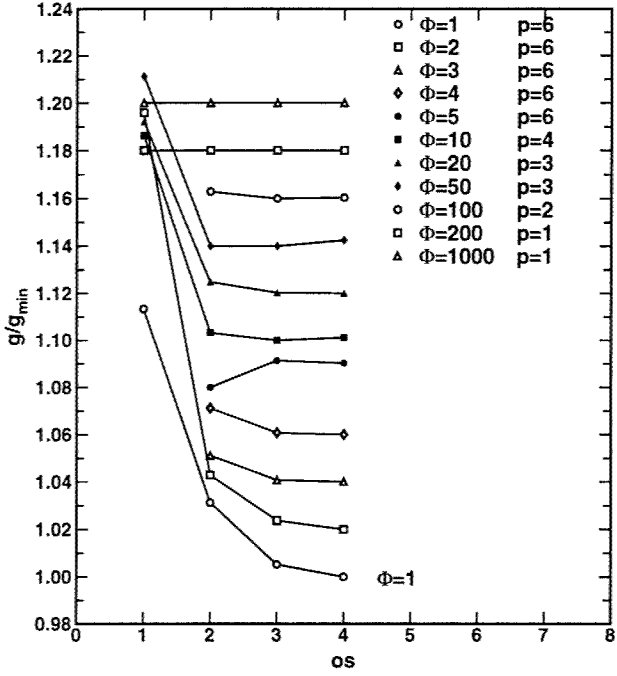


Figure 4. Performance vs. oversampling  $os$  for  $M=10$  and  $\Omega=0.3$ . Curves are offset by 0.02.  $1\sigma$  error bars are less than the symbol size.

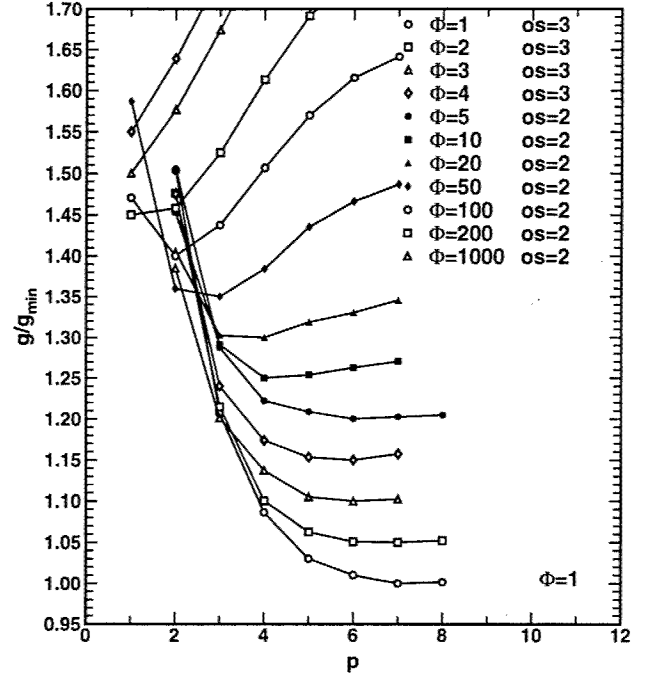


Figure 6. Performance vs. order  $p$  for  $M=10$  and  $\Omega=0.3$ . Curves are offset by 0.05.  $1\sigma$  error bars are less than the symbol size.

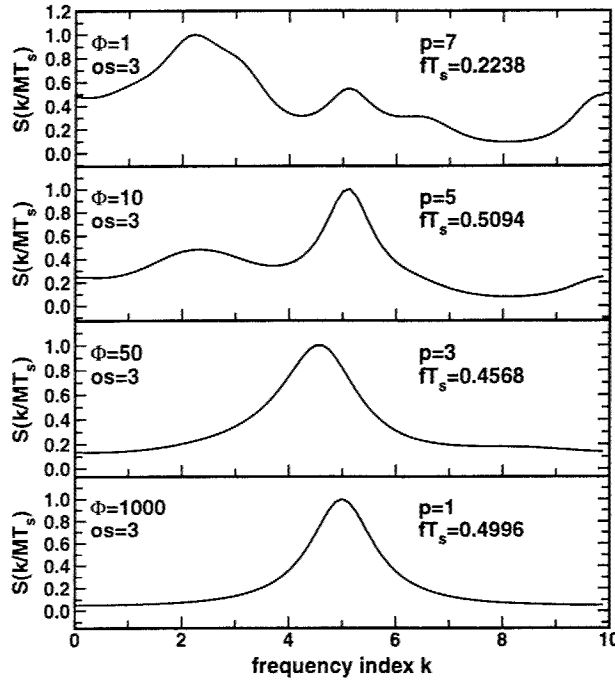


Figure 7. Single realizations of the CAPON spectral estimates for  $M = 10$  and  $\Omega=0.2$  for  $\Phi=1,10,50,1000$  with optimal estimator parameters as a function of frequency index  $k$ .

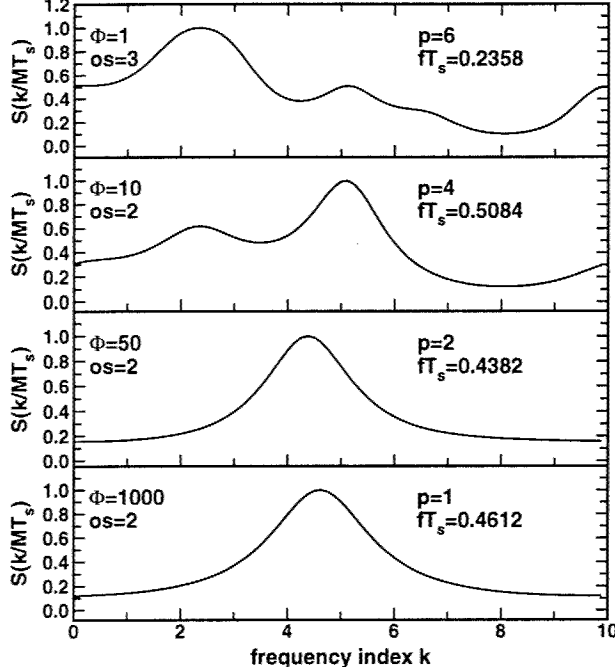


Figure 8. Single realizations of the CAPON spectral estimates for  $M=10$  and  $\Omega=0.3$  for  $\Phi=1,10,50,1000$  with optimal estimator parameters as a function of frequency index  $k$ .

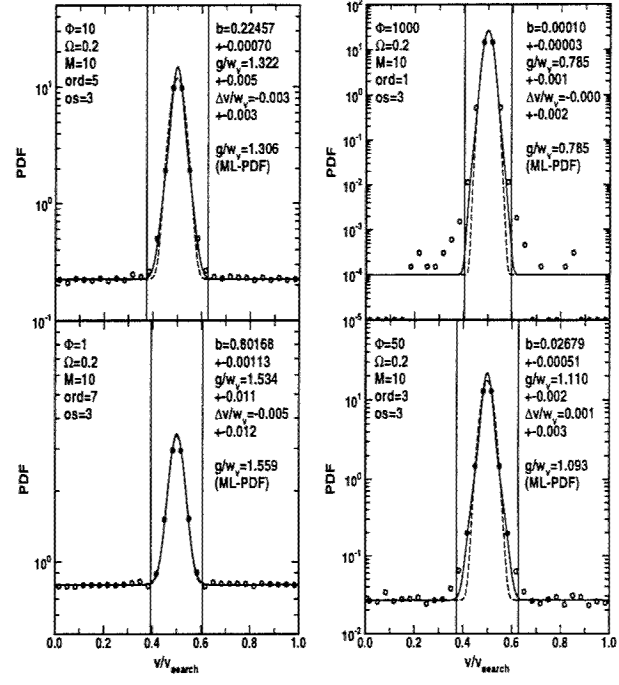


Figure 9. PDF of the Velocity Estimates using the CAPON estimator with  $M=10$  and  $\Omega=0.2$  for  $\Phi=1,10,50,1000$ .

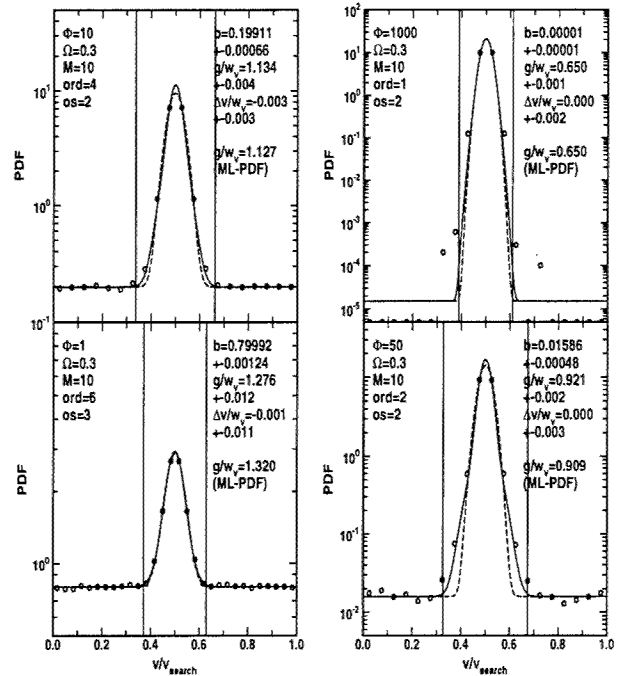
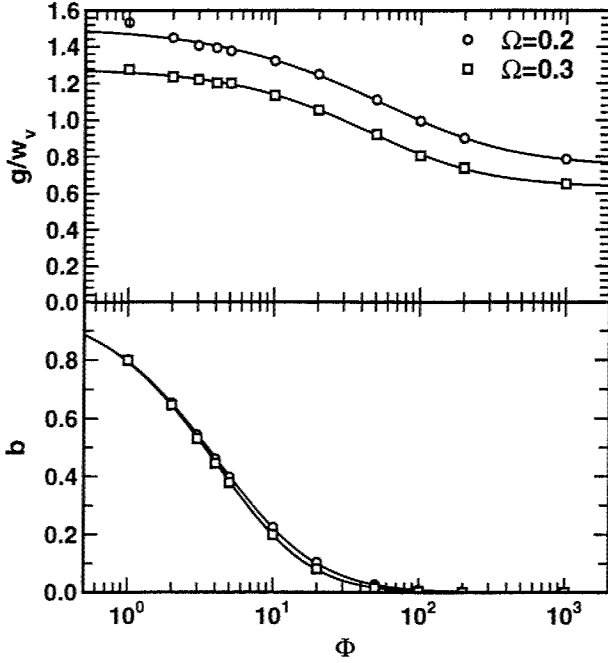
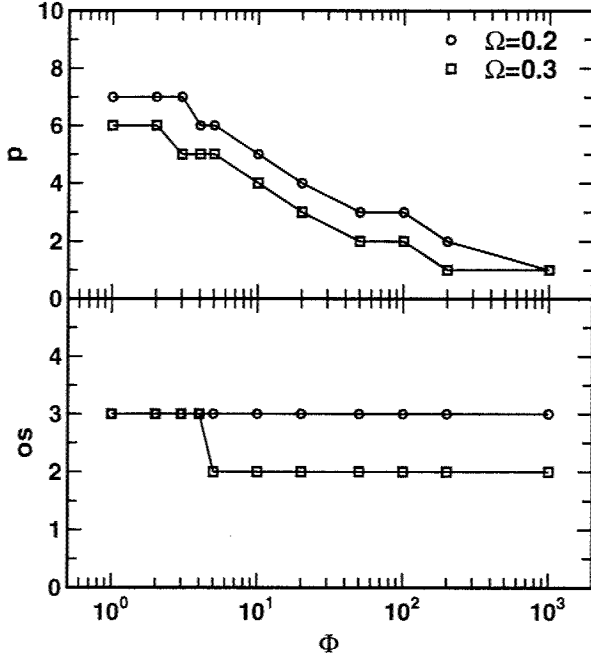


Figure 10. PDF of the Velocity Estimates using the CAPON estimator with  $M=10$  and  $\Omega=0.3$  for  $\Phi=1,10,50,1000$ .



**Figure 11.** Performance of the CAPON estimator with  $M=10$  and  $\Omega=0.2$  and  $0.3$  using optimal estimator parameters.  $1\sigma$  error bars are less than the symbol size. Best fit model is (-).



**Figure 12.** Optimal parameters with  $M=10$  and  $\Omega=0.2$  and  $0.3$ .

Reducing the order (from optimal) results in an increase in the standard deviation  $g$  of the good estimate. The minimum required estima-

tor order  $p$  with  $M=10$  and  $\Omega=0.2$  and  $0.3$  for no greater than 5% and 10% degradation (increase) in the standard deviation  $g$  of the good estimates are shown in Fig. 13.

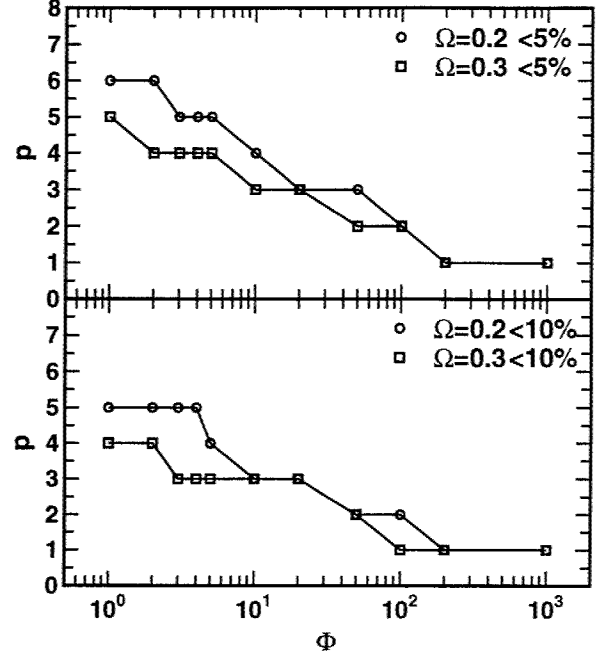


**Figure 13.** Minimum estimator order  $p$  with  $M=10$  and  $\Omega=0.2$  and  $0.3$  for no greater than 5% and 10% increase in the standard deviation  $g$  of the good estimates.

$\Omega$	%D	$b_0$	$\alpha$	$\gamma$	$\chi$
0.2	0.00	7.9381	.9796	1.8497	.7584
0.3	0.00	9.5469	.9885	2.2648	.6478
0.2	0.05	7.8439	.9846	1.8447	.7584
0.3	0.05	9.0815	.9974	2.2010	.6478
0.2	0.10	7.8968	.9850	1.8650	.7584
0.3	0.10	9.9245	.9827	2.3456	.6478
$\Omega$	%D	$g_0$	$\epsilon$	$\delta$	$\mu$
0.2	0.00	199.81	.6870	2.3680	.7554
0.3	0.00	77.824	.8576	1.5935	.6344
0.2	0.05	199.81	.6870	2.3680	.7554
0.3	0.05	77.824	.8576	1.5935	.6344
0.2	0.10	199.81	.6870	2.3680	.7554
0.3	0.10	77.824	.8576	1.5935	.6344

**Table 6.** Model Fit Parameters for  $M=10$ ,  $\Omega=0.2$  and  $0.3$ . Performance for the optimal and no more than 5% and 10% increase in the standard deviation  $g$  of the good estimates.

The performance curves are fitted to empirical models[10]. The parameters  $b$  and  $g/w_v$  are modeled as  $b(\Phi) = [1 + (\Phi/b_0)^\alpha]^{-\gamma}$  and  $g/w_v(\Phi) = \chi[1 + (\Phi/g_0)^\epsilon]^{-\delta} + \mu$  respectively. The parameters for optimal (% D=0) and degraded (% D=0.05 and % D=0.10) performance are listed in Table 6. Model fits are shown as the solid lines for every performance curve.

## 7 Results M=16

For this set, performance of the estimator will be evaluated for the  $\Omega=0.2, 0.3, 0.5, 1.0$  cases.

Performance vs. oversampling  $os$  is shown in Appendix A, Fig. A1 - A4. Performance vs. order  $p$  is shown in Appendix A, Fig. A5 - A8. Single realizations of the spectral estimates are shown in Appendix A, Fig. A9 - A12. The PDF's are shown in Appendix A, Fig. A13 - A16.

A summary of the performance for the  $M=16$  and  $\Omega=0.2, 0.3, 0.5$ , and 1.0 is shown in Fig. 14. A summary of the optimal order and oversampling is shown in Fig. 15.

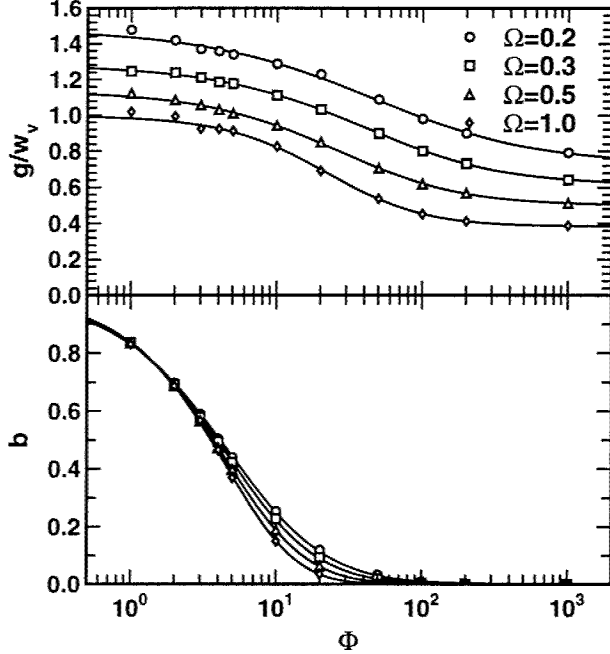


**Figure 14.** Performance of the CAPON estimator with  $M=16$  and  $\Omega=0.2, 0.3, 0.5$ , and 1.0 using optimal estimator parameters.  $1\sigma$  error bars are less than the symbol size.

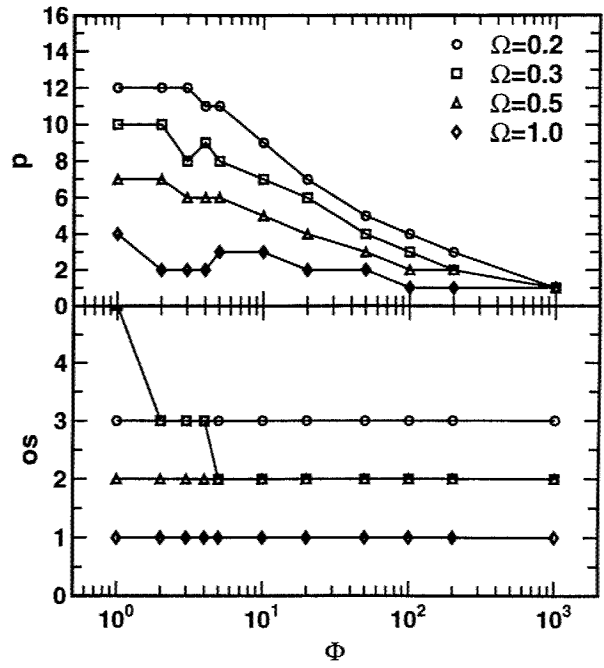


**Figure 15.** Optimal parameters with  $M=16$  and  $\Omega=0.2, 0.3, 0.5$ , and 1.0.

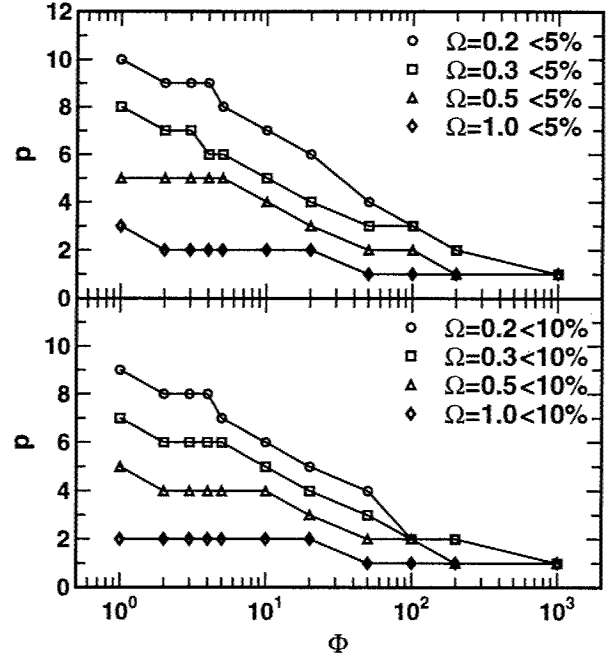


**Figure 16.** Minimum estimator order  $p$  with  $M=16$  and  $\Omega=0.2, 0.3, 0.5$ , and 1.0 for no greater than 5% and 10% increase in the standard deviation  $g$  of the good estimates.

The minimum required estimator order  $p$  with  $M=16$  and  $\Omega=0.2, 0.3, 0.5$  and  $1.0$  for no greater than 5% and 10% degradation (increase) in the standard deviation  $g$  of the good estimates are shown in Fig. 16.

The model parameters for optimal (% D=0) and degraded (% D=0.05 and % D=0.10) performance are listed in Table 7. Model fits are shown as the solid lines in Fig. 14.

$\Omega$	%D	$b_0$	$\alpha$	$\gamma$	$\chi$
0.2	0.00	8.2488	1.0338	1.7358	.7490
0.3	0.00	9.0784	1.0654	2.0114	.6659
0.5	0.00	10.759	1.0935	2.5561	.6362
1.0	0.00	15.860	1.1228	4.0381	.6143
0.2	0.05	7.7098	1.0484	1.6617	.7490
0.3	0.05	8.9319	1.0710	2.0077	.6659
0.5	0.05	11.164	1.0862	2.6444	.6362
1.0	0.05	23.727	1.0766	5.5904	.6143
0.2	0.10	7.6513	1.0457	1.6538	.7490
0.3	0.10	9.3928	1.0575	2.0820	.6659
0.5	0.10	10.879	1.0885	2.6020	.6362
1.0	0.10	24.253	1.0735	5.6868	.6143
$\Omega$	%D	$g_0$	$\epsilon$	$\delta$	$\mu$
0.2	0.00	67.5253	.7032	1.2938	.7337
0.3	0.00	59.6000	.8039	1.3699	.6164
0.5	0.00	35.7440	.8889	1.3207	.5004
1.0	0.00	25.8000	1.1844	1.2049	.3832
0.2	0.05	67.5253	.7032	1.2938	.7337
0.3	0.05	59.6000	.8039	1.3699	.6164
0.5	0.05	35.7440	.8889	1.3207	.5004
1.0	0.05	25.8000	1.1844	1.2049	.3832
0.2	0.10	67.5253	.7032	1.2938	.7337
0.3	0.10	59.6000	.8039	1.3699	.6164
0.5	0.10	35.7440	.8889	1.3207	.5004
1.0	0.10	25.8000	1.1844	1.2049	.3832

**Table 7.** Model Fit Parameters for  $M=16$ ,  $\Omega=0.2, 0.3, 0.5$  and  $1.0$ . Performance for the optimal (% D=0.0) and no more than 5% and 10% increase in the standard deviation  $g$  of the good estimates.

## 8 Results M=32

For this set, performance of the estimator will be evaluated for the  $\Omega=0.2, 0.3, 0.5, 1.0, 2.0$ , and  $3.0$  cases.

Performance vs. oversampling  $os$  is shown in Appendix B, Fig. B1 - B5. Performance vs. order  $p$  is shown in Appendix B, Fig. B6 - B10. Single realizations of the spectral estimates are shown in Appendix B, Fig. B11 - B15. The PDF's are shown in Appendix B, Fig. B16 - B20.

A summary of the performance for the  $M=32$  and  $\Omega=0.2, 0.3, 0.5, 1.0, 2.0$ , and  $3.0$  is shown in Fig. 17. A summary of the optimal order and oversampling is shown in Fig. 18.

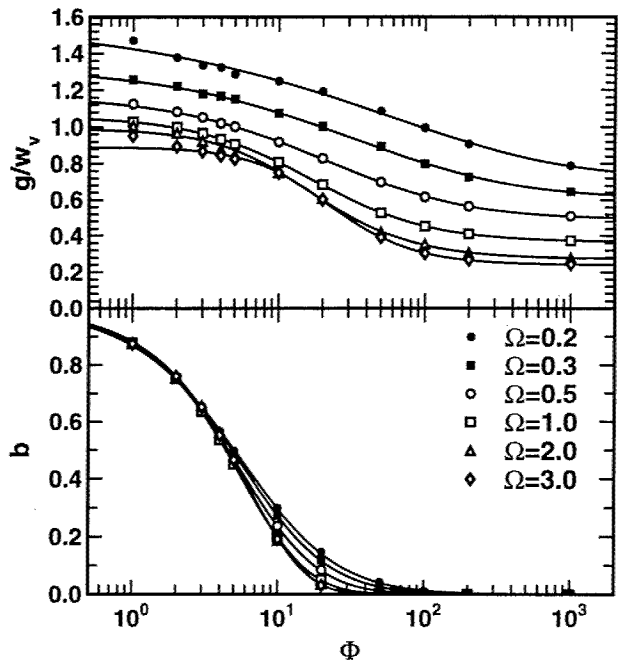


**Figure 17.** Performance of the CAPON estimator with  $M=32$  and  $\Omega=0.2, 0.3, 0.5, 1.0, 2.0$ , and  $3.0$  using optimal estimator parameters.  $1\sigma$  error bars are smaller than the symbol size.

The minimum required estimator order  $p$  with  $M=32$  and  $\Omega=0.2, 0.3, 0.5, 1.0, 2.0$ , and  $3.0$  for no greater than 5% and 10% degradation (increase) in the standard deviation  $g$  of the good estimates are shown in Fig. 19.

The model parameters for optimal (% D=0) and degraded (% D=0.05 and % D=0.10) performance are listed in Table 8. Model fits are the solid lines shown in Fig. 17.

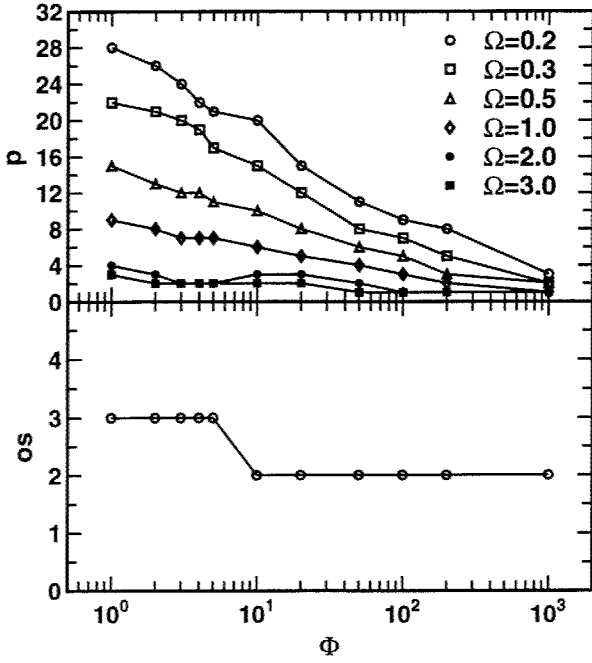


**Figure 18.** Optimal parameters with  $M=32$  and  $\Omega=0.2, 0.3, 0.5, 1.0, 2.0$ , and  $3.0$ . For  $\Omega \geq 1$ ,  $os=1$ . For  $\Omega = 0.2$  and  $0.5$ ,  $os=2$ .

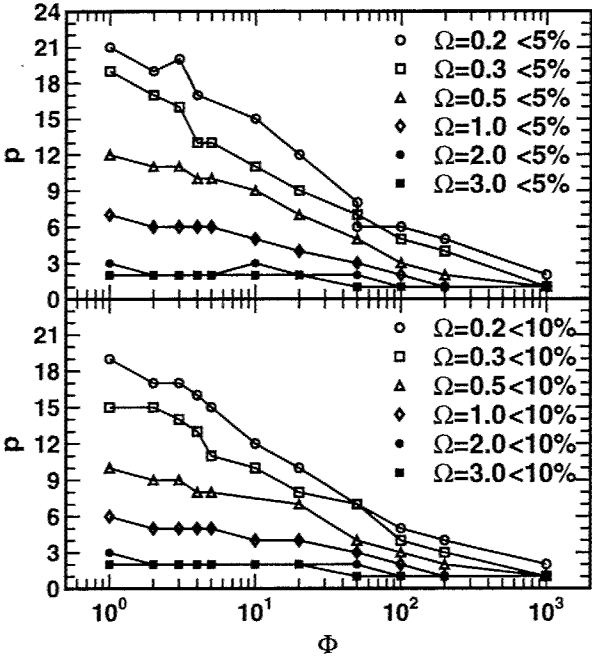


**Figure 19.** Minimum estimator order  $p$  with  $M=32$  and  $\Omega=0.2, 0.3, 0.5, 1.0, 2.0$  and  $3.0$  for no greater than 5% and 10% increase in the standard deviation  $g$  of the good estimates.

$\Omega$	%D	$b_0$	$\alpha$	$\gamma$	$\chi$
0.2	0.00	8.5182	1.0979	1.5455	.8411
0.3	0.00	9.2911	1.1373	1.7642	.7203
0.5	0.00	11.488	1.1614	2.3403	.6790
1.0	0.00	17.461	1.1849	3.8698	.6920
2.0	0.00	53.837	1.1454	12.015	.7178
3.0	0.00	106.39	1.1311	24.643	.6506
0.2	0.05	8.3578	1.1038	1.5246	.8411
0.3	0.05	8.9662	1.1434	1.7283	.7203
0.5	0.05	11.832	1.1541	2.4022	.6790
1.0	0.05	18.075	1.1784	4.0029	.6920
2.0	0.05	44.794	1.1657	10.196	.7178
3.0	0.05	127.13	1.1245	29.445	.6506
0.2	0.10	8.2038	1.1109	1.5136	.8411
0.3	0.10	9.0809	1.1380	1.7453	.7203
0.5	0.10	11.940	1.1494	2.4213	.6790
1.0	0.10	18.239	1.1746	4.0351	.6920
2.0	0.10	44.427	1.1664	10.121	.7178
3.0	0.10	127.18	1.1245	29.4586	.6506
$\Omega$	%D	$g_0$	$\epsilon$	$\delta$	$\mu$
0.2	0.00	14890.4	.4027	9.3678	.7309
0.3	0.00	84.4809	.6048	1.7585	.6077
0.5	0.00	33.8113	.7727	1.3989	.4927
1.0	0.00	18.544	1.0551	1.0714	.3664
2.0	0.00	14.1141	1.3774	.8169	.2729
3.0	0.00	18.6496	1.6891	.7894	.2385
0.2	0.05	14890.4	.4027	9.3678	.7309
0.3	0.05	84.4809	.6048	1.7585	.6077
0.5	0.05	33.8113	.7727	1.3989	.4927
1.0	0.05	18.544	1.0551	1.0714	.3664
2.0	0.05	14.1141	1.3774	.8169	.2729
3.0	0.05	18.6496	1.6891	.7894	.2385
0.2	0.10	14890.4	.4027	9.3678	.7309
0.3	0.10	84.4809	.6048	1.7585	.6077
0.5	0.10	33.8113	.7727	1.3989	.4927
1.0	0.10	18.544	1.0551	1.0714	.3664
2.0	0.10	14.1141	1.3774	.8169	.2729
3.0	0.10	18.6496	1.6891	.7894	.2385

**Table 8.** Model Fit Parameters for  $M=32$ ,  $\Omega=0.2, 0.3, 0.5, 1.0, 2.0$ , and  $3.0$ . Performance for the optimal (%D=0.0) and no more than 5% and 10% increase in the standard deviation  $g$  of the good estimates.

## 9 Results M=64

For this set, performance of the estimator will be evaluated for the  $\Omega=0.3, 0.5, 1.0, 2.0$ , and  $3.0$  cases.

Performance vs. oversampling  $os$  is shown in Appendix C, Fig. C1 - C5. Performance vs. order  $p$  is shown in Appendix C, Fig. C6 - C10. Single realizations of the spectral estimates are shown in Appendix C, Fig. C11 - C15. The PDF's are shown in Appendix C, Fig. C16 - C20.

A summary of the performance for the  $M=64$  and  $\Omega=0.3, 0.5, 1.0, 2.0$ , and  $3.0$  is shown in Fig. 20. A summary of the optimal order and oversampling is shown in Fig. 21.

The minimum required estimator order  $p$  with  $M=64$  and  $\Omega=0.3, 0.5, 1.0, 2.0$ , and  $3.0$  for no greater than 5% and 10% degradation (increase) in the standard deviation  $g$  of the good estimates are shown in Fig. 22.

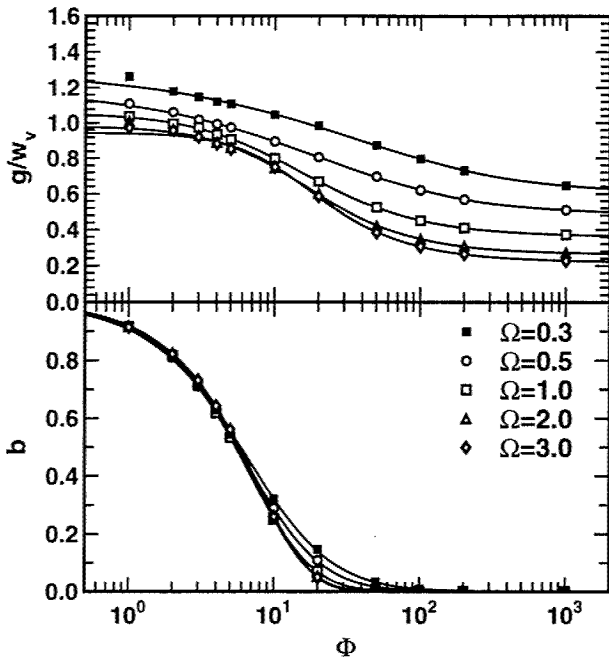


**Figure 20.** Performance of the CAPON estimator with  $M=64$  and  $\Omega=0.3, 0.5, 1.0, 2.0$ , and  $3.0$  using optimal estimator parameters.  $1\sigma$  error bars are smaller than the symbol size.

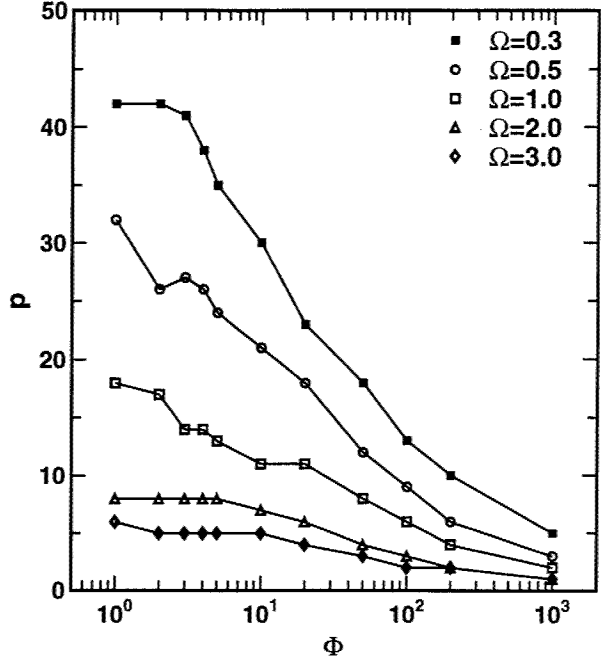


**Figure 21.** Optimal parameters with  $M=64$  and  $\Omega=0.3, 0.5, 1.0, 2.0$ , and  $3.0$ . For  $\Omega \geq 1$ ,  $os=1$ . For  $\Omega=0.3$  and  $0.5$ ,  $os=2$ .

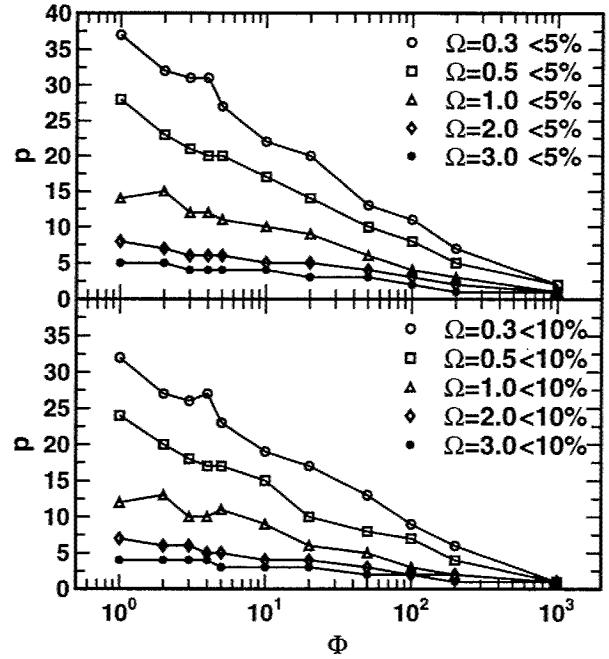


**Figure 22.** Minimum estimator order  $p$  with  $M=64$  and  $\Omega=0.3, 0.5, 1.0, 2.0$  and  $3.0$  for no greater than 5% and 10% increase in the standard deviation  $g$  of the good estimates.

The model parameters for optimal (% D=0) and degraded (% D=0.05 and % D=0.10) perfor-

mance are listed in Table 9. Model fits are the solid lines shown in Fig. 20.

$\Omega$	%D	$b_0$	$\alpha$	$\gamma$	$\chi$
0.3	0.00	10.2501	1.2046	1.6675	.6839
0.5	0.00	11.5370	1.2611	2.0474	.7069
1.0	0.00	16.9486	1.2893	3.3184	.6997
2.0	0.00	40.5676	1.2496	8.5421	.7208
3.0	0.00	146.179	1.2057	34.370	.7258
0.3	0.05	9.6026	1.2183	1.5856	.6839
0.5	0.05	11.5969	1.2543	2.0654	.7069
1.0	0.05	17.3629	1.2801	3.3904	.6997
2.0	0.05	41.8824	1.2443	8.8181	.7208
3.0	0.05	124.096	1.2052	28.291	.7258
0.3	0.10	9.3103	1.2252	1.5481	.6839
0.5	0.10	11.8990	1.2413	2.1025	.7069
1.0	0.10	17.0985	1.2775	3.3235	.6997
2.0	0.10	46.1708	1.2318	9.6375	.7208
3.0	0.10	531.599	1.1839	145.576	.7258
$\Omega$	%D	$g_0$	$\epsilon$	$\delta$	$\mu$
0.3	0.00	143.728	.5585	2.1787	.6095
0.5	0.00	40.6733	.6417	1.6238	.4871
1.0	0.00	11.8538	1.1825	.7792	.3593
2.0	0.00	12.3691	1.3978	.7169	.2625
3.0	0.00	11.9501	1.7884	.5551	.2183
0.3	0.05	143.728	.5585	2.1787	.6095
0.5	0.05	40.6733	.6417	1.6238	.4871
1.0	0.05	11.8538	1.1825	.7792	.3593
2.0	0.05	12.3691	1.3978	.7169	.2625
3.0	0.05	11.9501	1.7884	.5551	.2183
0.3	0.10	143.728	.5585	2.1787	.6095
0.5	0.10	40.6733	.6417	1.6238	.4871
1.0	0.10	11.8538	1.1825	.7792	.3593
2.0	0.10	12.3691	1.3978	.7169	.2625
3.0	0.10	11.9501	1.7884	.5551	.2183

**Table 9.** Model Fit Parameters for  $M=64$ ,  $\Omega=0.3, 0.5, 1.0, 2.0$ , and  $3.0$ . Performance for the optimal (no more than 5% and 10% increase in the standard deviation  $g$  of the good estimates.

## 10 Results M=128

For this set, performance of the estimator will be evaluated for the  $\Omega=0.5, 1.0, 2.0, 3.0$ , and  $7.0$  cases.

Performance vs. oversampling  $os$  is shown in Appendix D, Fig. D1 - D5. Performance vs. or-

der  $p$  is shown in Appendix D, Fig. D6 - D10. Single realizations of the spectral estimates are shown in Appendix D, Fig. D11 - D15. The PDF's are shown in Appendix D, Fig. D16 - D20.

A summary of the performance for the  $M=128$  and  $\Omega=0.3, 0.5, 1.0, 2.0$ , and  $3.0$  is shown in Fig. 23. A summary of the optimal order and oversampling is shown in Fig. 24.

The minimum required estimator order  $p$  with  $M=128$  and  $\Omega=0.3, 0.5, 1.0, 2.0$ , and  $3.0$  for no greater than 5% and 10% degradation (increase) in the standard deviation  $g$  of the good estimates are shown in Fig. 25.

The model parameters for optimal (% D=0) and degraded (% D=0.05 and % D=0.10) performance are listed in Table 10. Model fits are the solid lines shown in Fig. 23.

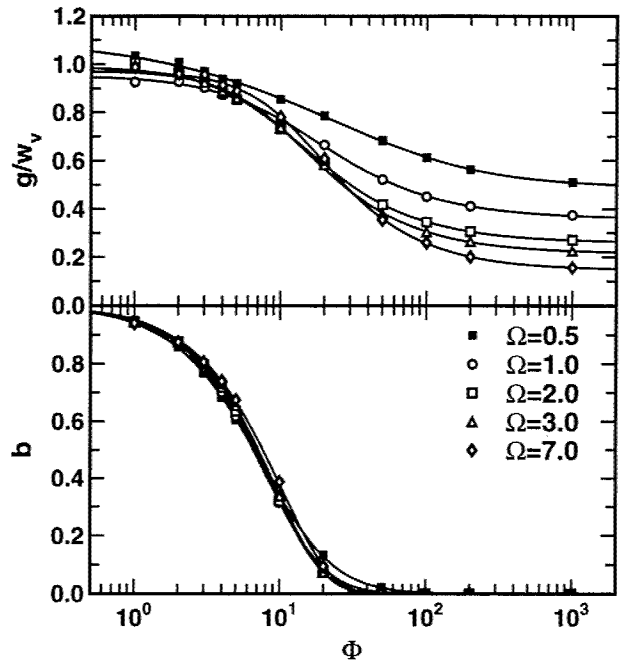


**Figure 23.** Performance of the CAPON estimator with  $M=128$  and  $\Omega=0.5, 1.0, 2.0, 3.0$ , and  $7.0$  using optimal estimator parameters.  $1\sigma$  error bars are smaller than the symbol size.

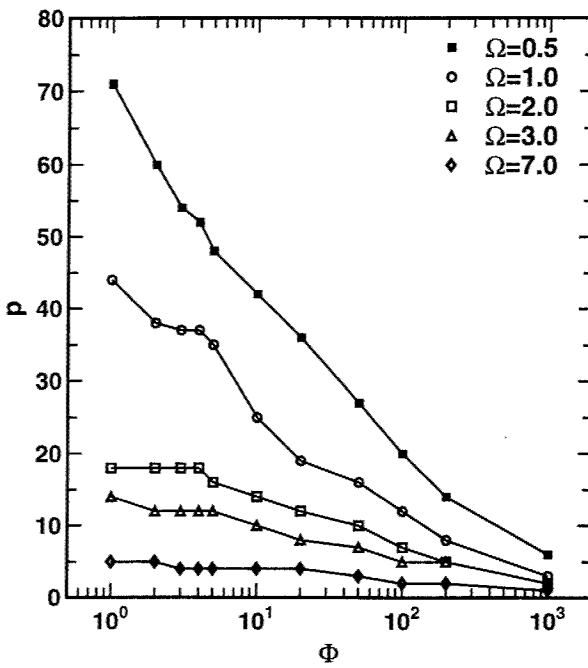


**Figure 24.** Optimal parameters with  $M=128$  and  $\Omega=0.5, 1.0, 2.0, 3.0$ , and  $7.0$ . For  $\Omega \geq 1$ ,  $os=1$ . For  $\Omega=0.5$ ,  $os=2$ .

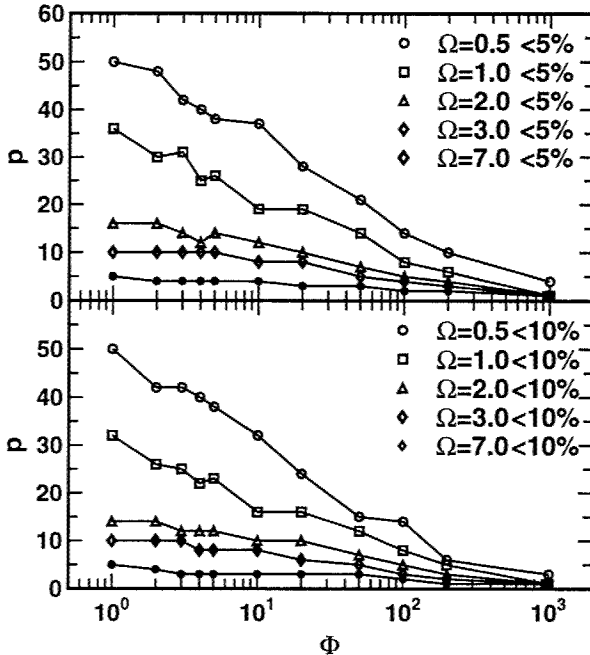


**Figure 25.** Minimum estimator order  $p$  with  $M=128$  and  $\Omega=0.5, 1.0, 2.0, 3.0$  and  $7.0$  for no greater than 5% and 10 % increase in the standard deviation  $g$  of the good estimates.

$\Omega$	%D	$b_0$	$\alpha$	$\gamma$	$\chi$
0.5	0.00	12.0831	1.3615	1.8761	.6101
1.0	0.00	16.4936	1.4240	2.8733	.5936
2.0	0.00	34.3710	1.3789	6.6881	.7308
3.0	0.00	67.3247	1.3519	14.6471	.7593
7.0	0.00	886.873	1.2707	289.570	.8251
0.5	0.05	11.8024	1.3638	1.8380	.6101
1.0	0.05	16.3219	1.4124	2.8298	.5936
2.0	0.05	37.2563	1.3622	7.2806	.7308
3.0	0.05	54.9006	1.3507	11.3052	.7593
7.0	0.05	1039.27	1.2678	349.622	.8251
0.5	0.10	11.5259	1.3682	1.7958	.6101
1.0	0.10	17.0047	1.3956	2.9235	.5936
2.0	0.10	39.6903	1.3543	7.7813	.7308
3.0	0.10	53.1581	1.3455	10.7559	.7593
7.0	0.10	1026.83	1.2704	348.030	.8251
$\Omega$	%D	$g_0$	$\epsilon$	$\delta$	$\mu$
0.5	0.00	59.1149	.6417	1.8396	.4927
1.0	0.00	13.2728	1.2783	.6908	.3590
2.0	0.00	10.5849	1.4301	.6542	.2598
3.0	0.00	10.5032	1.6436	.5669	.2142
7.0	0.00	13.4402	1.7921	.5521	.1449
0.5	0.05	59.1149	.6417	1.8396	.4927
1.0	0.05	13.2728	1.2783	.6908	.3590
2.0	0.05	10.5849	1.4301	.6542	.2598
3.0	0.05	10.5032	1.6436	.5669	.2142
7.0	0.05	13.4402	1.7921	.5521	.1449
0.5	0.10	59.1149	.6417	1.8396	.4927
1.0	0.10	13.2728	1.2783	.6908	.3590
2.0	0.10	10.5849	1.4301	.6542	.2598
3.0	0.10	10.5032	1.6436	.5669	.2142
7.0	0.10	13.4402	1.7921	.5521	.1449

**Table 10.** Model Fit Parameters for  $M=128$ ,  $\Omega=0.5, 1.0, 2.0, 3.0$ , and  $7.0$ . Performance for the optimal (%D=0.0) and no more than 5% and 10% increase in the standard deviation  $g$  of the good estimates.

## 11 Results M=512

For this set, performance of the estimator will be evaluated for the  $\Omega=7.0$  and  $10.0$  cases.

Performance vs. order  $p$  is shown in Appendix E, Fig. E1 - E2. Single realizations of the spectral estimates are shown in Appendix E, Fig. E3 - E4. The PDF's are shown in Appendix E, Fig. E5 - E6.

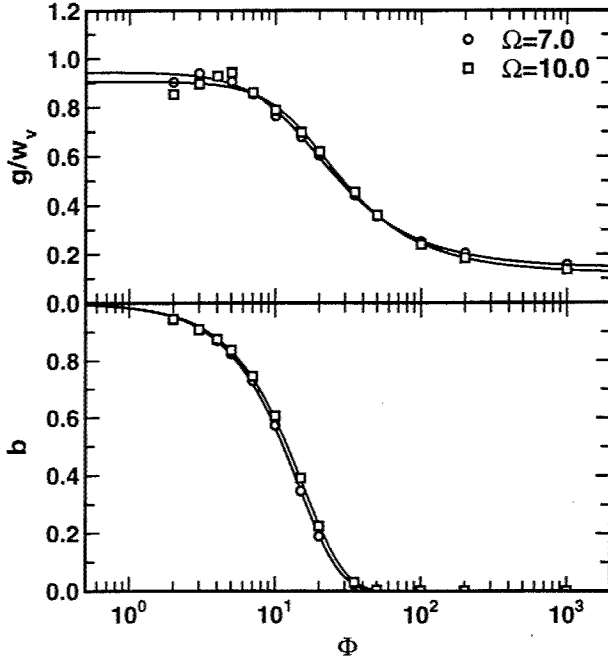


**Figure 26.** Performance of the CAPON estimator with  $M=512$  and  $\Omega=7.0$  and  $10.0$  using optimal estimator parameters.  $1\sigma$  error bars are smaller than the symbol size.

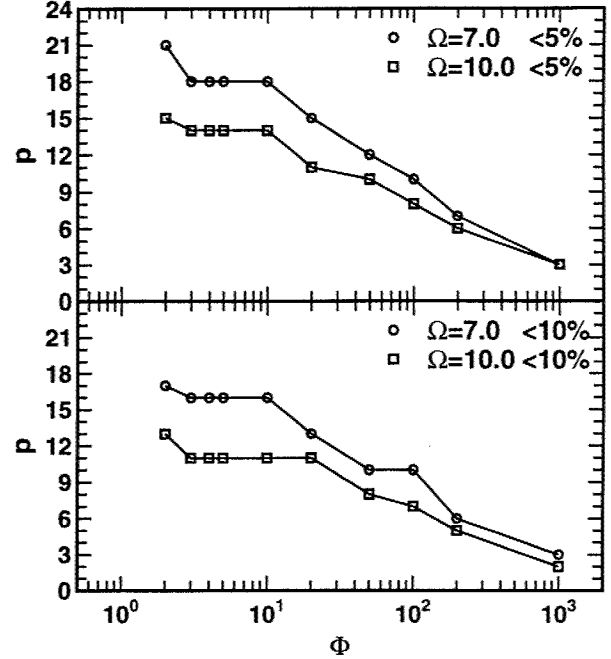


**Figure 28.** Minimum estimator order  $p$  with  $M=512$  and  $\Omega=7.0$  and  $10.0$  for no greater than 5 and 10 % increase in the standard deviation of the good estimates  $g$ .

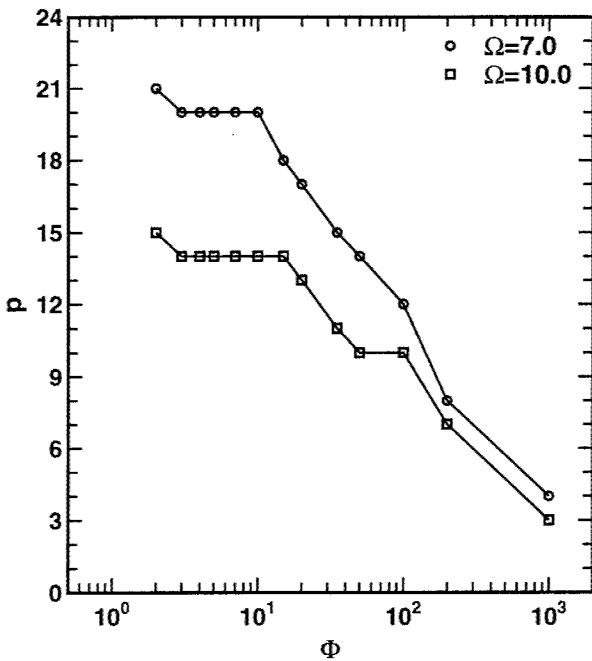


**Figure 27.** Optimal parameters with  $M=512$  and  $\Omega=7.0$  and  $10.0$ . For  $\Omega \geq 7$ ,  $os=1$ .

$\Omega$	%D	$b_0$	$\alpha$	$\gamma$	$\chi$
7.0	0.00	885.17	1.5233	526.17	.8025
10.0	0.00	1188.4	1.5060	687.78	.7857
7.0	0.05	918.63	1.4978	502.95	.8025
10.0	0.05	1350.2	1.4970	812.28	.7857
7.0	0.10	870.84	1.4904	447.34	.8025
10.0	0.10	1000.8	1.4840	492.19	.7857
$\Omega$	%D	$g_0$	$\epsilon$	$\delta$	$\mu$
7.0	0.00	12.9353	2.0414	.4662	.1428
10.0	0.00	14.7845	2.3502	.4090	.1206
7.0	0.05	12.9353	2.0414	.4662	.1428
10.0	0.05	14.7845	2.3502	.4090	.1206
7.0	0.10	12.9353	2.0414	.4662	.1428
10.0	0.10	14.7845	2.3502	.4090	.1206

**Table 11.** Model Fit Parameters for  $M=512$ ,  $\Omega=7.0$  and  $10.0$ . Performance for the optimal (%D=0.0) and no more than 5% and 10% increase in the standard deviation  $g$  of the good estimates.

A summary of the performance for the  $M=512$  and  $\Omega=7.0$  and  $10.0$  is shown in Fig. 26. A summary of the optimal order and oversampling is shown in Fig. 27.

The minimum required estimator order  $p$  with

$M=512$  and  $\Omega=7.0$  and  $10.0$  for no greater than 5% and 10% degradation (increase) in the standard deviation  $g$  of the good estimates are shown in Fig. 28.

The model parameters for optimal (% D=0) and degraded (% D=0.05 and % D=0.10) performance are listed in Table 11. Model fits are the solid lines shown in Fig. 26.

## 12 Acknowledgements

The authors acknowledge useful discussions with Michael Kavaya, Garry Spiers, and Barry Rye. This work was supported by the National Aeronautics and Space Administration, Marshall Space Flight Center under Research Grants NAG8-253 and NGT-51206 (Michael J. Kavaya, Technical Officer).

## Appendix A, $M=16$

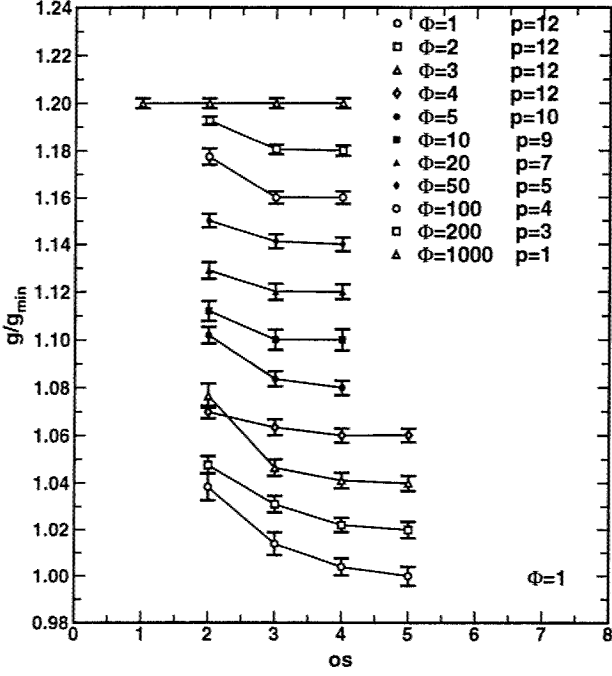


Figure A1. Performance vs. oversampling  $os$  for  $M = 16$  and  $\Omega=0.2$ . Curves are offset by 0.05. ( $1\sigma$  error bars).

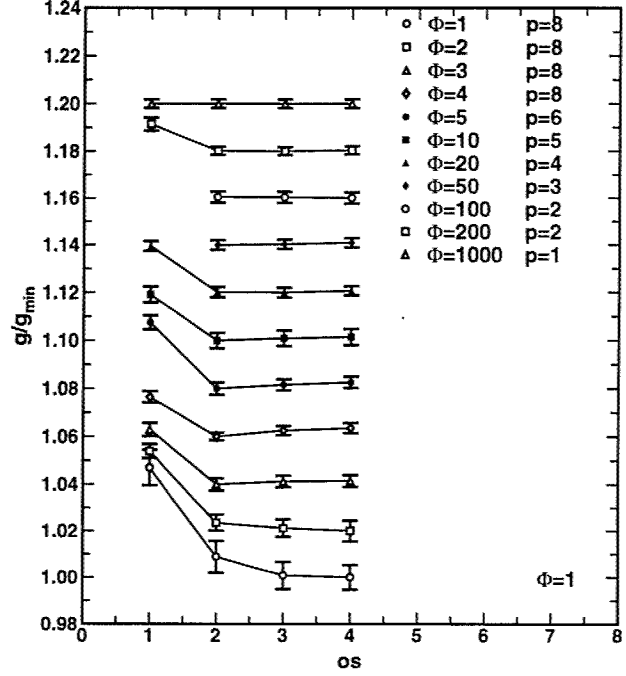


Figure A3. Performance vs. oversampling  $os$  for  $M = 16$  and  $\Omega=0.5$ . Curves are offset by 0.05. ( $1\sigma$  error bars).

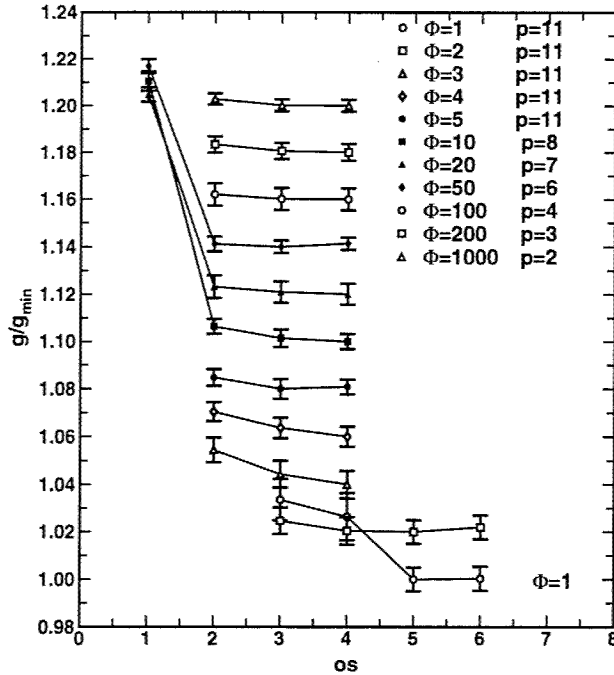


Figure A2. Performance vs. oversampling  $os$  for  $M = 16$  and  $\Omega=0.3$ . Curves are offset by 0.05. ( $1\sigma$  error bars).

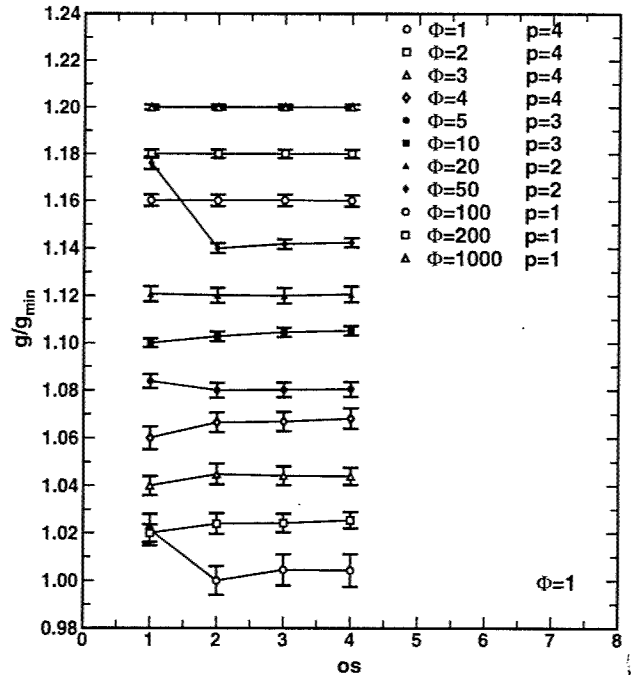


Figure A4. Performance vs. oversampling  $os$  for  $M = 16$  and  $\Omega=1.0$ . Curves are offset by 0.05. ( $1\sigma$  error bars).

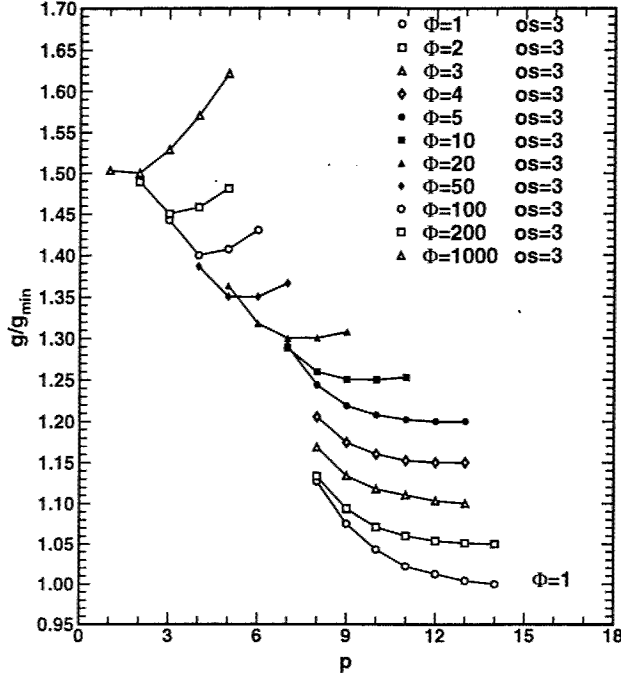


Figure A5. Performance vs. order  $p$  for  $M = 16$  and  $\Omega=0.2$ . Curves are offset by 0.05.  $1\sigma$  error bars are smaller than the symbol size.

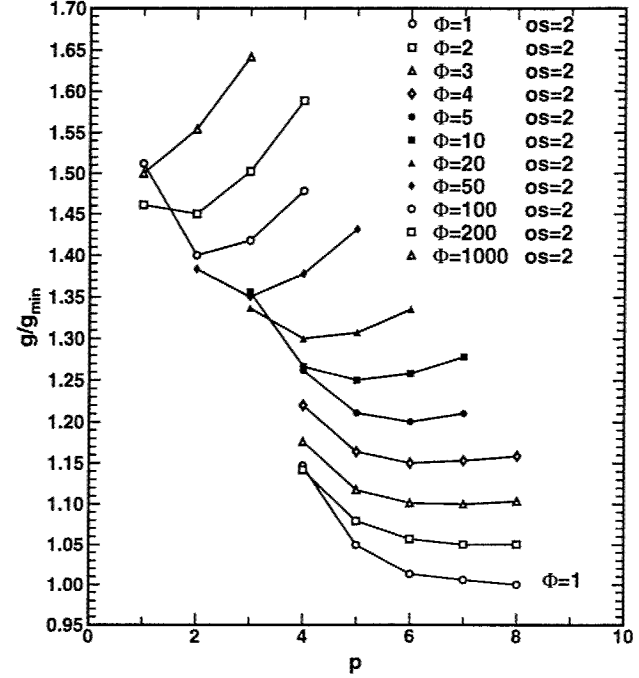


Figure A7. Performance vs. order  $p$  for  $M = 16$  and  $\Omega=0.5$ . Curves are offset by 0.05.  $1\sigma$  error bars are smaller than the symbol size.

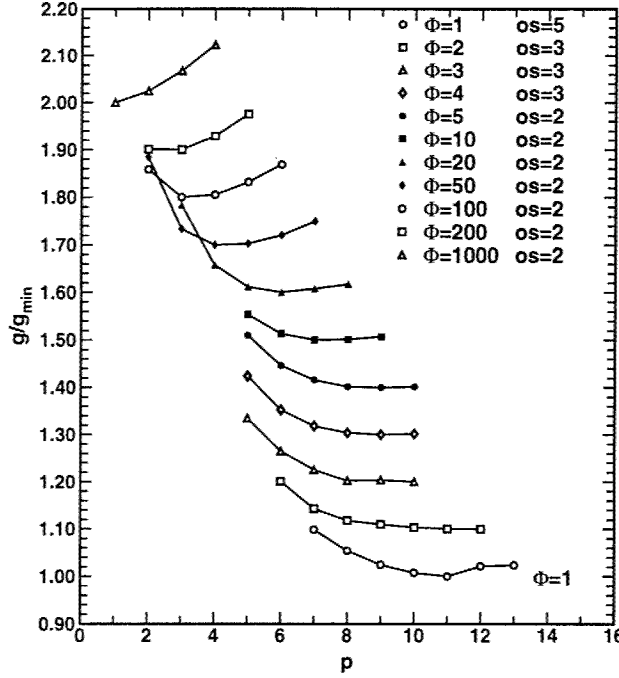


Figure A6. Performance vs. order  $p$  for  $M = 16$  and  $\Omega=0.3$ . Curves are offset by 0.05.  $1\sigma$  error bars are smaller than the symbol size.

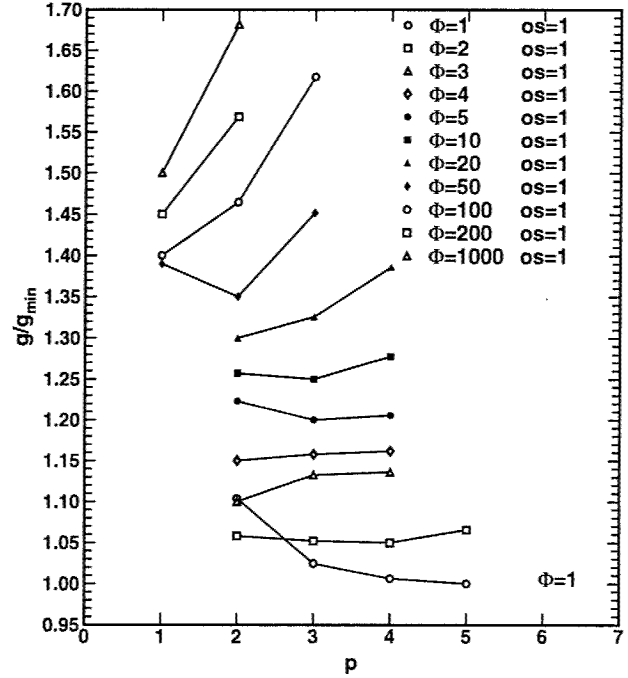


Figure A8. Performance vs. order  $p$  for  $M = 16$  and  $\Omega=1.0$ . Curves are offset by 0.05.  $1\sigma$  error bars are smaller than the symbol size.

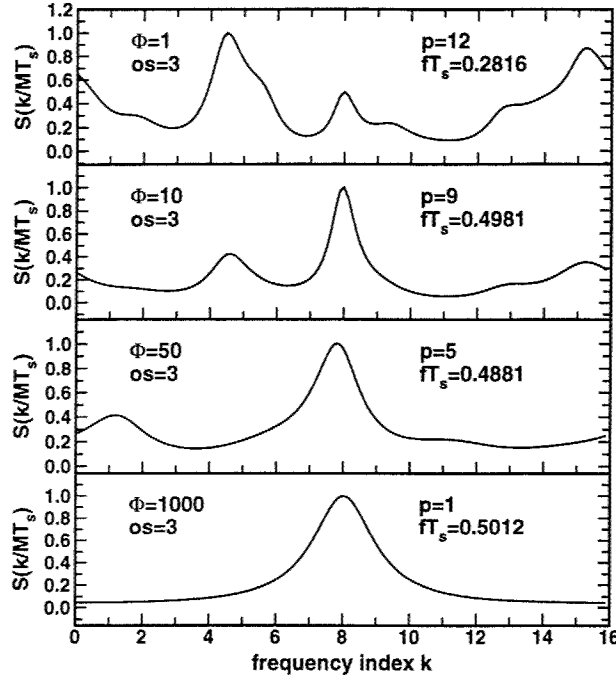


Figure A9. Single realizations of the CAPON spectral estimates for  $M=16$  and  $\Omega=0.2$  for  $\Phi=1,10,50,1000$  with optimal estimator parameters as a function of frequency index  $k$ .

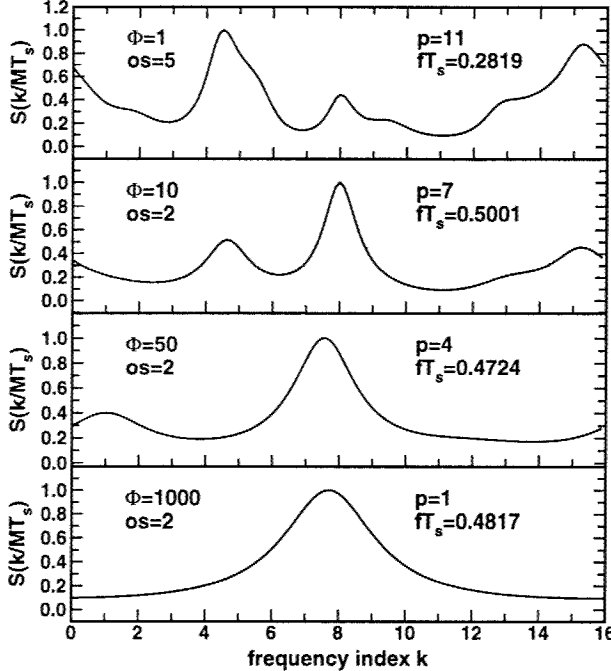


Figure A10. Single realizations of the CAPON spectral estimates for  $M=16$  and  $\Omega=0.3$  for  $\Phi=1,10,50,1000$  with optimal estimator parameters as a function of frequency index  $k$ .

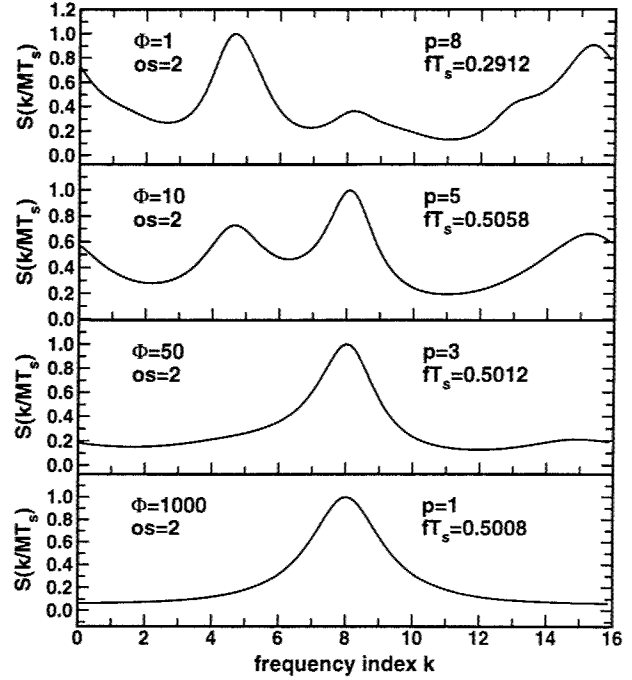


Figure A11. Single realizations of the CAPON spectral estimates for  $M=16$  and  $\Omega=0.5$  for  $\Phi=1,10,50,1000$  with optimal estimator parameters as a function of frequency index  $k$ .

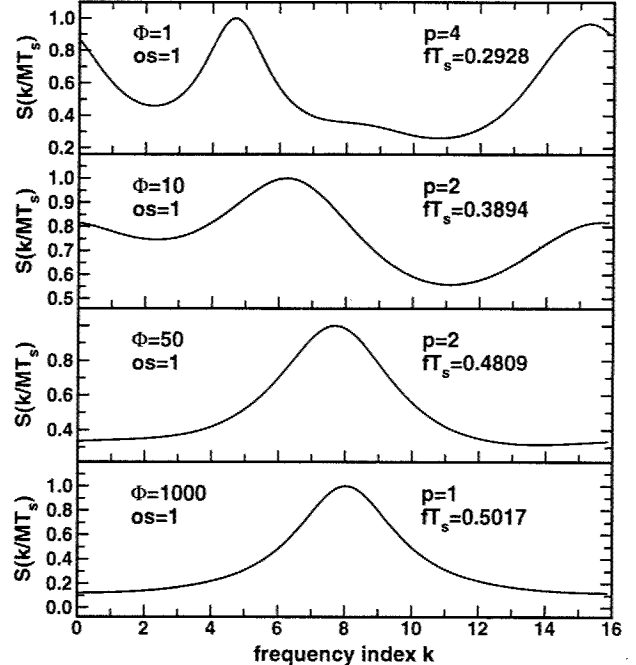
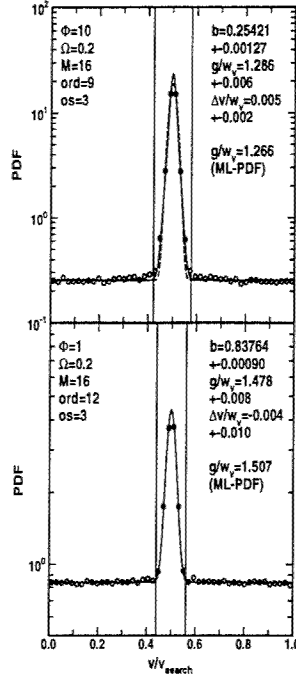
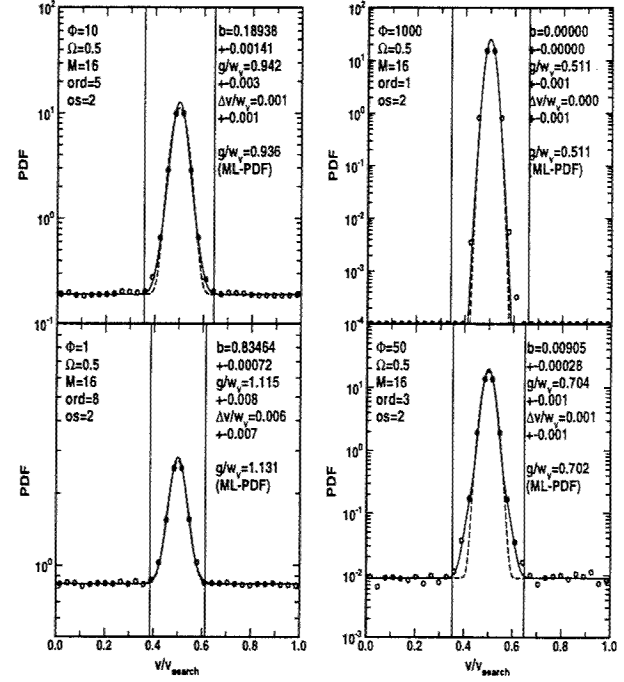
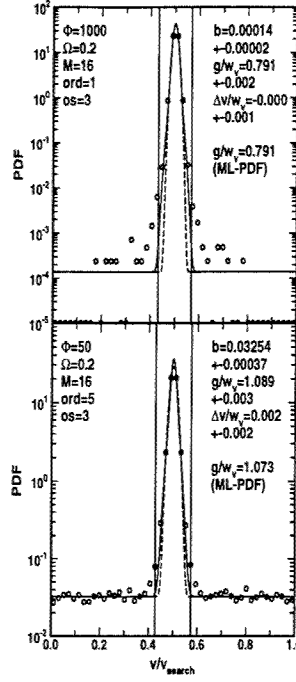


Figure A12. Single realizations of the CAPON spectral estimates for  $M=16$  and  $\Omega=1.0$  for  $\Phi=1,10,50,1000$  with optimal estimator parameters as a function of frequency index  $k$ .



**Figure A13.** PDF of the Velocity Estimates using the CAPON estimator with  $M=16$  and  $\Omega=0.2$  for  $\Phi=1,10,50,1000$ .



**Figure A15.** PDF of the Velocity Estimates using the CAPON estimator with  $M=16$  and  $\Omega=0.5$  for  $\Phi=1,10,50,1000$ .

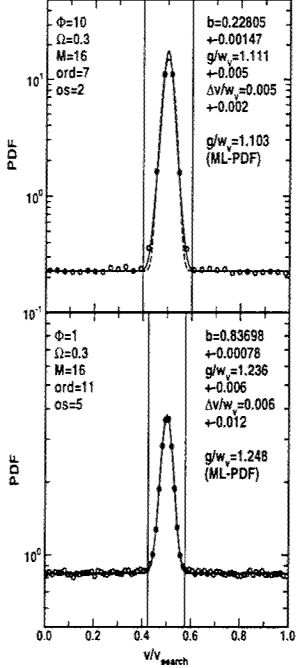


**Figure A14.** PDF of the Velocity Estimates using the CAPON estimator with  $M=16$  and  $\Omega=0.3$  for  $\Phi=1,10,50,1000$ .

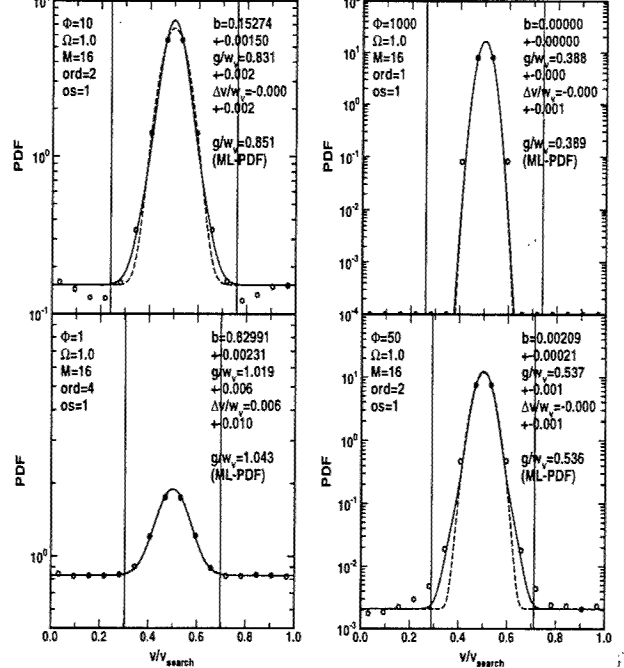
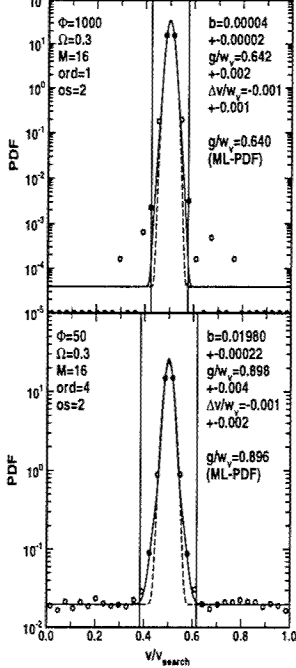


**Figure A16.** PDF of the Velocity Estimates using the CAPON estimator with  $M=16$  and  $\Omega=1.0$  for  $\Phi=1,10,50,1000$ .

## Appendix B, M=32

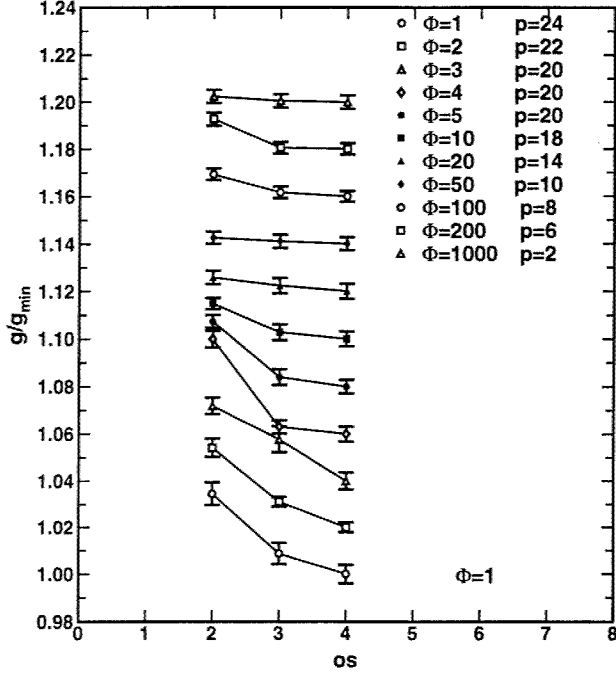


Figure B1. Performance vs. oversampling  $os$  for  $M=32$  and  $\Omega=0.2$ . Curves are offset by 0.05. ( $1\sigma$  error bars).

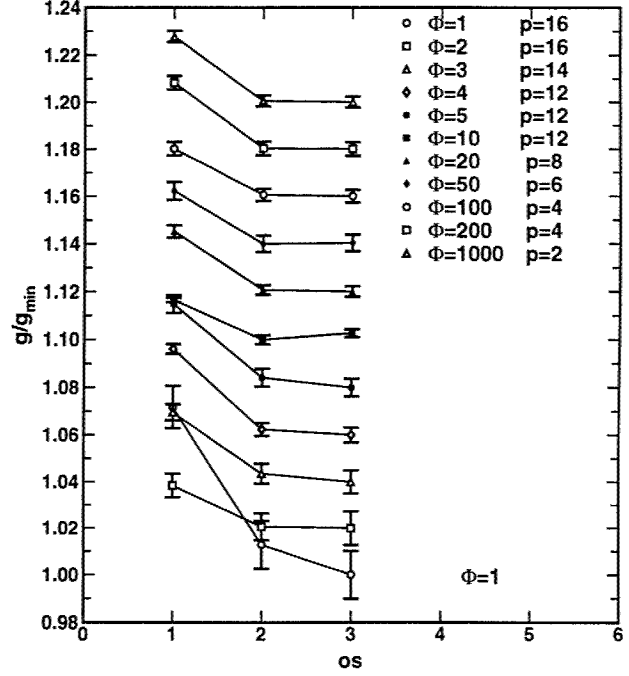


Figure B3. Performance vs. oversampling  $os$  for  $M=32$  and  $\Omega=0.5$ . Curves are offset by 0.05. ( $1\sigma$  error bars).

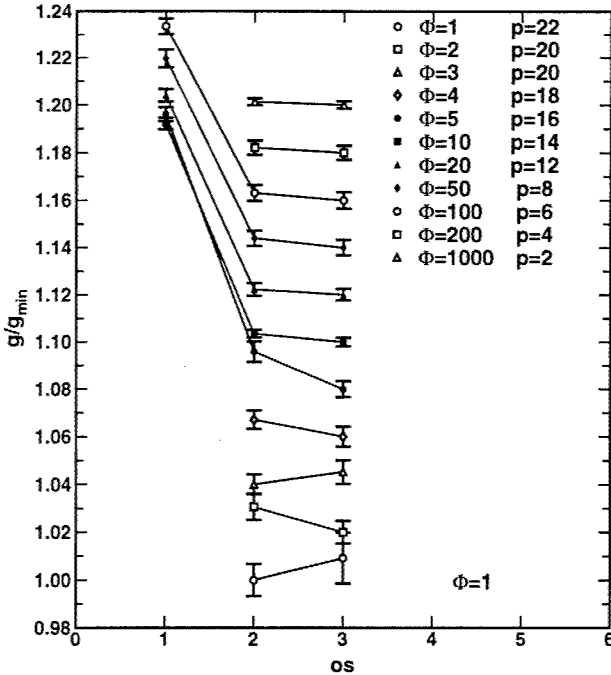


Figure B2. Performance vs. oversampling  $os$  for  $M=32$  and  $\Omega=0.3$ . Curves are offset by 0.05. ( $1\sigma$  error bars).

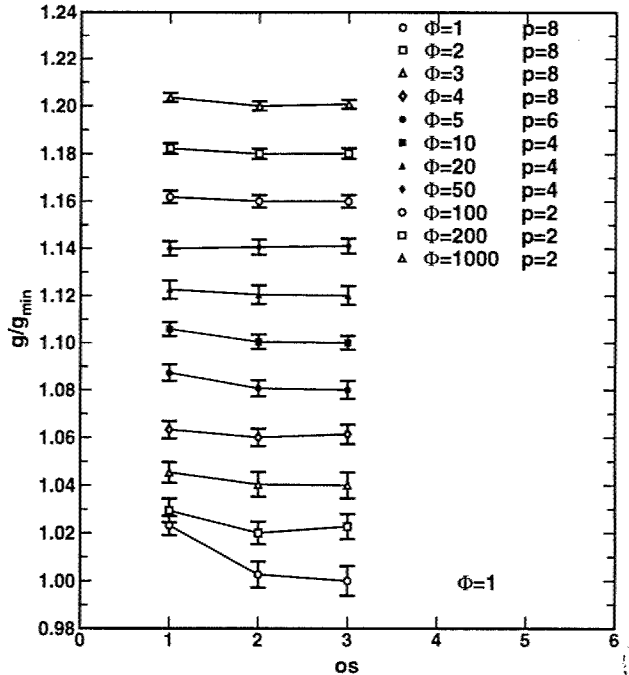
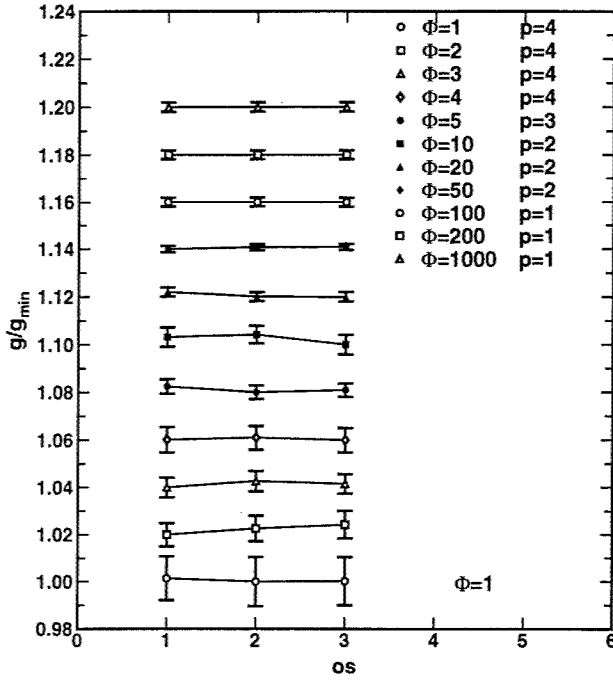
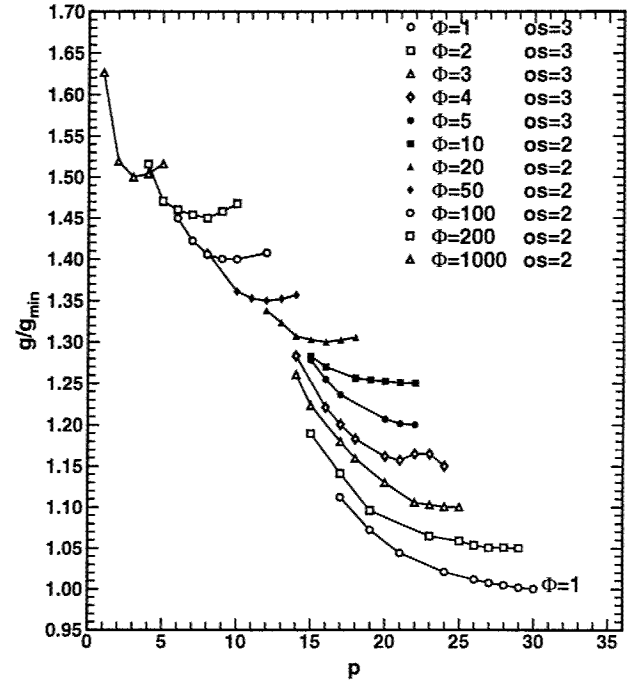


Figure B4. Performance vs. oversampling  $os$  for  $M=32$  and  $\Omega=1.0$ . Curves are offset by 0.05. ( $1\sigma$  error bars).



**Figure B5.** Performance vs. oversampling  $os$  for  $M=32$  and  $\Omega=2.0$ . Curves are offset by 0.05. ( $1\sigma$  error bars).



**Figure B7.** Performance vs. order  $p$  for  $M=32$  and  $\Omega=0.2$ . Curves are offset by 0.05.  $1\sigma$  error bars are less than the symbol size.

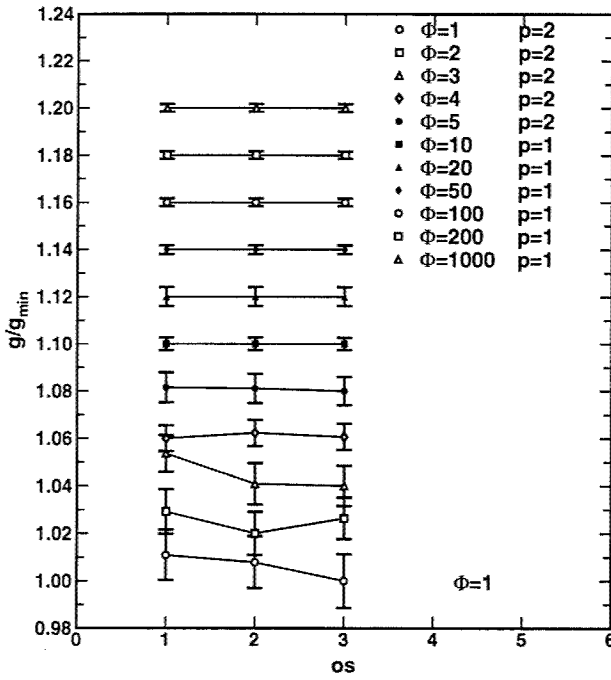


**Figure B6.** Performance vs. oversampling  $os$  for  $M=32$  and  $\Omega=3.0$ . Curves are offset by 0.05. ( $1\sigma$  error bars).

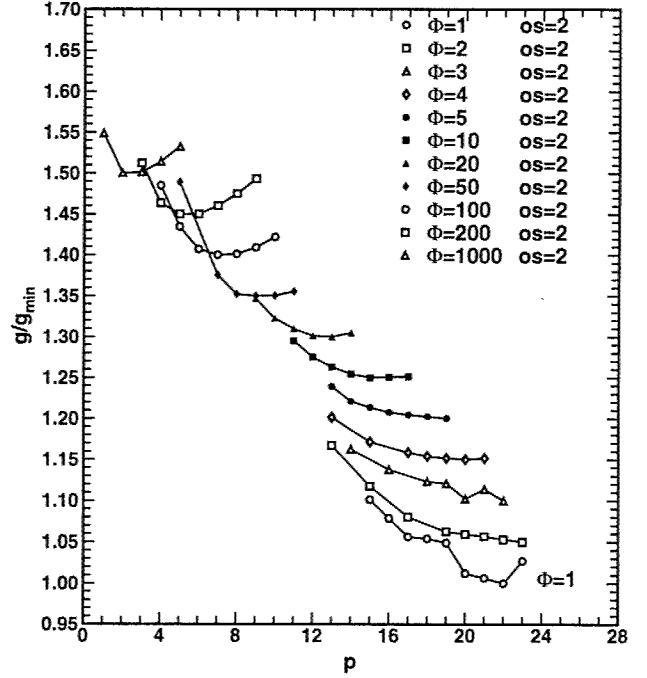


**Figure B8.** Performance vs. order  $p$  for  $M=32$  and  $\Omega=0.3$ . Curves are offset by 0.05.  $1\sigma$  error bars are less than the symbol size.

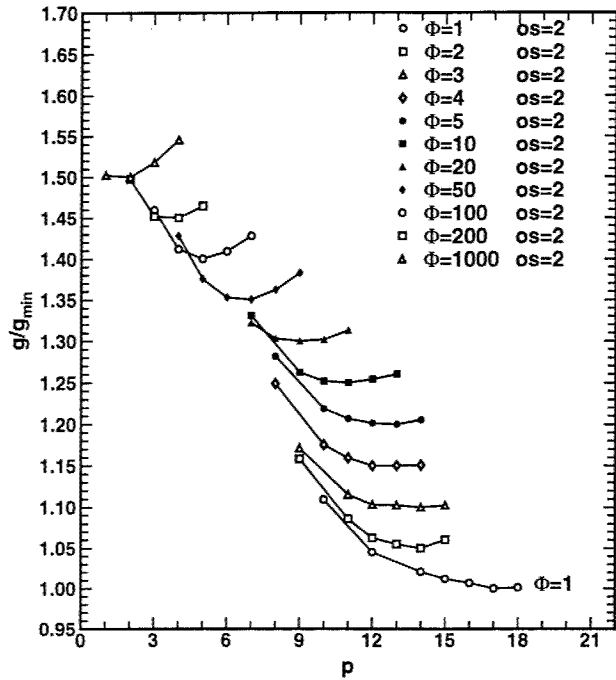


**Figure B9.** Performance vs. order  $p$  for  $M=32$  and  $\Omega=0.5$ . Curves are offset by 0.05.  $1\sigma$  error bars are less than the symbol size.

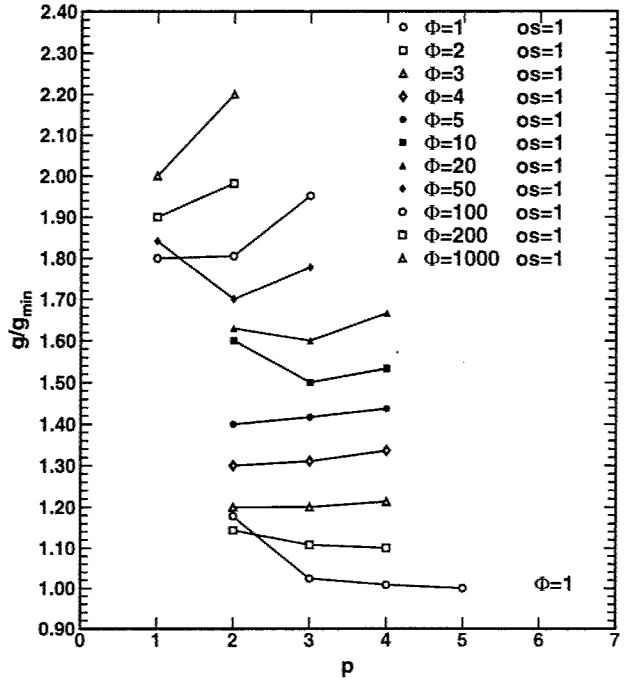


**Figure B11.** Performance vs. order  $p$  for  $M=32$  and  $\Omega=2.0$ . Curves are offset by 0.10.  $1\sigma$  error bars are less than the symbol size.

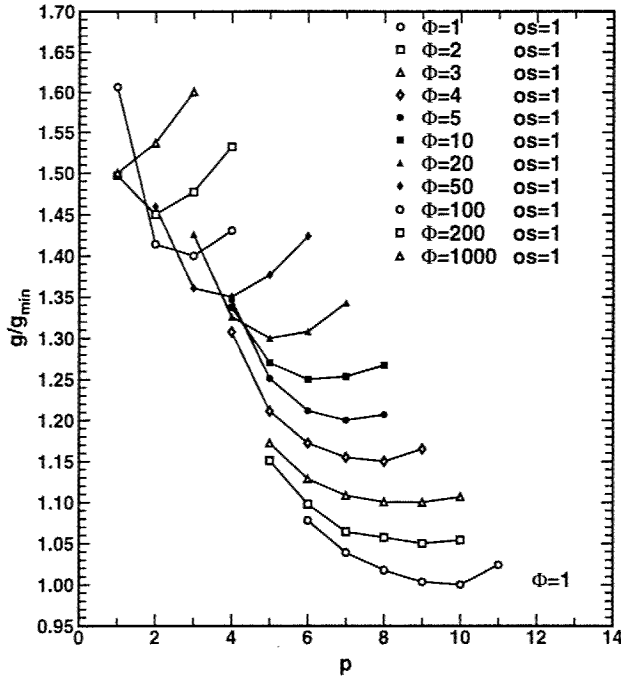


**Figure B10.** Performance vs. order  $p$  for  $M=32$  and  $\Omega=1.0$ . Curves are offset by 0.05.  $1\sigma$  error bars are less than the symbol size.

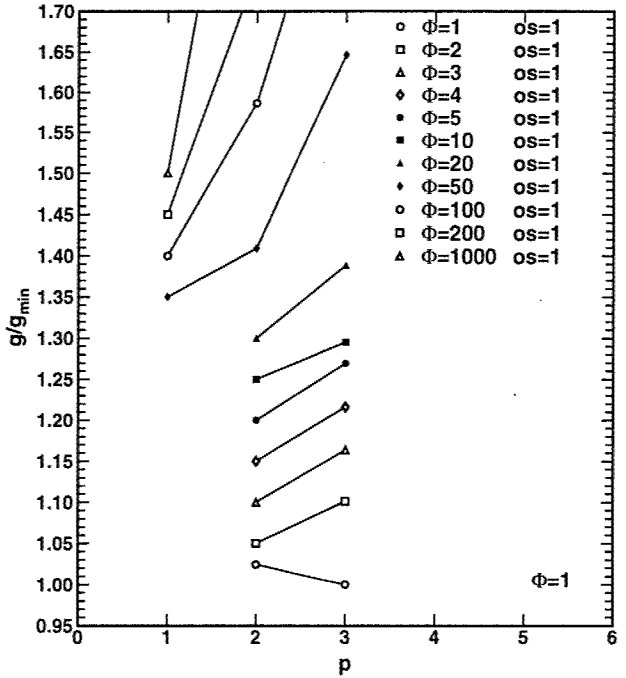


**Figure B12.** Performance vs. order  $p$  for  $M=32$  and  $\Omega=3.0$ . Curves are offset by 0.10.  $1\sigma$  error bars are less than the symbol size.

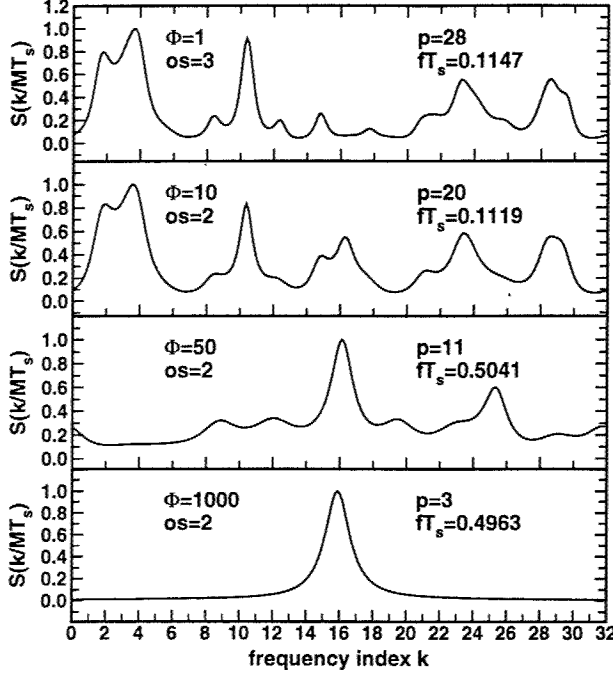


**Figure B13.** Single realizations of the CAPON spectral estimates for  $M=32$  and  $\Omega=0.2$  for  $\Phi=1, 10, 50, 1000$  with optimal estimator parameters as a function of frequency index  $k$ .

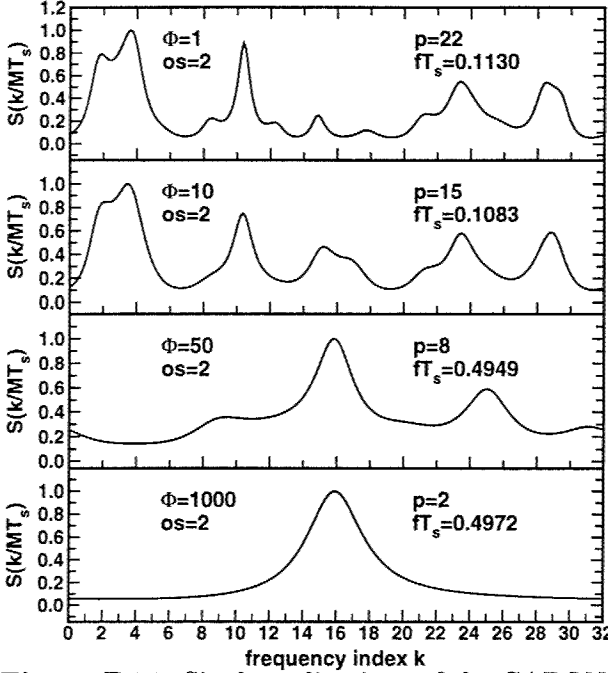


**Figure B14.** Single realizations of the CAPON spectral estimates for  $M=32$  and  $\Omega=0.3$  for  $\Phi=1, 10, 50, 1000$  with optimal estimator parameters as a function of frequency index  $k$ .

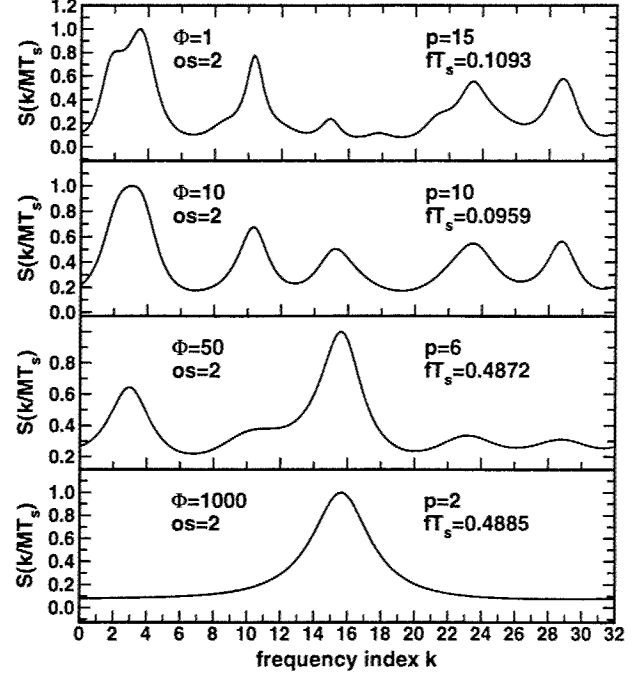


**Figure B15.** Single realizations of the CAPON spectral estimates for  $M=32$  and  $\Omega=0.5$  for  $\Phi=1, 10, 50, 1000$  with optimal estimator parameters as a function of frequency index  $k$ .

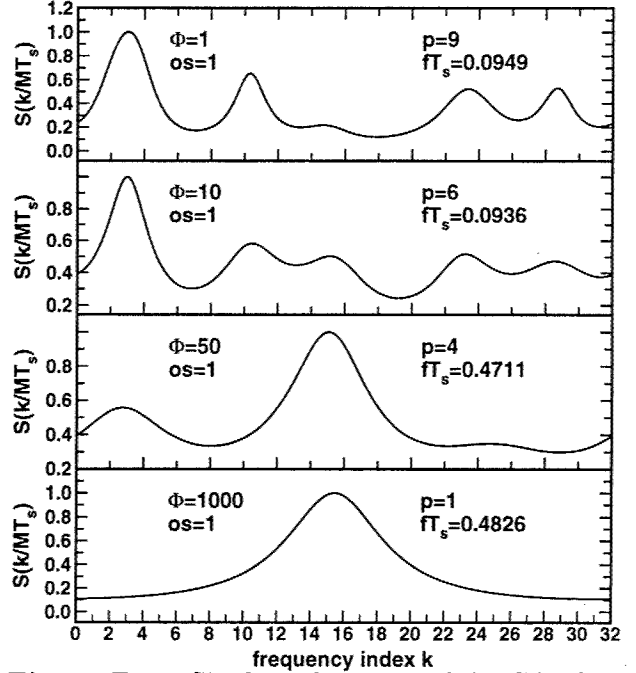


**Figure B16.** Single realizations of the CAPON spectral estimates for  $M=32$  and  $\Omega=1.0$  for  $\Phi=1, 10, 50, 1000$  with optimal estimator parameters as a function of frequency index  $k$ .

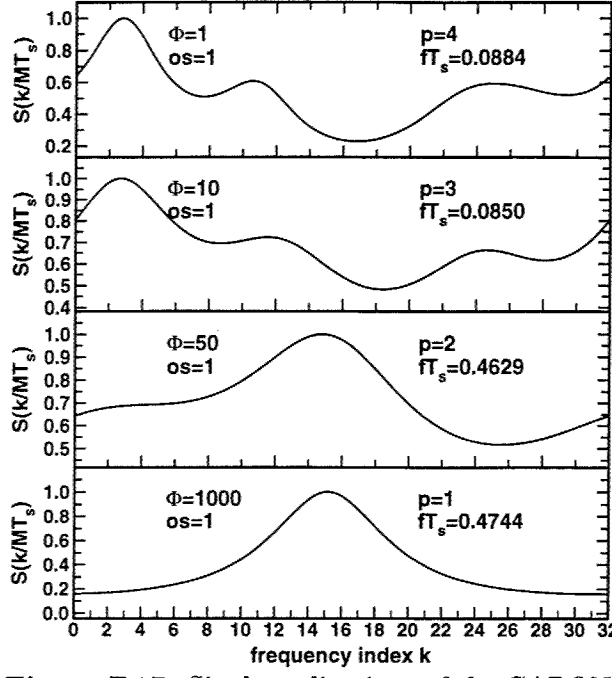


**Figure B17.** Single realizations of the CAPON spectral estimates for  $M=32$  and  $\Omega=2.0$  for  $\Phi=1, 10, 50, 1000$  with optimal estimator parameters as a function of frequency index  $k$ .

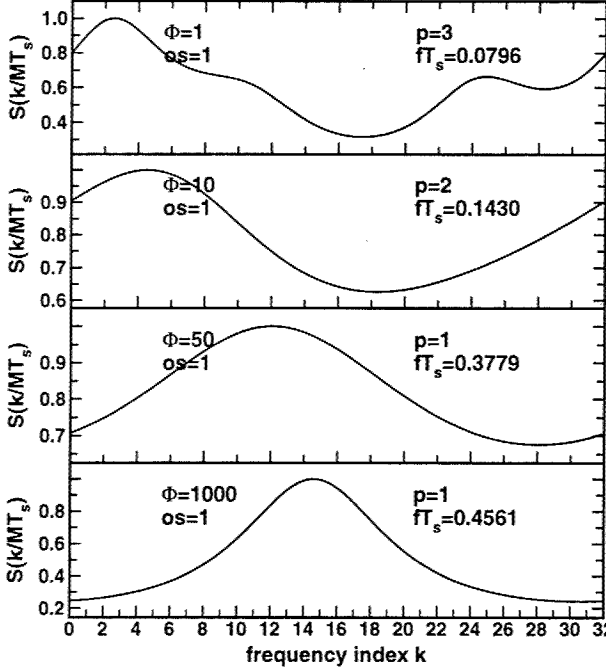


**Figure B18.** Single realizations of the CAPON spectral estimates for  $M=32$  and  $\Omega=3.0$  for  $\Phi=1, 10, 50, 1000$  with optimal estimator parameters as a function of frequency index  $k$ .

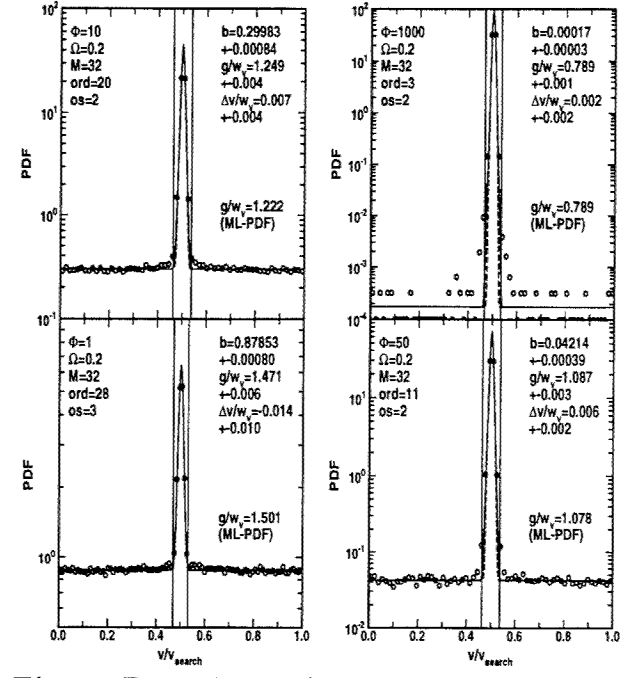


**Figure B19.** PDF of the Velocity Estimates using the CAPON estimator with  $M=32$  and  $\Omega=0.2$  for  $\Phi=1, 10, 50, 1000$ .

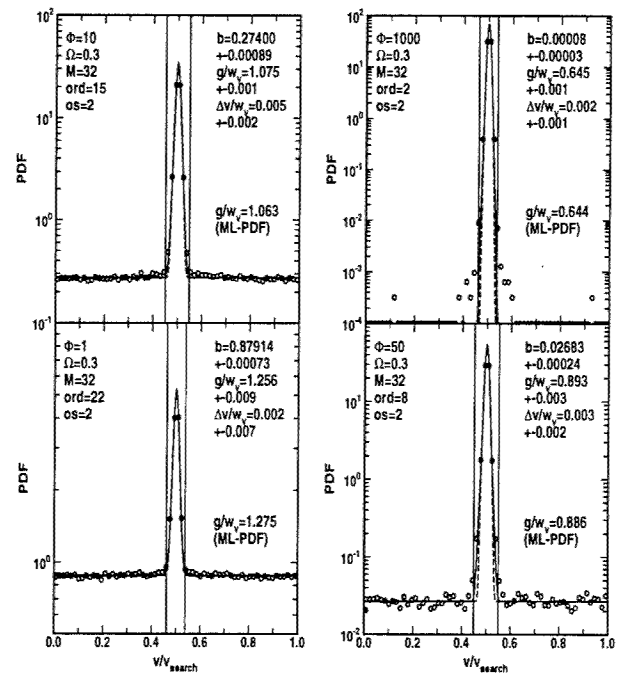


**Figure B20.** PDF of the Velocity Estimates using the CAPON estimator with  $M=32$  and  $\Omega=0.3$  for  $\Phi=1, 10, 50, 1000$ .

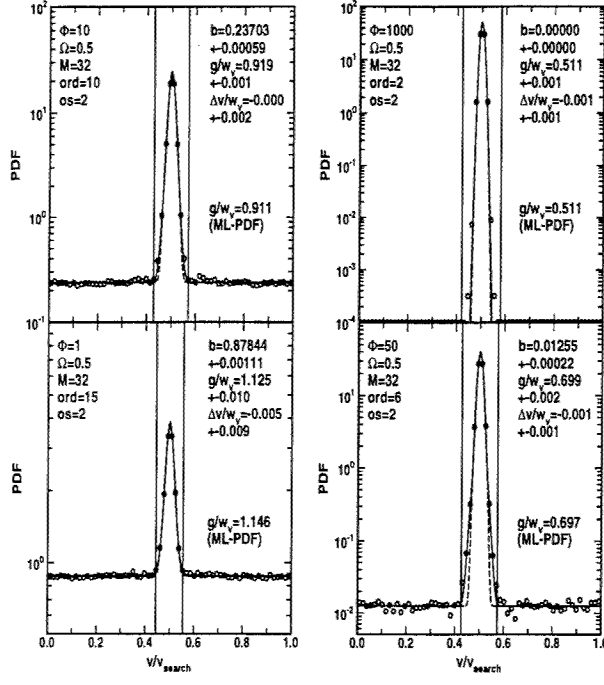


**Figure B21.** PDF of the Velocity Estimates using the CAPON estimator with  $M=32$  and  $\Omega=0.5$  for  $\Phi=1,10,50,1000$ .

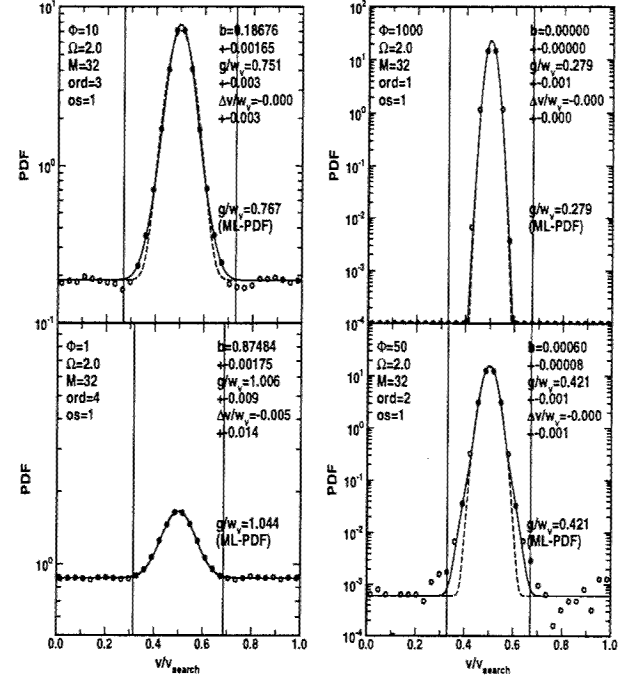


**Figure B23.** PDF of the Velocity Estimates using the CAPON estimator with  $M=32$  and  $\Omega=2.0$  for  $\Phi=1,10,50,1000$ .

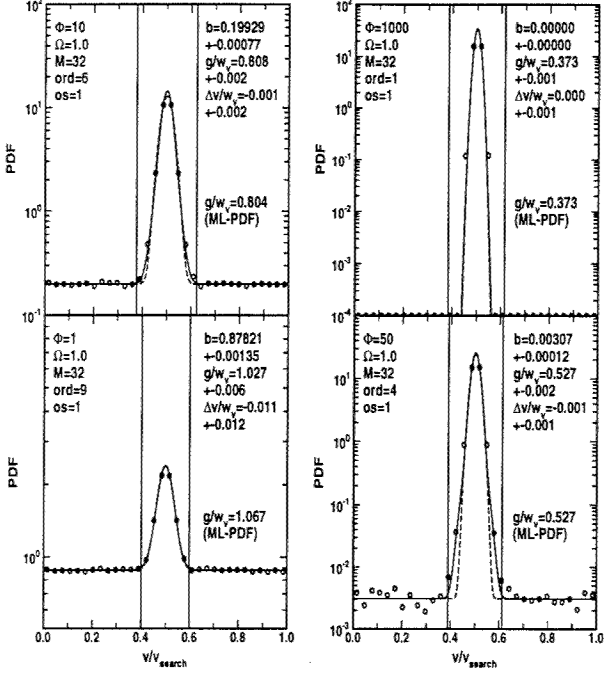


**Figure B22.** PDF of the Velocity Estimates using the CAPON estimator with  $M=32$  and  $\Omega=1.0$  for  $\Phi=1,10,50,1000$ .

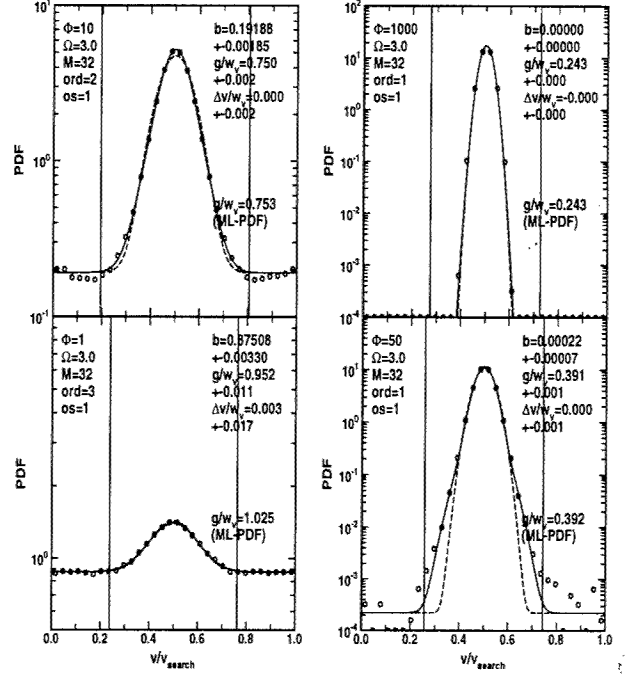


**Figure B24.** PDF of the Velocity Estimates using the CAPON estimator with  $M=32$  and  $\Omega=3.0$  for  $\Phi=1,10,50,1000$ .

## Appendix C, M=64

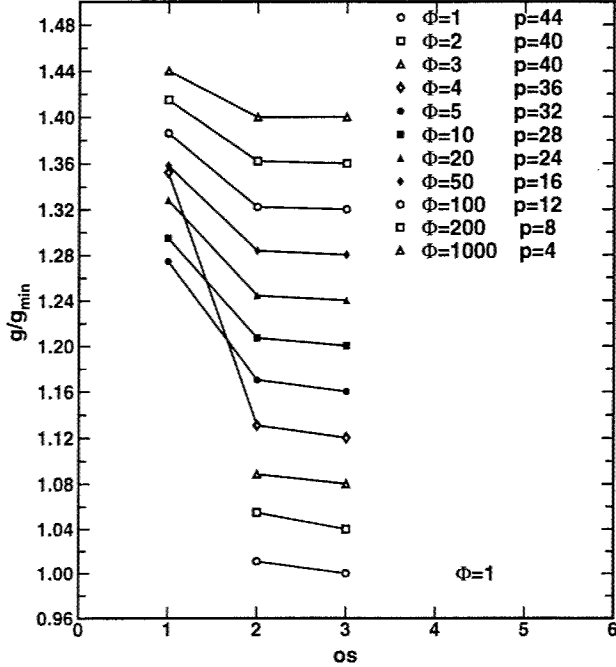


Figure C1. Performance vs. oversampling  $os$  for  $M=64$  and  $\Omega=0.3$ . Curves are offset by 0.05.  $1\sigma$  error bars are smaller than the symbol size.

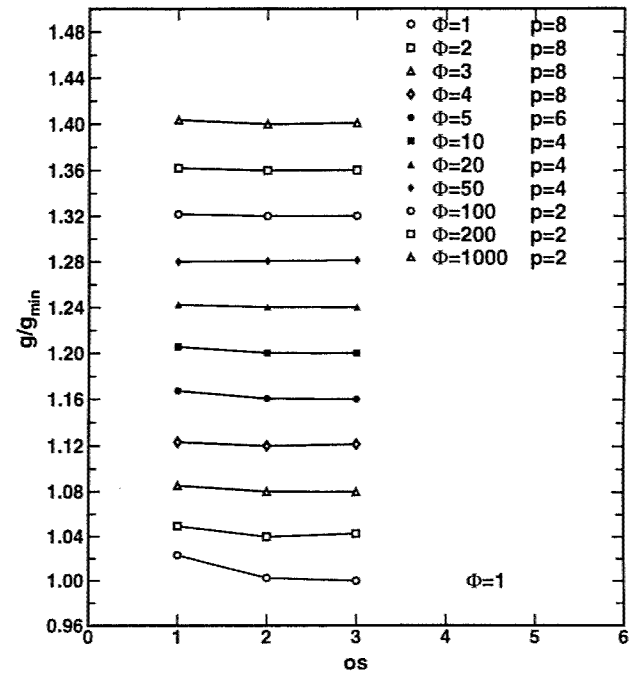


Figure C3. Performance vs. oversampling  $os$  for  $M=64$  and  $\Omega=1.0$ . Curves are offset by 0.05.  $1\sigma$  error bars are smaller than the symbol size.

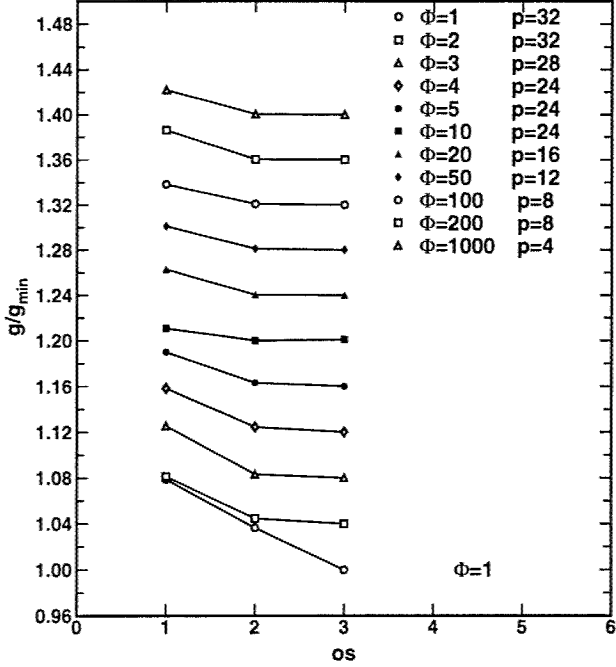


Figure C2. Performance vs. oversampling  $os$  for  $M=64$  and  $\Omega=0.5$ . Curves are offset by 0.05.  $1\sigma$  error bars are smaller than the symbol size.

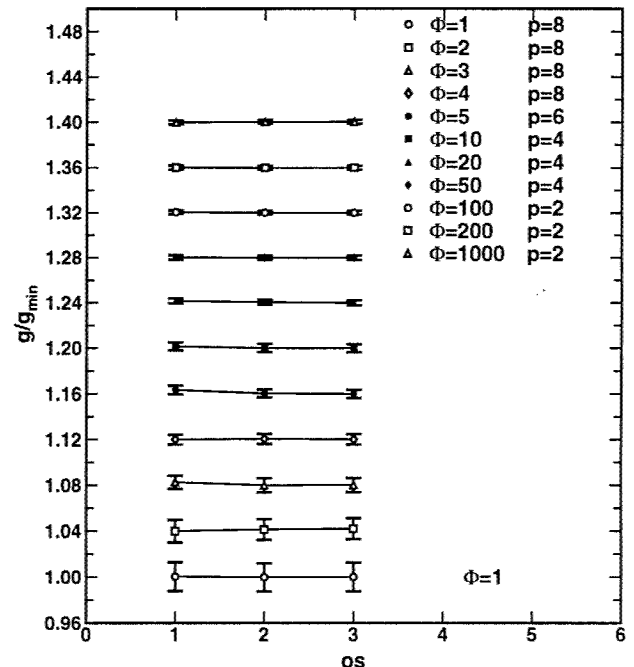
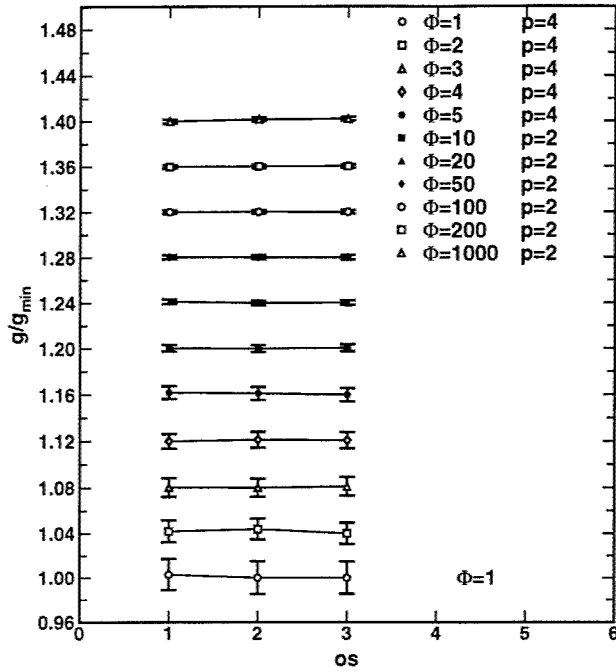
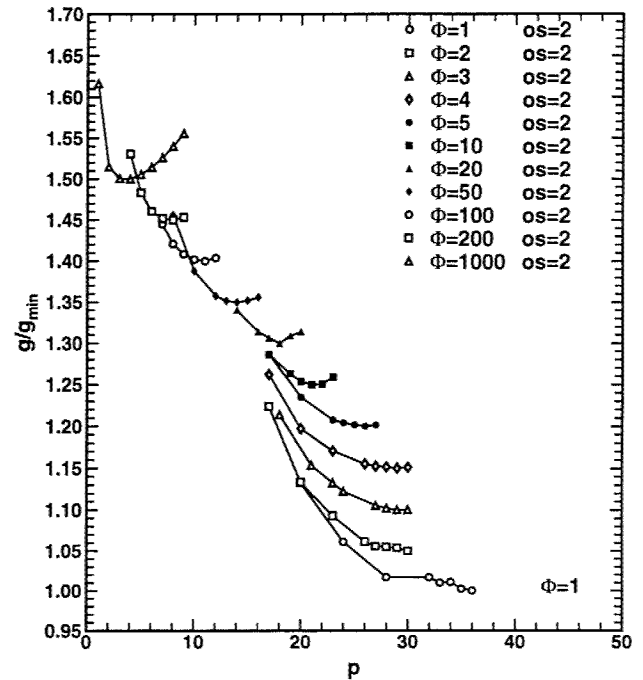


Figure C4. Performance vs. oversampling  $os$  for  $M=64$  and  $\Omega=2.0$ . Curves are offset by 0.05. ( $1\sigma$  error bars).



**Figure C5.** Performance vs. oversampling  $os$  for  $M=64$  and  $\Omega=3.0$ . Curves are offset by 0.05. ( $1\sigma$  error bars).



**Figure C7.** Performance vs. order  $p$  for  $M=64$  and  $\Omega=0.5$ . Curves are offset by 0.05.  $1\sigma$  error bars are less than the symbol size.

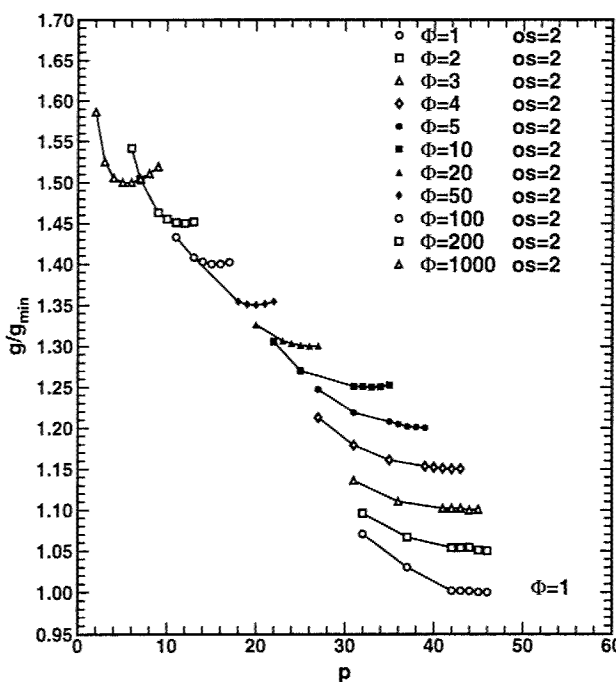


**Figure C6.** Performance vs. order  $p$  for  $M=64$  and  $\Omega=0.3$ . Curves are offset by 0.05.  $1\sigma$  error bars are less than the symbol size.

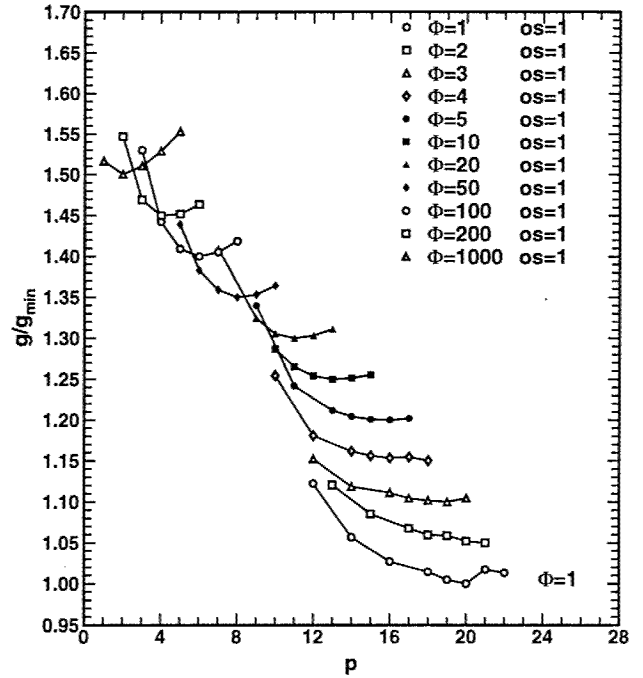


**Figure C8.** Performance vs. order  $p$  for  $M=64$  and  $\Omega=1.0$ . Curves are offset by 0.05.  $1\sigma$  error bars are less than the symbol size.

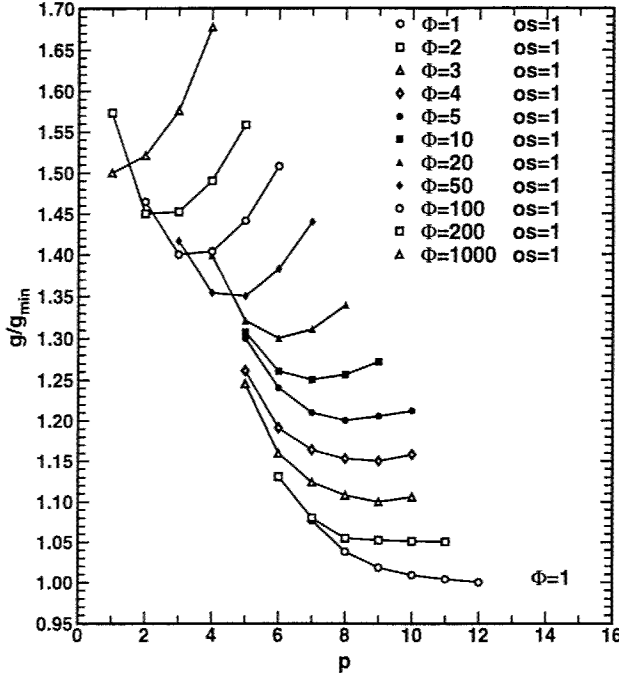


**Figure C9.** Performance vs. order  $p$  for  $M=64$  and  $\Omega=2.0$ . Curves are offset by 0.05.  $1\sigma$  error bars are less than the symbol size.

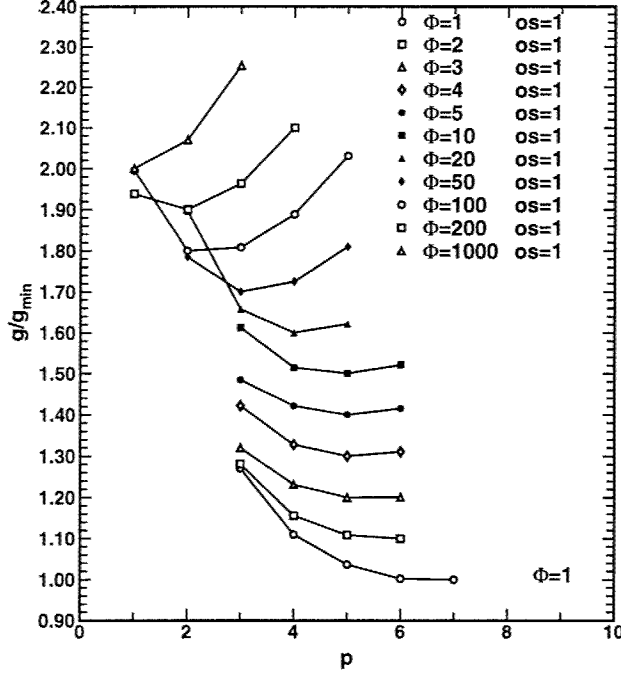


**Figure C10.** Performance vs. order  $p$  for  $M=64$  and  $\Omega=3.0$ . Curves are offset by 0.10.  $1\sigma$  error bars are less than the symbol size.

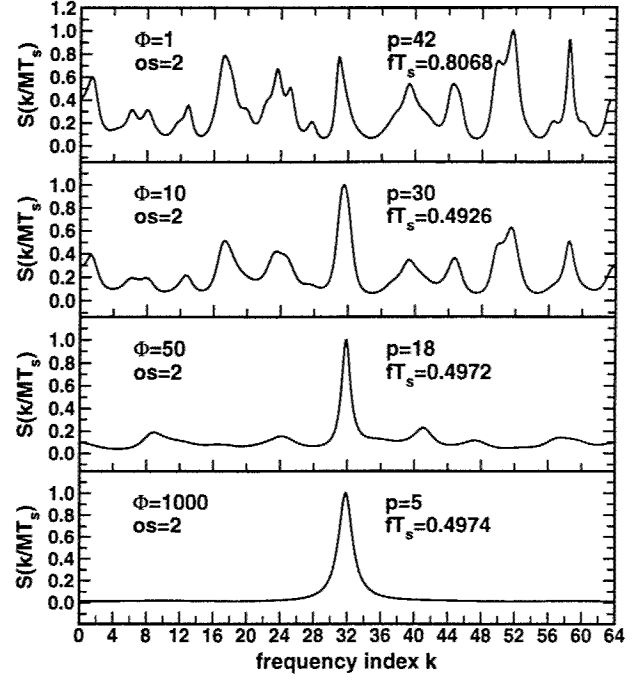


**Figure C11.** Single realizations of the CAPON spectral estimates for  $M=64$  and  $\Omega=0.3$  for  $\Phi=1, 10, 50, 1000$  with optimal estimator parameters as a function of frequency index  $k$ .

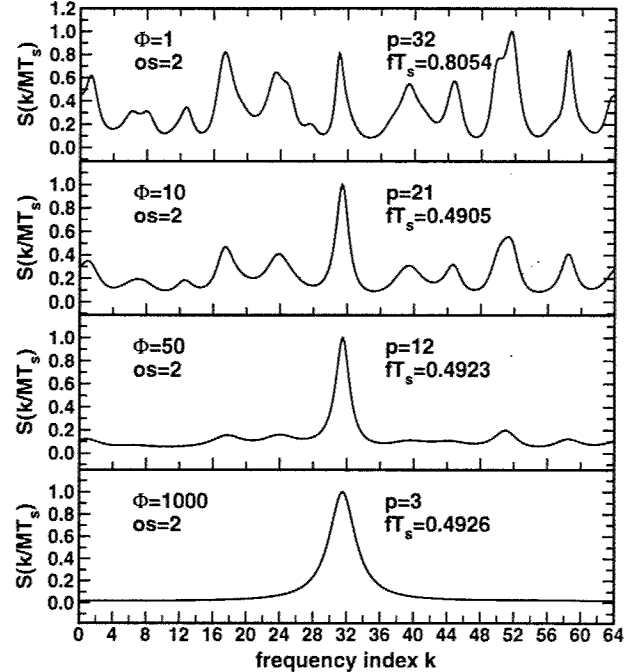


**Figure C12.** Single realizations of the CAPON spectral estimates for  $M=64$  and  $\Omega=0.5$  for  $\Phi=1, 10, 50, 1000$  with optimal estimator parameters as a function of frequency index  $k$ .

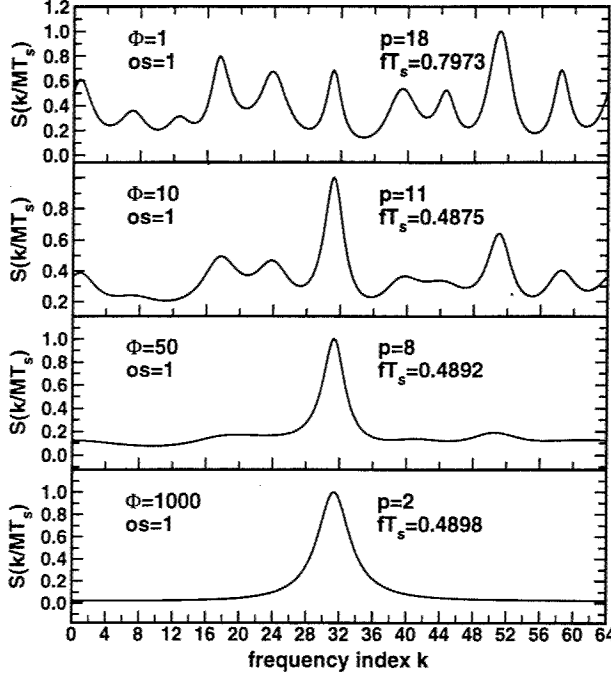


Figure C13. Single realizations of the CAPON spectral estimates for  $M=64$  and  $\Omega=1.0$  for  $\Phi=1, 10, 50, 1000$  with optimal estimator parameters as a function of frequency index  $k$ .

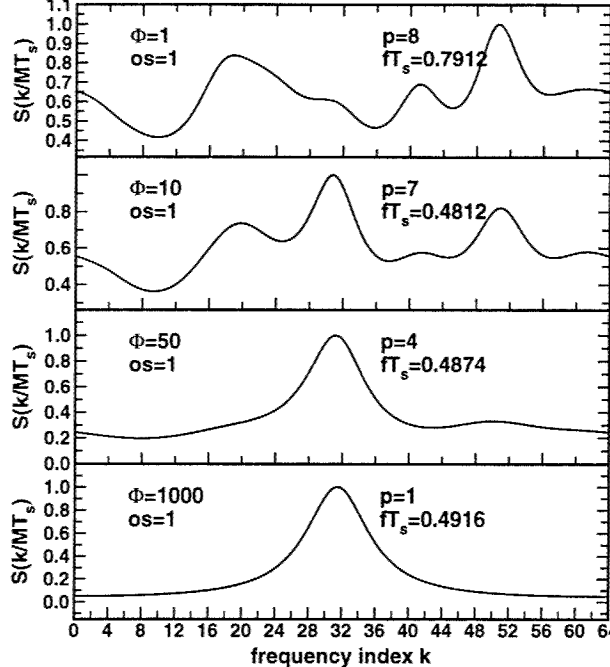


Figure C14. Single realizations of the CAPON spectral estimates for  $M=64$  and  $\Omega=2.0$  for  $\Phi=1, 10, 50, 1000$  with optimal estimator parameters as a function of frequency index  $k$ .

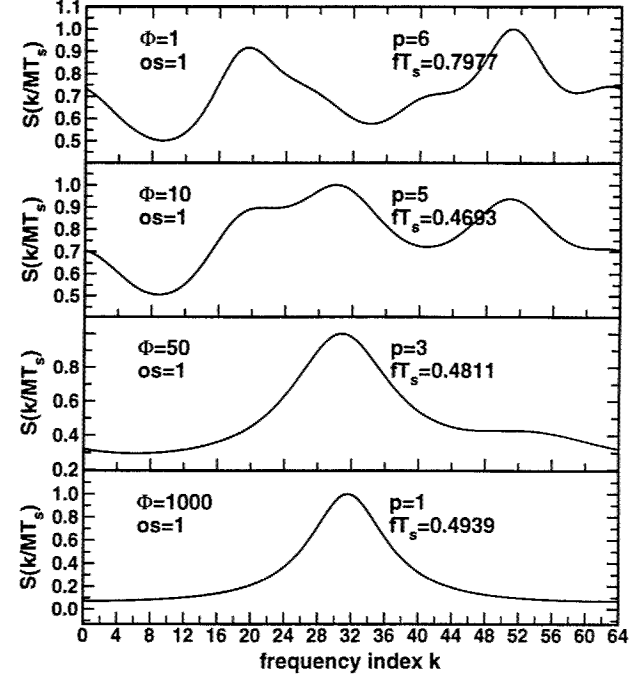


Figure C15. Single realizations of the CAPON spectral estimates for  $M=64$  and  $\Omega=3.0$  for  $\Phi=1, 10, 50, 1000$  with optimal estimator parameters as a function of frequency index  $k$ .

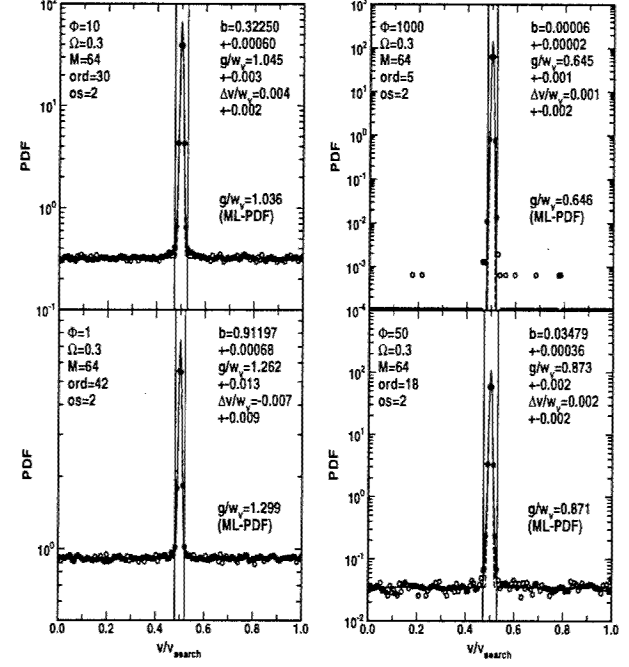
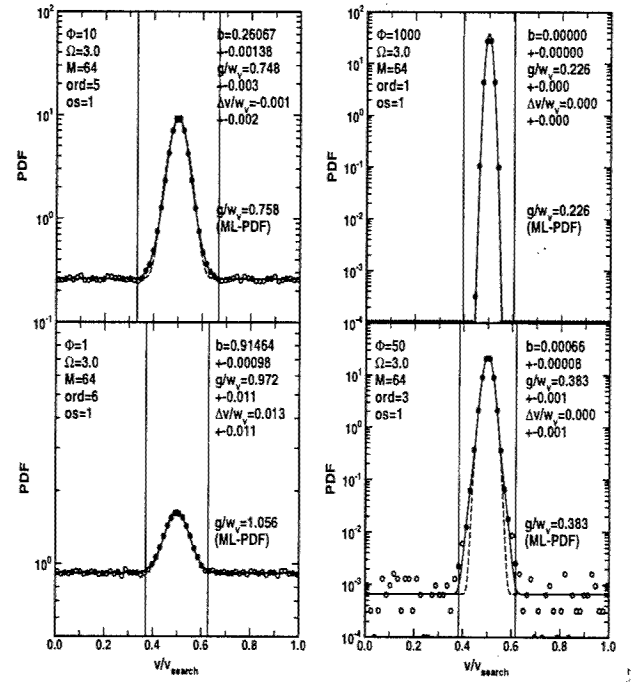
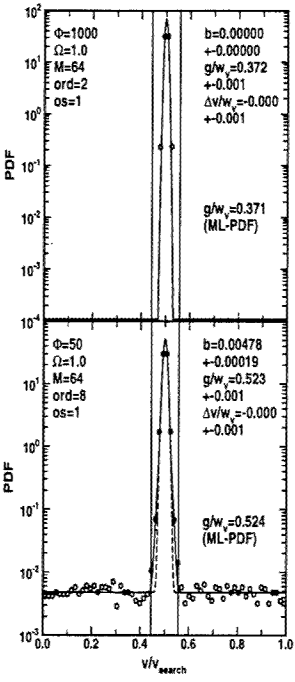
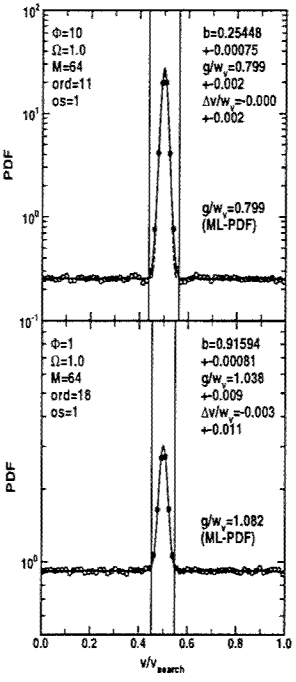
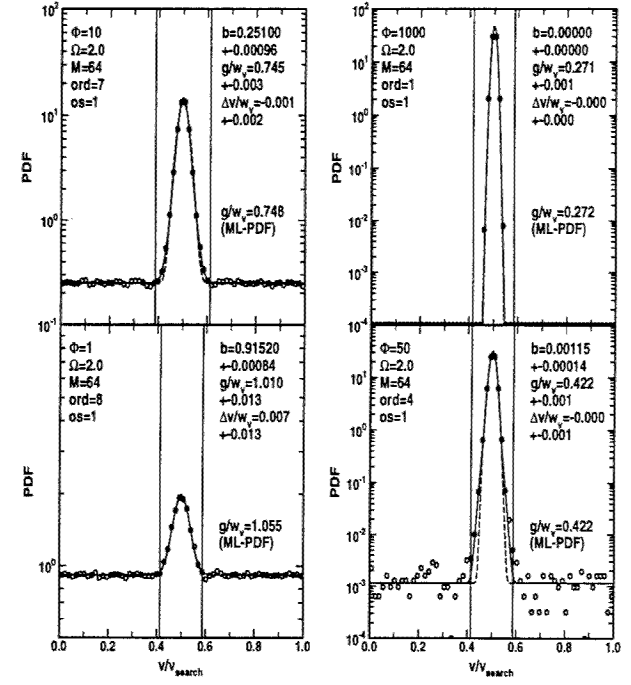
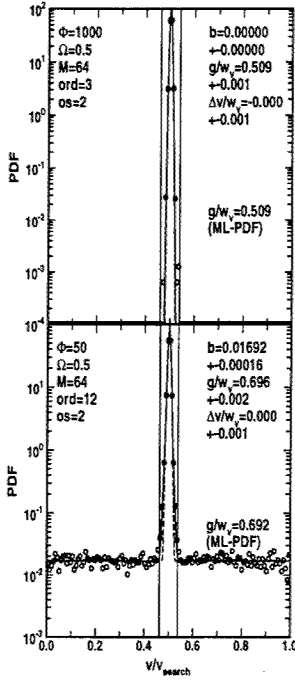
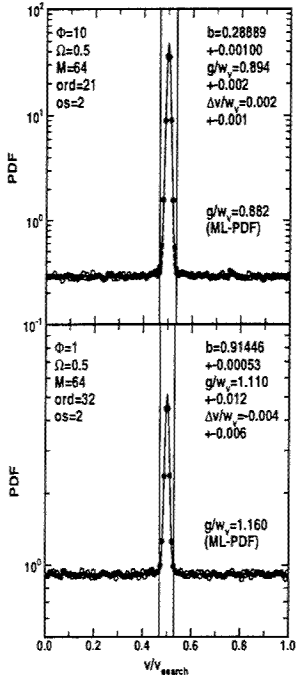
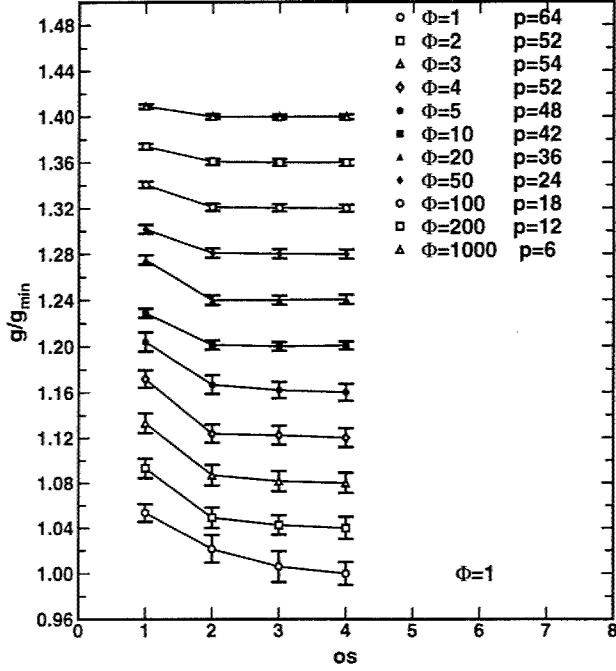


Figure C16. PDF of the Velocity Estimates using the CAPON estimator with  $M=64$  and  $\Omega=0.3$  for  $\Phi=1, 10, 50, 1000$ .



## Appendix D, M=128



**Figure D1.** Performance vs. oversampling  $os$  for  $M=128$  and  $\Omega=0.5$ . Curves are offset by 0.05. (1 $\sigma$  error bars).

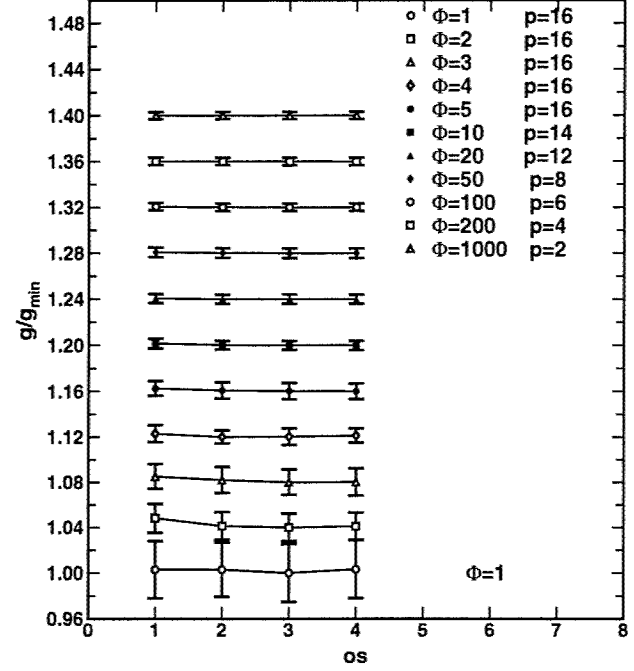


**Figure D3.** Performance vs. oversampling  $os$  for  $M=128$  and  $\Omega=2.0$ . Curves are offset by 0.05. (1 $\sigma$  error bars).

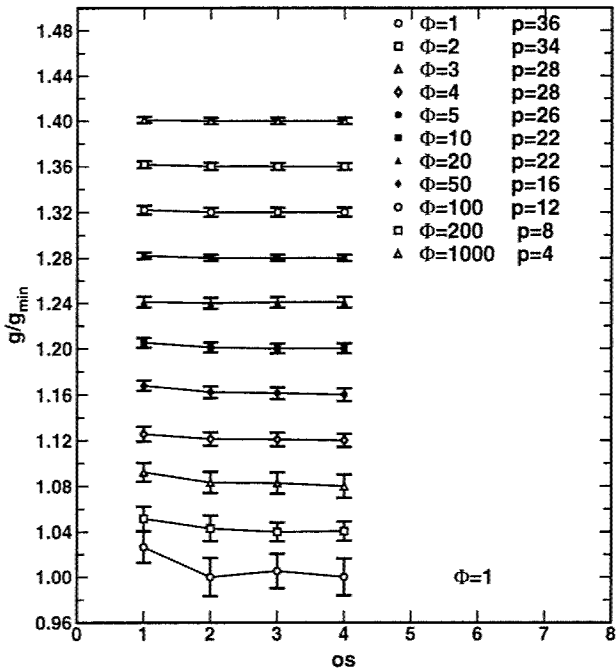


**Figure D2.** Performance vs. oversampling  $os$  for  $M=128$  and  $\Omega=1.0$ . Curves are offset by 0.05. (1 $\sigma$  error bars).

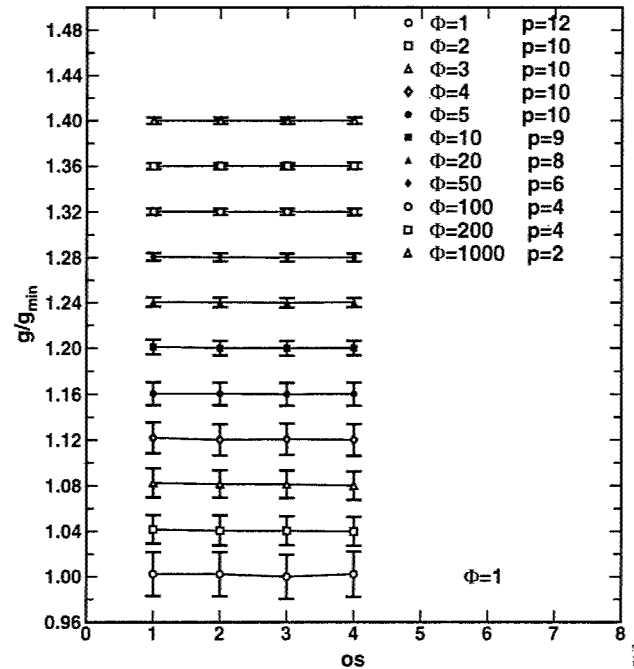


**Figure D4.** Performance vs. oversampling  $os$  for  $M=128$  and  $\Omega=3.0$ . Curves are offset by 0.05. (1 $\sigma$  error bars).

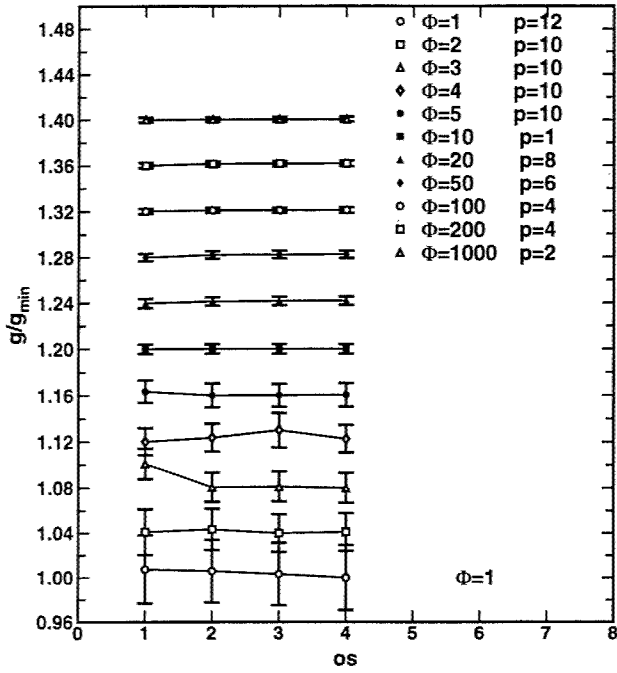


Figure D5. Performance vs. oversampling  $os$  for  $M=128$  and  $\Omega=7.0$ . Curves are offset by 0.05.  $1\sigma$  error bars are less than the symbol size.

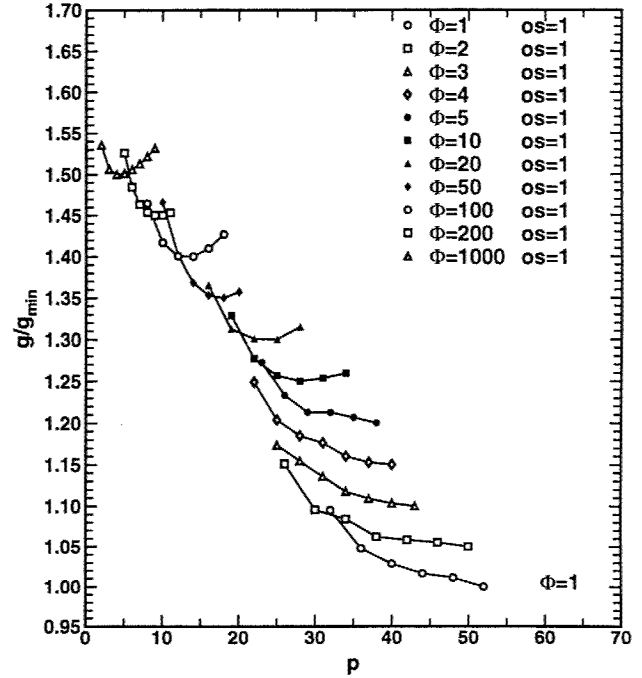


Figure D7. Performance vs. order  $p$  for  $M=128$  and  $\Omega=1.0$ . Curves are offset by 0.10.  $1\sigma$  error bars are less than the symbol size.

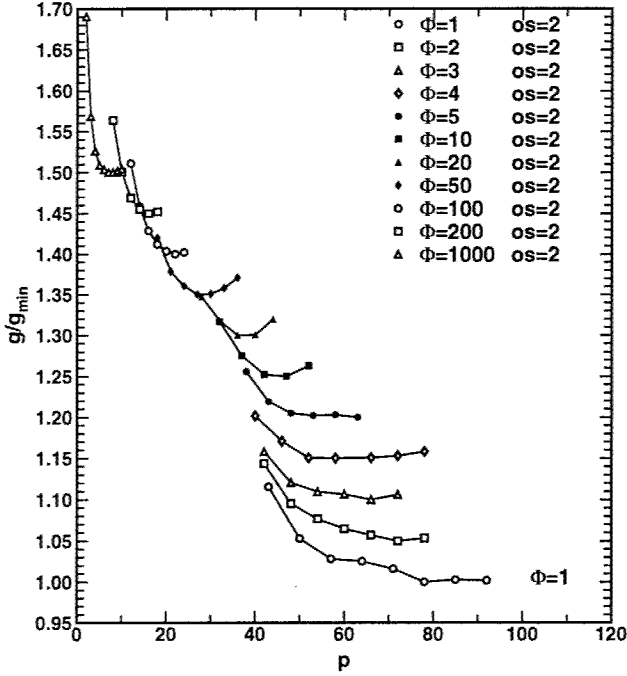


Figure D6. Performance vs. order  $p$  for  $M=128$  and  $\Omega=0.5$ . Curves are offset by 0.10.  $1\sigma$  error bars are less than the symbol size.

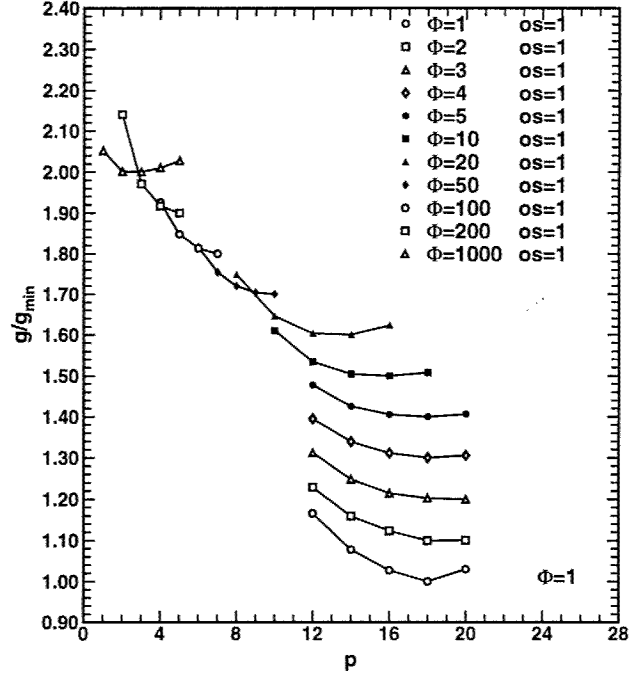


Figure D8. Performance vs. order  $p$  for  $M=128$  and  $\Omega=2.0$ . Curves are offset by 0.10.  $1\sigma$  error bars are less than the symbol size.

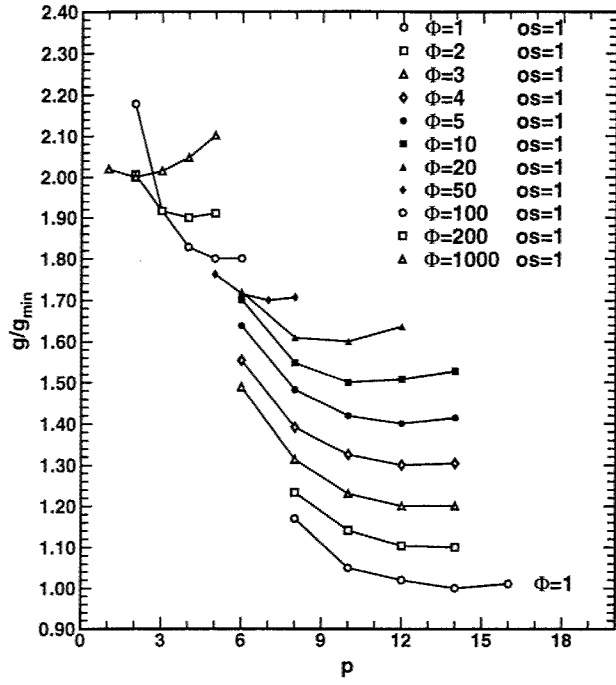


Figure D9. Performance vs. order  $p$  for  $M=128$  and  $\Omega=3.0$ . Curves are offset by 0.10.  $1\sigma$  error bars are less than the symbol size.

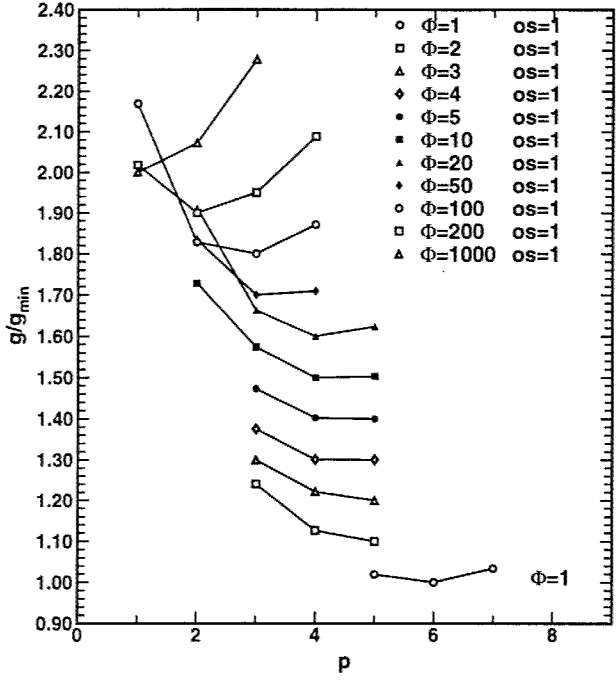


Figure D10. Performance vs. order  $p$  for  $M=128$  and  $\Omega=7.0$ . Curves are offset by 0.10.  $1\sigma$  error bars are less than the symbol size.

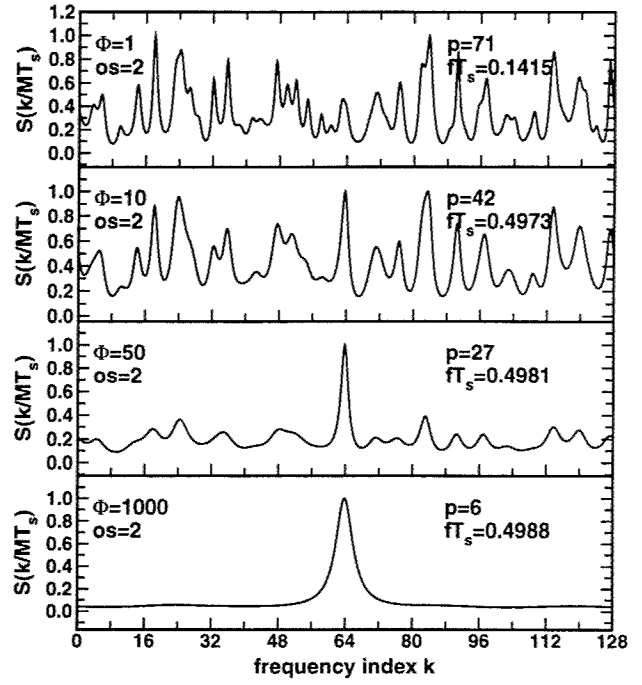


Figure D11. Single realizations of the CAPON spectral estimates for  $M=128$  and  $\Omega=0.5$  for  $\Phi=1, 10, 50, 1000$  with optimal estimator parameters as a function of frequency index  $k$ .

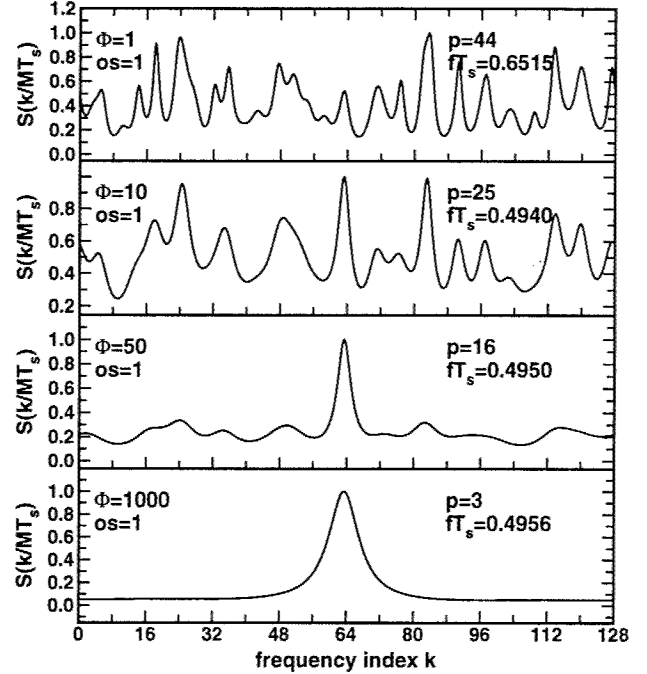
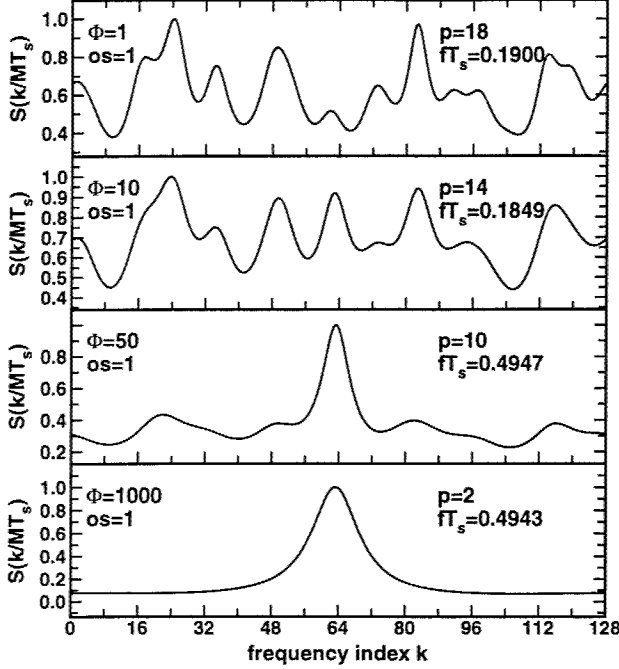
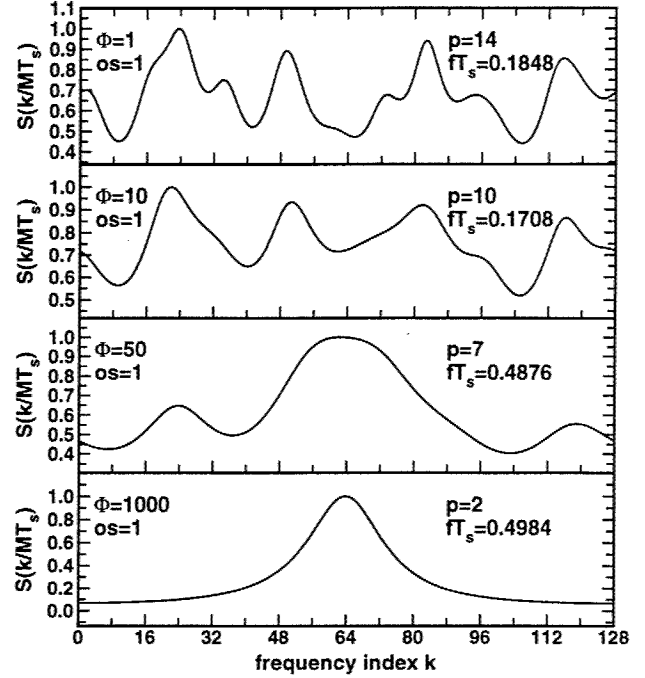


Figure D12. Single realizations of the CAPON spectral estimates for  $M=128$  and  $\Omega=1.0$  for  $\Phi=1, 10, 50, 1000$  with optimal estimator parameters as a function of frequency index  $k$ .



**Figure D13.** Single realizations of the CAPON spectral estimates for  $M=128$  and  $\Omega=2.0$  for  $\Phi=1,10,50,1000$  with optimal estimator parameters as a function of frequency index  $k$ .



**Figure D15.** Single realizations of the CAPON spectral estimates for  $M=128$  and  $\Omega=7.0$  for  $\Phi=1,10,50,1000$  with optimal estimator parameters as a function of frequency index  $k$ .

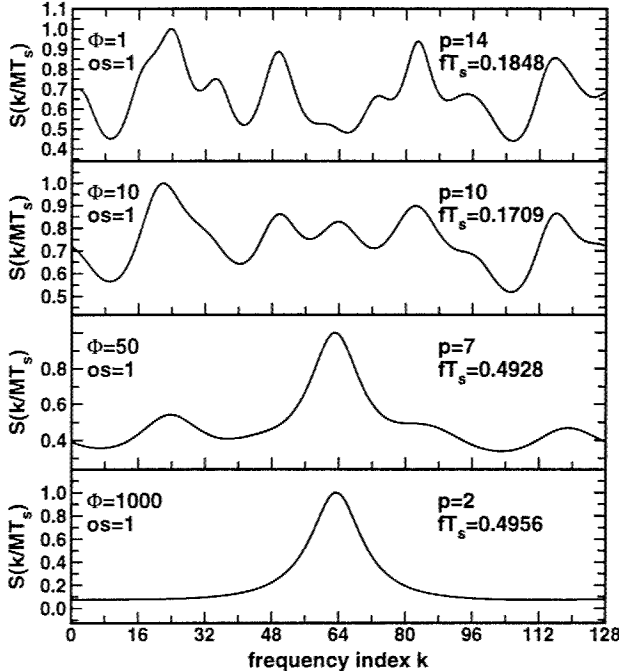


**Figure D14.** Single realizations of the CAPON spectral estimates for  $M=128$  and  $\Omega=3.0$  for  $\Phi=1,10,50,1000$  with optimal estimator parameters as a function of frequency index  $k$ .

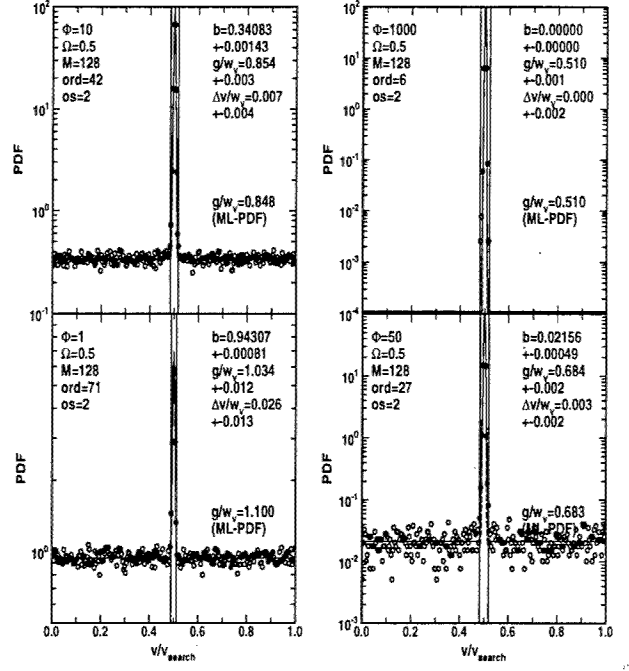


**Figure D16.** PDF of the Velocity Estimates using the CAPON estimator with  $M=128$  and  $\Omega=0.5$  for  $\Phi=1,10,50,1000$ .

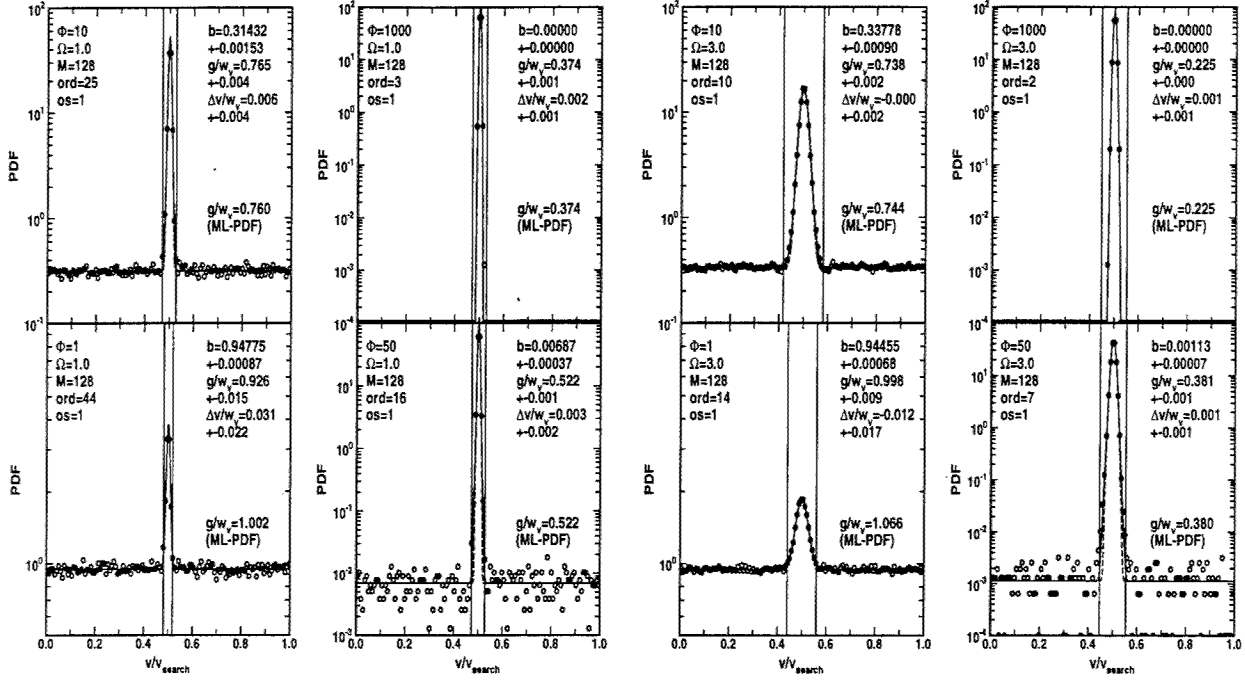


**Figure D17.** PDF of the Velocity Estimates using the CAPON estimator with  $M=128$  and  $\Omega=1.0$  for  $\Phi=1,10,50,1000$ .

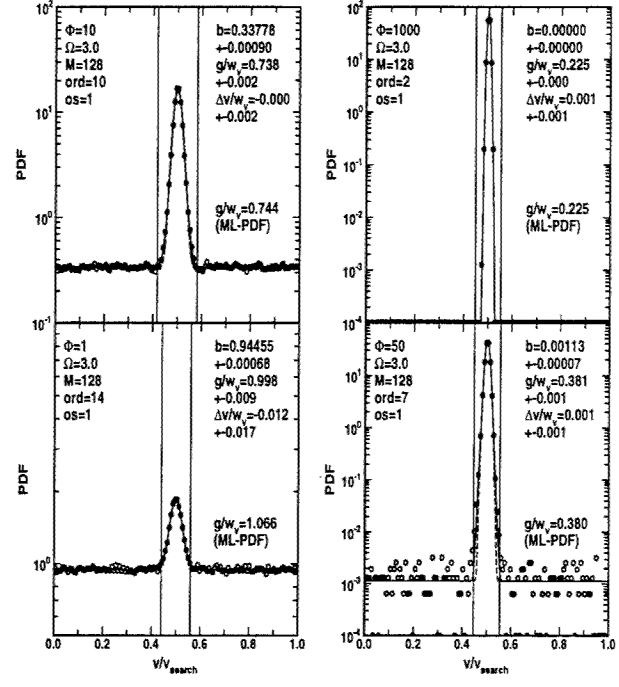


**Figure D19.** PDF of the Velocity Estimates using the CAPON estimator with  $M=128$  and  $\Omega=3.0$  for  $\Phi=1,10,50,1000$ .

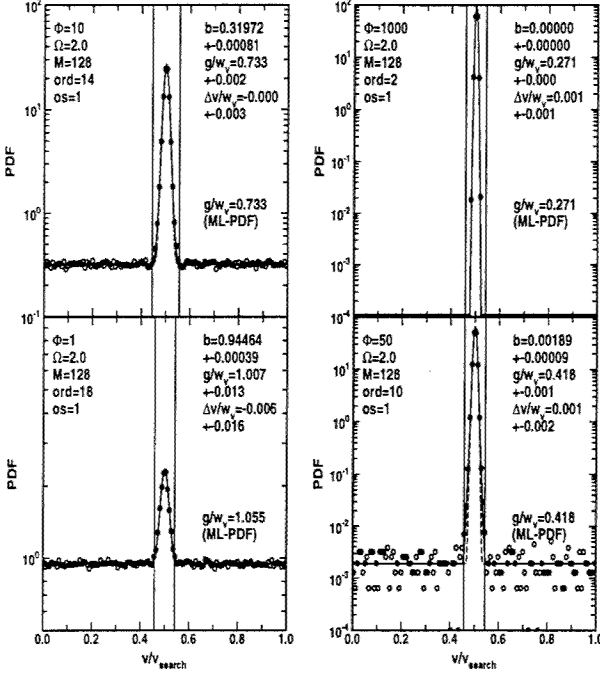


**Figure D18.** PDF of the Velocity Estimates using the CAPON estimator with  $M=128$  and  $\Omega=2.0$  for  $\Phi=1,10,50,1000$ .

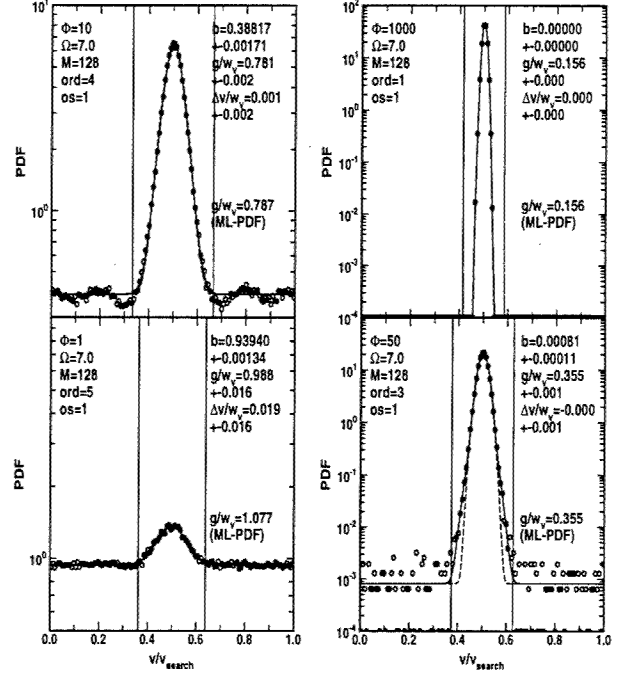


**Figure D20.** PDF of the Velocity Estimates using the CAPON estimator with  $M=128$  and  $\Omega=7.0$  for  $\Phi=1,10,50,1000$ .

## Appendix E, $M=512$

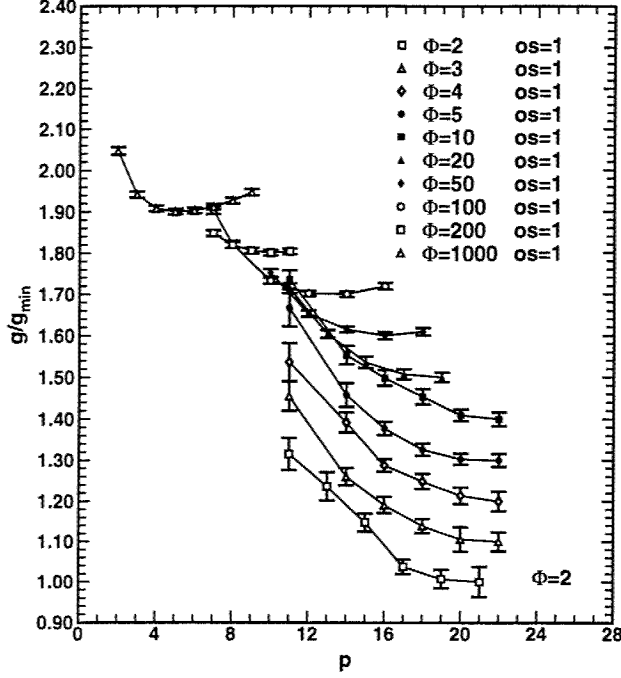


**Figure E1.** Performance vs. order  $p$  for  $M=512$  and  $\Omega=7.0$ . Curves are offset by 0.05. ( $1\sigma$  error bars).

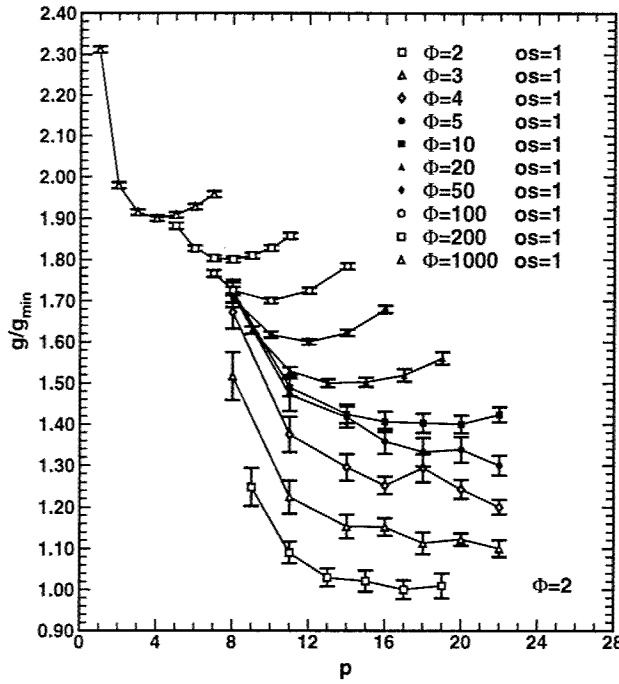


**Figure E2.** Performance vs. order  $p$  for  $M=512$  and  $\Omega=10.0$ . Curves are offset by 0.05. ( $1\sigma$  error bars).

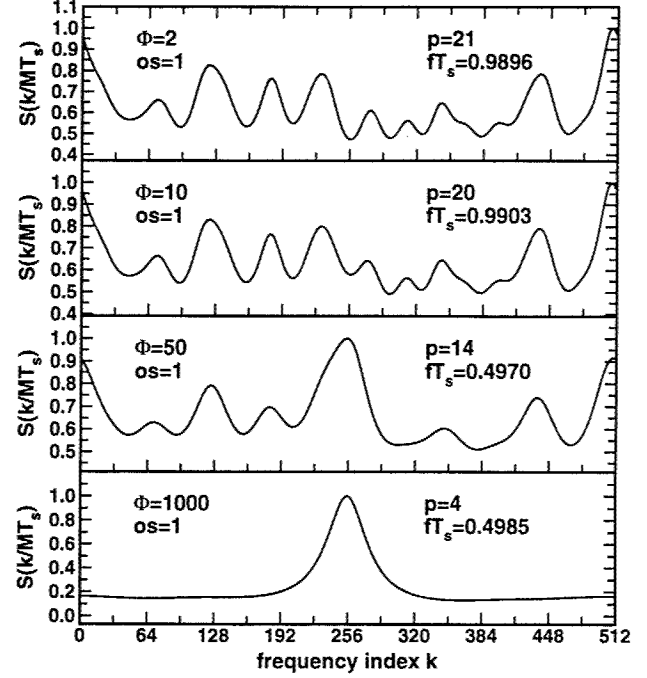


**Figure E3.** Single realizations of the CAPON spectral estimates for  $M=512$  and  $\Omega=7.0$  for  $\Phi=2, 10, 50, 1000$  with optimal estimator parameters as a function of frequency index  $k$ .

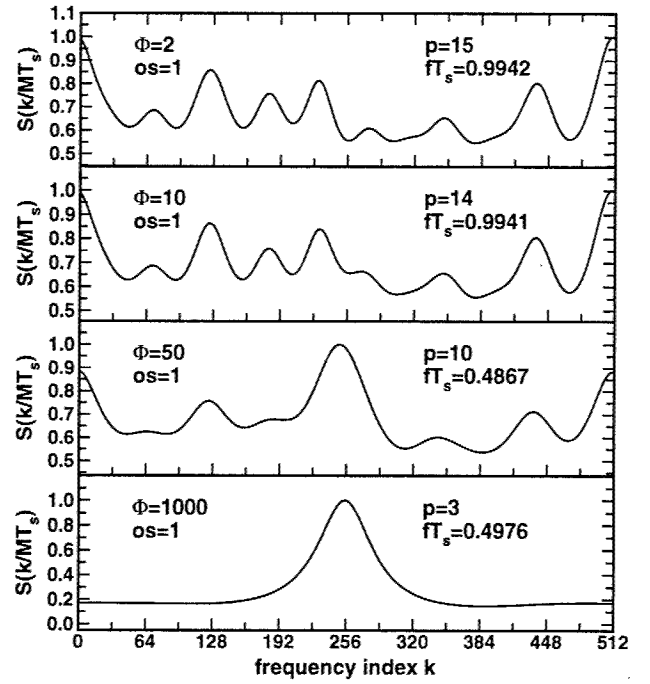


**Figure E4.** Single realizations of the CAPON spectral estimates for  $M=512$  and  $\Omega=10.0$  for  $\Phi=2, 10, 50, 1000$  with optimal estimator parameters as a function of frequency index  $k$ .

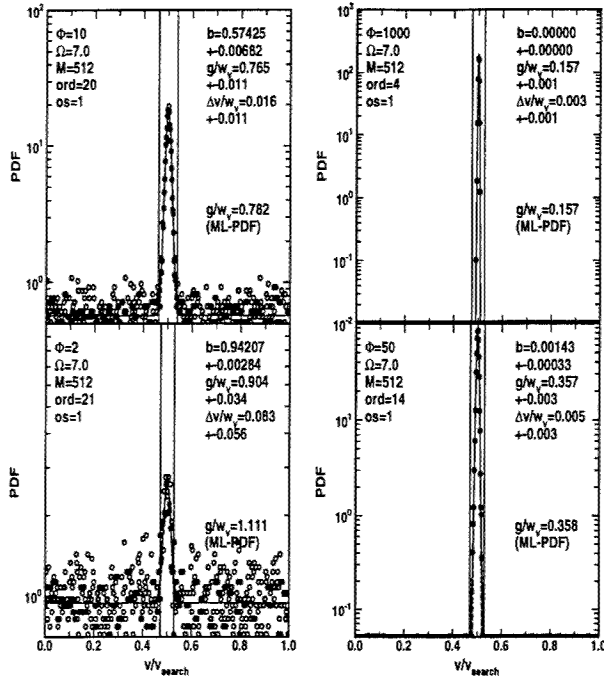


**Figure E5.** PDF of the Velocity Estimates using the CAPON estimator with  $M=512$  and  $\Omega=7.0$  for  $\Phi=2, 10, 50, 1000$ .

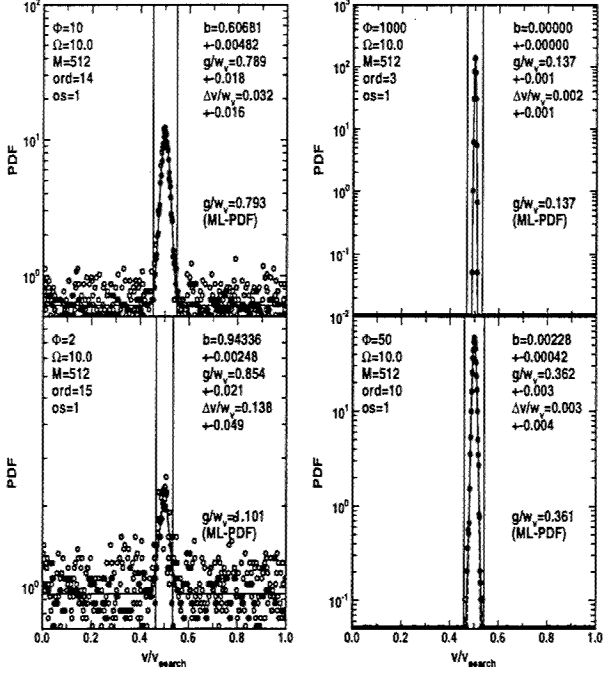


**Figure E6.** PDF of the Velocity Estimates using the CAPON estimator with  $M=512$  and  $\Omega=10.0$  for  $\Phi=2, 10, 50, 1000$ .

## References

- [1] T. R. Lawrence, D. J. Wilson, C. E. Craven, I. P. Jones, R. M. Huffaker and J. A. L. Thomson: "A laser velocimeter for remote wind sensing," *Rev. Sci. Instr.*, **43** 512-518, (1972).
- [2] J. W. Bilbro, C. DiMarzio, D. Fitzjarrald, S. Johnson, and W. Jones: "Airborne Doppler lidar measurements," *Appl. Opt.* **25**, 2952-2960 (1986).
- [3] J. C. Petheram, G. Frohbeiter, and A. Rosenberg: "Carbon dioxide Doppler lidar wind sensor on a space station polar platform," *Appl. Opt.* **28**, 834-839 (1989).
- [4] M. J. Post and R. E. Cupp: "Optimizing a pulsed Doppler lidar," *Appl. Opt.* **29**, 4145-4158 (1990).
- [5] M. J. Kavaya, S. W. Henderson, J. R. Magee, C. P. Hale, and R. M. Huffaker: "Remote wind profiling with a solid-state Nd:YAG coherent lidar system," *Opt. Lett.* **14**, 776-778 (1992).
- [6] S. W. Henderson, C. P. Hale, J. R. Magee, M. J. Kavaya, and A. V. Huffaker: "Eye-safe coherent laser radar system at  $2.1\text{ }\mu\text{m}$  using Tm,Ho:YAG lasers," *Opt. Lett.* **16**, 773-775 (1991).
- [7] S. W. Henderson, P. J. M. Suni, C. P. Hale, S. M. Hannon, J. R. Magee, D. L. Bruns, and E. H. Yuen: "Coherent laser radar at  $2\text{ }\mu\text{m}$  using solid-state lasers," *IEEE Trans. Geo. Remote Sensing* **31**, 4-15 (1993).
- [8] M. R. Huffaker, T.R. Lawrence, M. J. Post, J.T. Priestley, F. F. Hall, Jr., R.A. Richter, and R.J. Keeler: "Feasibility studies for a global wind measuring satellite system (Windsat): analysis of simulated performance," *Appl. Opt.* **23**, 2523-2536 (1984).
- [9] W. E. Baker, G. D. Emmitt, P. Robertson, R. M. Atlas, J. E. Molinari, D. A. Bowdle, J. Paegle, R. M. Hardesty, R. T. Menzies, T. N. Krishnamurti, R. A. Brown, M. J. Post, J. R. Anderson, A. C. Lorenc, T. L. Miller, and J. McElroy: "Lidar measured winds from space: an essential component for weather and climate prediction," *Bull. Amer. Met. Soc.* **76**, 869-888 (1995) .
- [10] R. G. Frehlich, and M. J. Yadlowsky: "Performance of mean frequency estimators for Doppler radar and lidar," *J. Atm. Ocean. Tech.*, **11**, 1217-1230 (1994) .
- [11] Anderson, J. R.: "High performance velocity estimators for coherent laser radars," *Sixth Topical Meeting on Coherent Laser Radar: Technology and Applications*, (Snowmass-at-Aspen, CO, USA), Optical Society of America, 216-218, (1991).
- [12] B. J. Rye, and R. M. Hardesty: "Discrete spectral peak estimation in incoherent backscatter heterodyne lidar. I. Spectral accumulation and the Cramer-Rao lower bound," *IEEE Trans. Geo. Sci. Remote Sensing* **31**, 16-27 (1993).
- [13] B. J. Rye and R. M. Hardesty: "Discrete spectral peak estimation in incoherent backscatter heterodyne lidar. II. Correlogram accumulation," *IEEE Trans. Geo. Sci. Remote Sensing* **31**, 28-35 (1993).
- [14] R. Frehlich, S. Hannon, and S. Henderson: "Performance of a  $2\text{ }\mu\text{m}$  coherent Doppler lidar for wind measurements", *J. Atm. Ocean. Tech.* **11**, 1517-1528 (1994).
- [15] Marple, S.Lawrence Jr.: "Digital Spectral Analysis with Applications" performance," Prentice-Hall Signal Processing Series, (1987).
- [16] Frehlich, R. G.: "Effects of wind turbulence on coherent Doppler lidar performance," submitted to *J. Atmos. Ocean. Tech.*, Dec. (1994).

REPORT DOCUMENTATION PAGE			Form Approved OMB No. 0704-0188
<p>Public reporting burden for this collection of information is estimated to average 1 hour per response, including the time for reviewing instructions, searching existing data sources, gathering and maintaining the data needed, and completing and reviewing the collection of information. Send comments regarding this burden estimate or any other aspect of this collection of information, including suggestions for reducing this burden, to Washington Headquarters Services, Directorate for Information Operations and Reports, 1215 Jefferson Davis Highway, Suite 1204, Arlington, Va 22202-4302, and to the Office of Management and Budget, Paperwork Reduction Project (0704-0188), Washington, DC 20503.</p>			
1. AGENCY USE ONLY (Leave Blank)	2. REPORT DATE January 1997	3. REPORT TYPE AND DATES COVERED Contractor Report (Final)	
4. TITLE AND SUBTITLE  Evaluation of the MV (CAPON) Coherent Doppler Lidar Velocity Estimator			5. FUNDING NUMBERS NAG8-253 NGT-51206
6. AUTHOR(S)  B. Lottman and R. Frehlich			
7. PERFORMING ORGANIZATION NAME(S) AND ADDRESS(ES) University of Colorado CIRES - Campus Box 216 Boulder, CO 80309-0216			8. PERFORMING ORGANIZATION REPORT NUMBERS  M-824
9. SPONSORING/MONITORING AGENCY NAME(S) AND ADDRESS(ES) George C. Marshall Space Flight Center Marshall Space Flight Center, Alabama 35812			10. SPONSORING/MONITORING AGENCY REPORT NUMBER  NASA CR-4763
11. SUPPLEMENTARY NOTES Technical Monitor: Dr. Michael Kavaya, Astrionics Laboratory, Science and Engineering Directorate			
12a. DISTRIBUTION/AVAILABILITY STATEMENT  Unclassified-Unlimited  Subject Category 43			12b. DISTRIBUTION CODE
13. ABSTRACT (Maximum 200 words)  The performance of the CAPON velocity estimator for coherent Doppler lidar is determined for typical space-based and ground-based parameter regimes. Optimal input parameters for the algorithm were determined for each regime. For weak signals, performance is described by the standard deviation of the good estimates and the fraction of outliers. For strong signals, the fraction of outliers is zero. Numerical effort was also determined.			
14. SUBJECT TERMS Doppler Lidar Velocity Estimation			15. NUMBER OF PAGES 44
			16. PRICE CODE A03
17. SECURITY CLASSIFICATION Unclassified	18. SECURITY CLASSIFICATION OF THIS PAGE Unclassified	19. SECURITY CLASSIFICATION OF ABSTRACT Unclassified	20. LIMITATION OF ABSTRACT Unlimited

National Aeronautics and  
Space Administration  
Code JTT  
Washington, DC  
20546-0001

*Official Business  
Penalty for Private Use, \$300*

*Postmaster: If Undeliverable (Section 158 Postal Manual), Do Not Return*

---